

Water Resources Center

Annual Technical Report

FY 2000

Introduction

None

Research Program

Basic Information

Title:	A coupled hydraulic-ecosystem model for evaluation of habitat and wildlife in restored rivers, focusing on dam operations and removal.
Project Number:	B-07
Start Date:	3/1/2000
End Date:	2/28/2001
Research Category:	Water Quality
Focus Category:	Models, Water Quantity, Ecology
Descriptors:	
Lead Institute:	Ohio State University
Principal Investigators:	Tim Granata, Diane L. Foster

Publication

1. Articles in Refereed Journals: One article in preparation: Cheng, F. Zika, Keith Banachowski, Granata, T.C. in preparation. Modeling the effects of dam removal on migratory walleye life stages in a coastal watershed. To be submitted to Regulated Rivers in 2001.
2. None.
3. Cheng, Fang. Modeling the effects of dam removal on migratory walleye life stages in a coastal watershed; to be completed August 2001. Environmental Science Graduate Program, OSU, Columbus, Ohio. Banachowski, Keith. Hydraulic and management models for a coastal watershed to assess the impact of dam removal; to be completed Spring 2002. Department of Civil and Environmental Engineering and Geodetic Science, OSU, Columbus, Ohio.
4. Timothy C. Granata, Virginie Bouchard, Ann Christy, Diane Foster, Roy Stein. 2001. A coupled hydraulic-ecosystem model for evaluation of habitat and wildlife restoration in rivers, focusing on dam operations and removal. Water Resources Center, Ohio State University, Columbus, OH. pp.

- 17.
5. None.
6. Conference Presentations: Two papers presented at National Conferences: Modeling the effects of dam removal on migratory walleye life stages in a coastal watershed. Cheng, F. Zika, U. Granata, T.C. American Society of Limnology and Oceanography, Winter Meeting 2001. Feb. 11-16, 2001, Albuquerque, NM. Hydrologic and hydraulic modeling of a coastal watershed to assess the impact of dam removal on geomorphology and fish habitat. Banachowski, K. and Granata, T.C. American Society of Limnology and Oceanography, Winter Meeting 2001. Feb. 11-16, 2001, Albuquerque, NM.
7. Timothy C. Granata, Virginie Bouchard, Ann Christy, Diane Foster, Roy Stein. 2001. A coupled hydraulic-ecosystem model for evaluation of habitat and wildlife restoration in rivers, focusing on dam operations and removal. Water Resources Center, Ohio State University, Columbus, OH. pp. 20.

Problem and Research Objectives

Statement of the problem

Within the last 5 years in the USA, several state and federal programs have begun to address restoration of aquatic habitat and wildlife in watersheds (NOAA, 1995; Nettle, 1999). A report from the Wisconsin Department of Natural Resources (1995) states that dams are among the most significant obstacles to restoring the integrity of riverine systems. Critics, however, cite that evidence of the recovery of aquatic communities and habitats after restoration is scarce and needs to be approached with caution (Ebersole et al., 1997). Thus, a major problem in river restoration is the gap in our knowledge of ecosystem response to hydrologic changes after dam removal.

The primary nature of a fluvial ecosystem is the dynamic equilibrium of the physical system, which in turn provides feedback to the biological components. Functional processes in a river-floodplain are characterized by fluxes of matter between each system and the input, processing, and retention of matter (Lorenz et al., 1997). Therefore, the goal of restoration should be to restore rivers to their original dynamics.

Dams modify hydraulic patterns (altering fluxes, composition, and movement of particles and sediments), reduce connectivity between habitats (effectively decoupling river channels and their floodplains/wetlands), and change habitat quality of aquatic wildlife (mainly fish and invertebrates). Dam operations not only change water levels in rivers but also in the ground water table which will affect recharge of the river. Since biological and physical processes are so closely linked in riverine systems, any river restoration project requires a fundamental understanding of river mechanics and transport. This is particularly important for restoration projects associated with dam operations and subsequent removal since dams alter material fluxes and modify suitable habitat for keystone species.

One of the clearest effects of dams is the blockage of anadromous fish migration in watersheds that connect to lakes and oceans. While most dam removals in the United States have been caused by natural destruction of structures (Born et al., 1998), a dam in the state of Maine was recently removed to promote restoration of the environment for spawning of salmon in rivers (Columbus Dispatch, 1999).

In Ohio, a dam removal project has been proposed for the Ballville Dam, a 120 m wide, 10 m high dam located south of the city of Fremont, Ohio, and 17 km south of Sandusky Bay, on Lake Erie.

The Sandusky River is one of the primary tributaries for spawning of walleye (*Stizostedion vitreum*) and small mouth bass (*Micropterus dolomieu*). Walleye is a terminal predator, an important sport and commercial fish, and is highly valued both ecologically and economically. Variability in recruitment to the adult population and changes in year-class-strength of Lake Erie walleye are believed to be caused by variable survival during the egg and larval life stages. In the Sandusky River, variability in river discharge underlies variability of walleye year-class-strength (Mion et al. 1998). Currently, the upstream movement of walleye in the Sandusky is prohibited by the Ballville Dam (Mion et al. 1998). Removal of the dam would potentially increase the amount of spawning habitat, since potential habitat upstream, near Tiffin, OH, would become accessible. Unfortunately, insufficient data exist to evaluate how removal of the Ballville Dam will affect habitat and walleye populations. Therefore, a joint physical-biological investigation is needed to fill the data gap so that responsible management decisions can be made.

Objectives

An initial approach to filling the gap in data was to develop a hydraulic-ecology model capable of simulating the response of a river-floodplain ecosystem to dam operations and removal. This response is evaluated for river morphology, water quality, usable habitat, and larval walleye populations. Development of the model was beneficial for several reasons. First, the model was a cost-effective way to compare interactions in dam operations with changes in water quality, river morphology, habitat, and wildlife. Second, model results will be publicly available for use by environmental managers, grass roots organizations and scientists, among others. Third, the model could be applied and extended to other coastal watersheds throughout the USA. Fourth, the model was developed and used within a restricted time frame (1 year) of the project.

The model uses available field data on the Sandusky River, provided by the U.S. Geological Survey, the Ohio Department of Natural Resources and others, to parameterize and set boundary conditions for model runs. Temporal scales of ecosystem responses were quantified and spatial scales described based on river morphology and hydraulic parameters. Scenarios were simulated over seasonal and spawning cycles with diurnal fluctuations resolved, thus providing an unaltered data set compatible with statistical procedures, e.g., time series, cross sections, longitudinal profiles, and horizontal maps.

Methodology

General Overview

Since this proposal only provides one year of funding, we purchased an existing model and add the capacity for habitat restoration and dam removal. To simulate nominal flow and flooding conditions in the Sandusky River system, we selected the commercially available package Mike11 for one-dimensional modeling of complex river mechanics, dam structures, sediment transport, and water quality in rivers. The modular design ensured that physical processes in the main program were automatically transferred between modules to couple river flow with river morphology, sediment resuspension, and water quality.

The basic MIKE11 software includes modules for: a) hydrodynamics, b) advection-dispersion; c) non-cohesive sediment transport; and d) water quality. A fish model, designed by our group, was developed to address walleye population dynamics. Dr. Foster worked on part of the sediment submodule, Dr. Christy with groundwater assessments; Dr. Bouchard with the ecological submodule; and Dr. Zika, a post-doctoral researcher with Dr. Stein, with the fish population model. Dr. Granata was be responsible for the hydrodynamic, and sediment transport submodules, plus coordinated all aspects of the global model.

Development of the conceptual model

To understand the mechanism of physical and biological parameters influencing walleye habitat and population, we process a thorough literature review. Based on the previous study on the life history of river-spawning walleye, we determined all the functional relationships and developed a conceptual model to specify the relationships between hydrological condition and walleye spawning, egg survival, and larval walleye drifting mortality. Historical data sources are summarized as shown in the Table 1.

Development of the mathematical model

Adult walleye natural mortality

The instantaneous mortality is:

$$InsMortality = \exp\left(\frac{\ln(AnnualMortality) \times dt}{T}\right) \quad (1)$$

T is one year, dt is one day, and the annual mortality rate is 0.505 year⁻¹ (ODNR data report, 1998-2000).

Walleye spawning

Walleye is assumed to spawn when temperature is between 3.3°C and 11°C, and egg density is smaller than the maximum egg density, 5000/m² (Jaworska, 1997, Paragamian, 1989). The habitat suitability is evaluated by the habitat suitability index (HSI), which is calculated using Leclerc's model (1996).

$$HSI = (I_V \times I_D \times I_S)^{\frac{1}{3}} \quad (2)$$

I_V is velocity preference index; I_D is depth preference index; and I_S is substrate preference index. I_V and I_D are functions of velocity and depth respectively. The best conditions for spawning are at depths from 0.6 to 1.2m (Geiling et al. 1996) and velocity is between 0.4 and 1.0 m/s. The I_V , I_D , and I_S curves are shown in Figures 2 to 4. Based on the velocity, depth and substrate preference indices, spawning habitat suitability is linked to hydrological conditions as function of time. In this way, stability is predictable based on the changing rate of HSI. Consequently, habitat suitability is a dynamic parameter.

Egg Production

Jensen's model (1992) is applied to simulate egg deposition (E). However as a result of insufficient data on river-spawning walleye length and weigh distribution, average values are used.

$$E = H \times \prod_{x=4}^8 P \times N(x) \times W(x) \quad (3)$$

H = 74 eggs / gram of female walleye

P = 0.5, sex ratio of female walleye in the whole walleye population

N (x): number of walleye at age x

W (x): mean weight of walleye at age x

It was assumed that walleye spawning in the Sandusky have the same age and weight distribution as those of spawning walleye in the Lake Erie. Walleye were taken as mature at an age of 3 year and spawn to the oldest age of 8 years. The average weight of all mature walleye was about 882g/female walleye (ODNR report 1998-2000).

The maximum egg density in saturated spawning ground depends on the substrate size. In general, walleye prefer gravel and cobble where the maximum egg density is 6421 eggs/m² (Corbett 1986), but Jones's report recommended the average value of 4325 eggs/m² (Jones, 1998). An average maximum egg density of 5000 eggs/m² was assumed in this model.

Egg Mortality and Hatching

It is well known that egg survival is function of water velocity, dissolved oxygen, and water temperature and warming rate (Roseman, et al 1996, Peterman, 1987, Auer, 1990,

Jaworska et. al, 1997). Because of a lack of data for river walleye, it was assumed that eggs either are hatched or die. The natural hatching rate is a function of water temperature (Jones 1998, Hartman, 1973), simulated by

$$HatchingRate = \frac{-5.481 + 1.062 \times T}{100} \quad (4)$$

where T is daily averaged water temperature (°C)

If dissolved oxygen is less than 6 mg/l, or velocity is greater than 0.3 m/s, or the warming rate is less than 1°C/day (Lit Review), the mortality is randomly selected from 0.5 to 1.0. Or else, the mortality is equal to 100% - hatching rate.

Larvae Mortality

Larval walleye mortality is 0.2/day (Jaworska et. al, 1997) for a pH < 9.8. In the Sandusky River, no pH higher than 9.0 has been reported (USGS data), therefore pH and ammonia probably do not affect walleye mortality.

Another component of larval mortality is larva drift since the greater the distance between the spawning ground and the Lake, the higher mortality. If river velocity is less than 0.3 m/s, transport is slow compared with the period of yolk absorption, which causes fry die. While if velocity is greater than 0.3 m/s, walleye survival is lower than less velocity (Mion et al, 1998). Krise and Meade (1986) use degree-days (DD) to measure the period of larval drift. They hypothesized a result of increased metabolism that yolk was completely consumed when larvae accumulated 100 to 128 DD. Combined advective transport, DD and drifting mortality of an individual larva give three possible outcomes. If the accumulated DD are greater than 128, larvae absorbed all the yolk before reaching the Lake, and survival rate is greatly reduced. Zero survival rate is used in the model. If the accumulated DD are less than 100, survival rate is randomly selected from 0 to 0.7 (Jones, 1998). If the accumulated DD are between 100 and 128, survival rate is randomly selected from 0 to 0.2.

Boundary conditions and Initial conditions

Upper boundary is set at the Sandusky River at the city of Tiffin, and the downstream boundary is at the Sandusky Bay where the Sandusky River enters the Lake Erie. Daily water discharge data at Tiffin, and daily water level data at the Sandusky Bay are needed for running the hydrodynamic model. Daily water velocity and depth at the spawning grounds are output from the hydrodynamic model. Water quality data including water temperature, DO, pH, and ammonia at Tiffin and the Sandusky Bay are essential for the advection-dispersion module providing daily water quality over the spawning grounds.

Due to insufficient water quality data at Tiffin boundary, water temperature and DO data at Fremont are assigned to the site of Sandusky River at Tiffin. The reason is that the Sandusky River at Tiffin and Fremont have very similar situation: they both have a dam

right upstream, so warm water effect from dam is the same. All the parameters and variables from adult spawning to larval drifting simulated in the fish model programmed with STELLA 5.0 software.

Hydraulic river model

The basic model, the hydrodynamic (HD) module, implicitly solves a finite difference scheme of integrated equations for the conservation of continuity and momentum, i.e. the Saint Venant equations:

$$\frac{\partial Q}{\partial t} + \frac{\partial}{\partial x} \left(\alpha \frac{Q^2}{A} \right) + gA \frac{\partial h}{\partial x} + \frac{gQQ}{C^2 AR} \quad (5)$$

$$\frac{\partial Q}{\partial x} + \frac{\partial A}{\partial t} = q$$

for the river network, where Q is flow (m³/s), t is time, A is cross sectional area, α is the weighting factor for flow, x is downstream distance, g is the gravitational constant, h is water height, C is the wave speed, and R is the hydraulic radius. The river network was defined from USGS maps and areal photographs. The HD module was applied to the branched network that included the main channel and two side streams (Wolf Creek and Sugar Creek). The computational scheme of MIKE11 was driven by outflow from USGS stream gages at the upstream boundary and lake level at the downstream boundary, cross sections 0 m and 62328 m, respectively. Over 100 cross sections between Tiffin and Sandusky bay were uploaded from a FEMA data base of the Sandusky River and used to define area of cross sections along the network. The HD module was calibrated with hourly discharge data from 1953 to 1977 and validated with data from 1978 to 1993. The numerical scheme adapted according to the local flow conditions so that subcritical and supercritical flows were simulated. For each time interval, the fully dynamic, non-linear equations (Saint Venant) for channel flow were solved between grid points for the boundary conditions. The HD module's advanced computational formulations permitted flow for weirs, culverts, and dam structures to be simulated. Errors in water levels were small (< 10%) when compared to FEMA HEC-RAS simulated output.

Advection-Dispersion, Water Quality and Sediment Transport Modules

Transport of water quality variables and non-cohesive sediments was done with the advection-dispersion (AD) module, the water quality (WQ) module and the sediment transport (ST) module (for erosion and deposition terms). An advection-dispersion equation was solved using an implicit finite difference scheme with negligible numerical

dispersion of mass for dissolved and particulate materials; thus concentration profiles with very steep fronts can be simulated accurately. The module required spatial and temporal output from the hydrodynamic module for discharge and water level, cross-sectional area and hydraulic radius. The non-cohesive sediment transport module was used to verify morphological conditions in the river using the Engelund-Hansen method (Mike11 reference manual, 1997). Sediment was classified by average particle size and standard deviation of the grain size distribution. Calculations were done in the morphological mode with feedback to sediment continuity and bed resistance. Outputs were sediment transport rates and bed level changes. The water quality module, developed by the Danish Water Quality Institute (VRI) was coupled to the transport advection-diffusion module to simulate the reaction processes of pH, BOD, DO, NH_4^+ and bacteria. This also described the BOD-DO relationship, nitrification, the influence from bottom vegetation, sedimentation and resuspension, and oxygen consumption from reduced chemicals. The mass balances were calculated for all grid points at all time steps using a rational extrapolation method in an integrated two-step procedure. Advection-dispersion module, declaring water quality components and their initial conditions and the boundary conditions, was run for the spatial distribution using time series of water quality parameters from 1984 to 1993. Based on the conceptual model, dissolved oxygen, water temperature, pH, and unionized ammonia nitrogen were considered as AD model components. The boundary conditions were all the time series of concentrations at the upstream and downstream boundaries (i.e. chainages 0 m and 62328 m).

The one-dimensional advection-dispersion equation was used with the following assumptions: the considered substance is completely mixed over the cross section; substances are conservative or subject to a first order reaction (linear decay); and Fick's diffusion law applies, i.e. the dispersion transport is proportional to the concentration gradient (Mike 11 user reference manual). The AD equation is:

$$\frac{AC}{t} + \frac{QC}{x} - \frac{AD}{x} \left(AD \frac{C}{x} \right) = -AKC + C_2 \times q \quad (6)$$

C = concentration (arbitrary unit)

D = dispersion coefficient (m^2/s)

A = cross-sectional area (m^2)

K = linear decay coefficient (s^{-1})

C_2 = source/sink concentration

q = lateral inflow

x = space coordinate (m)

t = time coordinate (t)

Boundary conditions

The open transport boundary was at the upstream and close boundary at the down stream. The boundary concentration calculated at open transport boundaries was multiplied with the calculated boundary concentration and added to the AD equation in the first grid point. The calculation is based on the equation (8):

$$C = C_{bf} + (C_{out} - C_{bf})e^{-t_{mix}K_{mix}} \quad (7)$$

C = calculated concentration

C_{bf} = the boundary concentration at the boundary immediately before the flow direction changed.

C_{out} = the concentration at the boundary immediately before the flow direction changed.

K_{mix} = a time scale specified in the input, hr⁻¹

t_{mix} = the time since the flow direction changed

Close boundary is calculated by C/ x = 0;

Initial condition and modeling coefficients setting

Mike 11 used equation 8 to calculate Dispersion coefficient (D):

$$D = aV^b \quad (8)$$

where a is the dispersion factor, b is the dispersion exponent, and V is mean velocity.

Fisher (1979) estimated the dispersion coefficient as a function of mean velocity, riverbank width, water depth, and shear velocity.

$$D = \frac{0.011u^2W^2}{du^*} \quad (9)$$

u is cross section mean velocity, W is width of open channel flow, d is depth and u* is shear velocity at a channel bottom. He concluded the experimental value of D/(du*) ranged from 140 to 500. du* = D/(140~500), so D = (0.011(140~500))^{1/2} Wu = (1.24 ~ 2.345) Wu. For an average value we get D = 1.7925 u×W. Mean channel width of the Sandusky River is 59m (USGS data), D = C × u, so C = 1.7625*59 = 104.

Model runs spanned March 1, 1984 to September 30, 1993. The initial value of each component was set according to the value on March 1st. Time series of water quality and quantity components output from the four modules were input into the fish model to simulate the responses of egg deposition and larvae survival.

Principal Findings and Significance

Results

Scenario One - Before Dam Removal

The number of adult migrating into the river is assumed to be 5% of the total walleye in the Lake Erie. It was assumed the migration period is 40 days, and the number of

migrating walleye each day is constant. Table 3 shows the abundance of walleye in the Lake Erie, and Table 4 the estimated number of migrating walleye from 1984-1993.

Habitat Characteristics

Habitat suitability of a spawning site varied with water velocity, depth, temperature, and egg density. Since all of these variables change with time, the habitat suitability index (HSI) is also dynamic. Time series of HSI from 1984-1993 show that the habitat suitability index varied for each year (Figure 5). In 1991, 1990, 1989, 1992, and 1987, the habitat suitability indices were higher than in the other years. The percentage of spawning calculated each year (Figure 6) and the percent of adult walleye spawned in 1987, 1988, 1991 and 1984 were higher than in other years. Comparing Figure 6 and Figure 7, the most suitable spawning situation and the greatest percentage of spawning adult walleye do not coincide, but both the habitat suitability index and percentage of spawning were greatest in 1987, 1988, and 1991.

Averages of I_v , I_d , and I_s , calculated each year (Figure 7), do not discriminate which of the parameters is more critical to the value of habitat suitability index. The substrate index (I_s) accounted for almost 1/3 of the HSI, suggesting it is possible to improve spawning habitat suitability by restoring gravel, cobble and pebble on spawning ground. It should be noted that these coarse substrates would increase the bed resistance, decreasing the velocity, increasing the depth and positively affecting spawning through I_v and I_s .

Spawning Adults

As shown in the Figure 8, the period of spawning varies from 2 to 12 days for 1984-1993. There is not direct relationship between days of spawning with larval walleye population, that is the longer spawning period does not mean greater larval walleye population. In fact, longer spawning period results in more adult walleye spawn successfully (See Figures 6 and 9). The larval walleye population was controlled by not only the habitat suitability, but also by the water temperature and egg density. When the egg density was less than the maximum, the spawning habitat was not saturated and so available for walleye to spawn. In this case the longer the unsaturated period the more eggs were deposited. Both optimal water temperatures and increased spawning area positively affected the absolute numbers of larval walleye.

Scenario 2 Completely remove the dam

Removal of the dam caused the downstream spawning habitat to be destroyed by the deposition of sediment behind the dam (Figure 10); however connectivity was restored so additional upstream habitat was available to walleye. The total area of potential spawning habitat is 654.3 thousand m^2 , which is 9 times greater than the downstream

area. Figure 11 shows the estimated number of larval walleye before and after dam removal. In most years, the latter scenario had a 58-fold increase in the number of larvae drifting back to the lake. In 1984 and 1987 walleye numbers were less than in the dam simulation. The reason could be a simulation error, since some of the parameter values were stochastically selected

Sensitivity Analysis

Uncertainty of this model is from three major sources. First, the number of adult walleye migrating into the Sandusky River is unknown. Secondly, the number of eggs produced per gram female walleye (H), and the weight of mature walleye (W) are based on averaged values, so they are imprecise. Third, the maximum egg density is also set up with an average value. So, it is necessary to process sensitivity analysis to determine the error bound of the model.

The number of adult walleye migrating (Adult-In)

The daily Adult-In parameter is the number of adult walleye migrating into the Sandusky River, and it is assumed to be equal for each day, if fact, the number depends on water temperature. In April and May, more adult migration occurs than in March and June. To investigate the change of the number of larval walleye resulted from the number of migrating adult walleye; it is assumed that the number of migrating walleye had normal distribution.

As shown in the Figure 12, the change in the amount of larval walleye produced and drifting back to the Lake varies from year to year, and the most variation occurs in 1992, which has 8 times fold increase compared with the constant adult walleye migration situation. In 1987, the larval walleye production with normal distributed number of adult walleye migration is only 20% of the situation with constant adult walleye migration each day. Consequently, the number of adult walleye migrating into the river in each day is a critical parameter for the model simulation.

Average Weight of adult walleye and Fecundity (W and H)

Weight of mature female walleye in the Lake Erie spans from 770g to 1292g (ODNR report), and the average value, 882, is used in this model. The number of eggs produced by each gram fish is believed to be 74/g (Jenson, 1992). But, the ODNR reported the fecundity ranges from 61.3 /g to 82.69 /g fish in the Lake Erie.

To test the effect of H and W on the larval walleye population, run the model under parameter setting of 61.3/g for H, and 770 g for W. While another situation is H is 82.69/g and W is 1292g. As seen in the Figure 13, the number of larval walleye fluctuates at most 50%. So, the value of H and W does not affect the production of larval walleye seriously.

Maximum egg density

In the model, maximum egg density is set to be 4800/m². Jones (1998) summarized the maximum egg density on cobble and gravel is about 4325, while Corbett (1986) reported the observed value of maximum egg density is about 6421 eggs /m². Run the sensitivity analysis with maximum egg density of 4325 and 6421 respectively. The results (Figure 14) show that larval walleye production varies at most 96.6%.

References

Auer, Martin T. and Auer, Nancy A., Chemical suitability of substrates for walleye egg development in the lower Fox river, Wisconsin, Transactions of the American Fisheries Society, 119: 871-876, 1990

Born, S.M., K.D. Genskow, T.L. Filbert, N. Hernandez-Mora, M. Keefer, K.A. White 1998. Socioeconomic and institutional dimensions of dam removal: the Wisconsin experience. Environ. Manag., 33: 359-370.

Columbus Dispatch 1999. Dam removal spawns return of the salmon. *Columbus Dispatch*, November 6, 1999.

Corbett, B. W., and Powles, P. M., 1986, Spawning and larva drift of sumpatric walleyes and white suckers in an Ontario stream, Trans. Am. Fish. Soc. 115:41-46

Ebersole, J.L., W.J. Liss, and C.A. Frissell 1998. Forum: Restoration of stream habitats in the Western United States. Restoration as reexpression of habitat capacity. Env. Manag., 21: 1-14.

Fischer H., E.J. List, R.C.Y. Koh, J. Imberger, and N.H. Brooks. 1979. Mixing in Inland and Coastal Waters. Academic Press, NY, pp. 483.

Geiling, W.D. et al., Benefits from incremental additions to walleye spawning habitat in the Curent River, with reference to habitat modification as a walleye management tool on Ontario, Can J. Fish. Aquat. Sci. 53 (suppl.1): 79-87, 1996

Krise, W. F. and Meade, J. W., Review of intensive culture of walleye fry, Progressive Fish Culturist, 48: 81-89

Liaw, W.K., Habitat suitability criteria for walleye spawning and egg incubation in Saskatchewan, Fisheries Technical Report 91-1, 1991

Lorenz, C.M., G.M. Van Dijk, A.G.M. Van Hattum, and W.P. Cofino 1997. Concepts in river ecology: implications for indicator development. *Reg. Rivers: Res. and Manag.*, 13: 501-516.

Jaworska, Joanna S., Rose, Kenneth A., and Barnhouse, W., General response patterns of fish populations to stress: an evaluation using an individual-based simulation model, *Journal of Aquatic Ecosystem Stress and Recovery*, 6: 15-31, 1997

Jensen, A.L., Relation between mortality of young walleye (*Stizostedion vitreum*) and recruitment with different forms of compensation, *Environmental pollution* 76 (1992) 177-181

Jones, M. L., et al., Linking habitat supply to fish community objectives using a population dynamics approach, Annual Progress Report to Great Lake Fishery Commission, 1998

Mike11 Reference Manual, 1997. General Reference Manual, version 3.2. First Edition. The Danish Hydraulic Institute.

Mion, J. B., et al., River discharge drives survival of larval walleye, *Ecological Applications*, 8 (1), 88-103, 1998

NOAA Coastal Ocean Program 1995. *Watershed Restoration: A Guide for Citizen Involvement in California*. Decision Analysis Series No.8. National Oceanic and Atmospheric Administration, Coastal Ocean Office, Silver Springs, MD. 114 pp.

Nuttle, W. 1999. Ecosystem restoration a challenge for unified hydrologic science. *EOS* 80(40): 469.

Ohio Department of Natural Resources, Report of the Lake Erie walleye task group, 1998

Ohio Department of Natural Resources, Ohio's Lake Erie Fisheries, 1998

Ohio Department of Natural Resources, Ohio's Lake Erie Fisheries, 1999

Paragamian, Vaughn L. Seasonal habitat use by walleye in a warmwater river system, as determined by radiotelemetry, *North American Journal of Fisheries Management*, vol, 9: 392-401, 1989.

Peterman, R. M. and Bradford, M. J., Statistical power of trends in fish abundance, Can. J. Fish. Aquat. Sci. Vol., 44: 1879-1899, 1987

Roseman, E. F. et al, Walleye egg deposition and survival on reefs in Western lake Erie (USA), Ann. Zool. Fennici 33: 341-351, November 1996

Table 1. Data Sources for models

Data Type	Year	Location	Source
Water Level, Discharge	1976-1995	Tiffin to Sandusky Bay	USGS
Water Temperature, pH, DO	1966-1980	Below Fremont	USGS
Water Temperature	1967-1980	Near Fremont	MSU
Water Temperature, pH	1999-2001	At Tiffin	Tiffin city

Table 2. Abundance of walleye in Lake Erie, 1983-1992.

Year	1983	1984	1985	1986	1987	1988	1989	1990	1991	1992
Walleye (Millions)	37.2	149.2	115.6	117.4	117.8	159.7	129.0	107.5	83.7	82.3

Table 3. Estimated abundance of walleye migrating to the Sandusky River, 1984-1993.

Year	1984	1985	1986	1987	1988	1989	1990	1991	1992	1993
Walleye (Thousands)	46.5	186.5	144.5	146.8	147.3	199.6	161.3	134.4	104.6	102.9

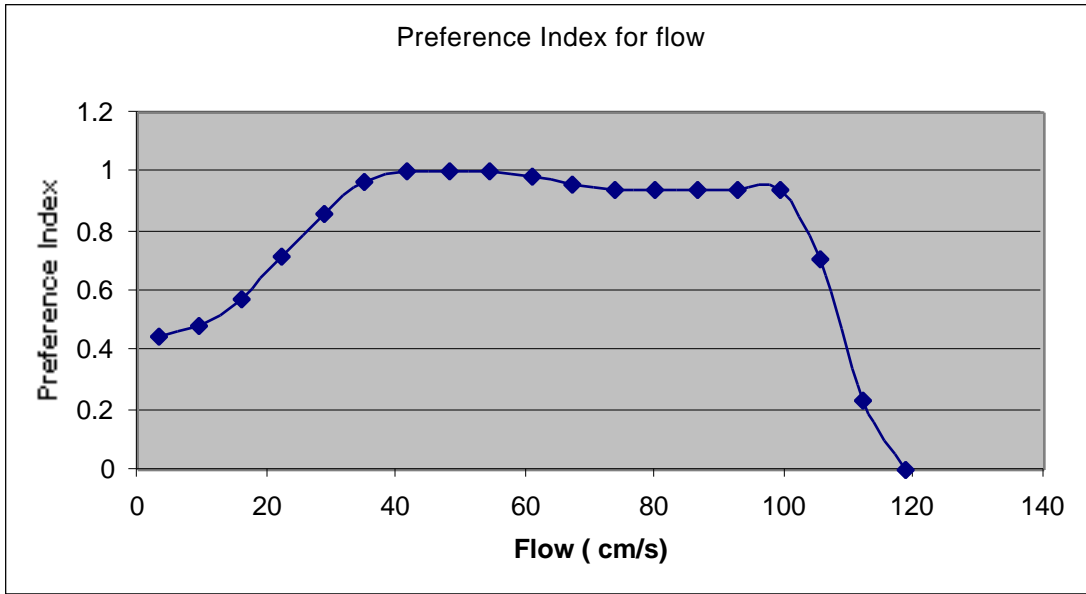


Figure 1. Velocity Preference Index, I_v .

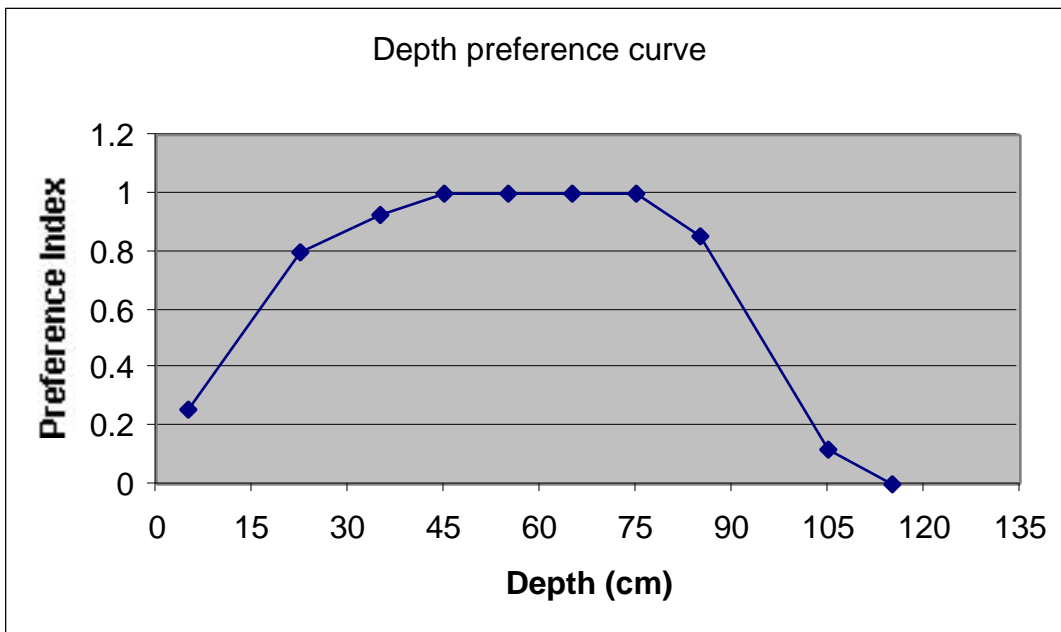


Figure 2. Depth Preference Index, I_D .

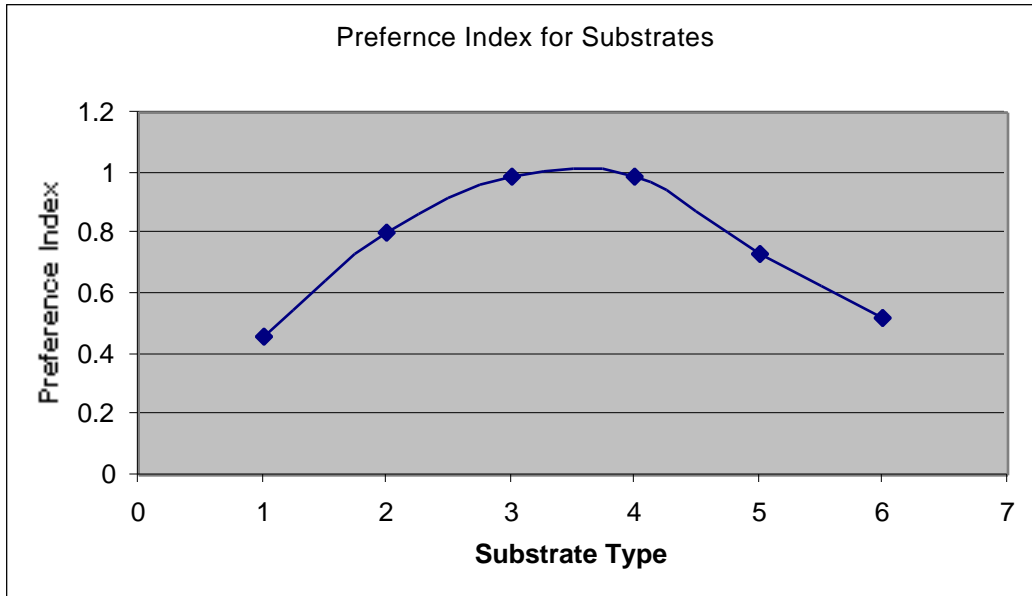


Figure 3. Preference Index for substrates, I_s , for spawning grounds.

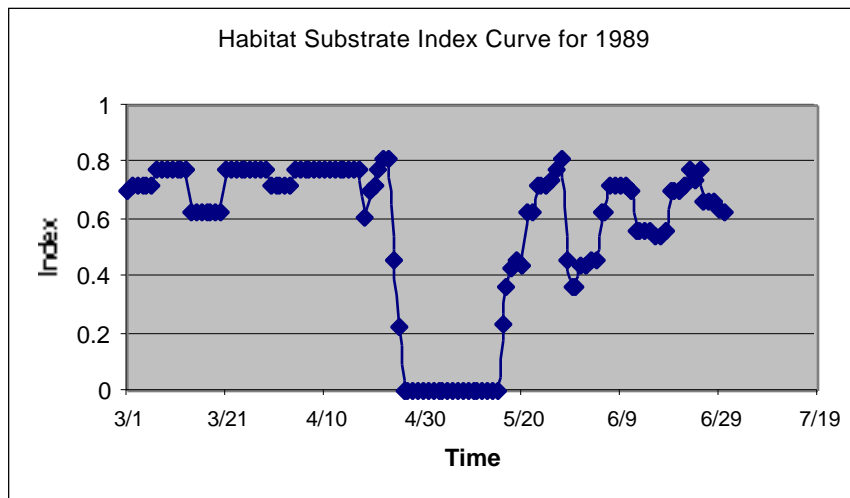


Figure 4. Habitat Suitability Index for the 1989 simulation before dam removal. 1: Sand; 2: Gravel, 3: Pebble, 4: Cobble, 5: Boulder, 6: bedrock.

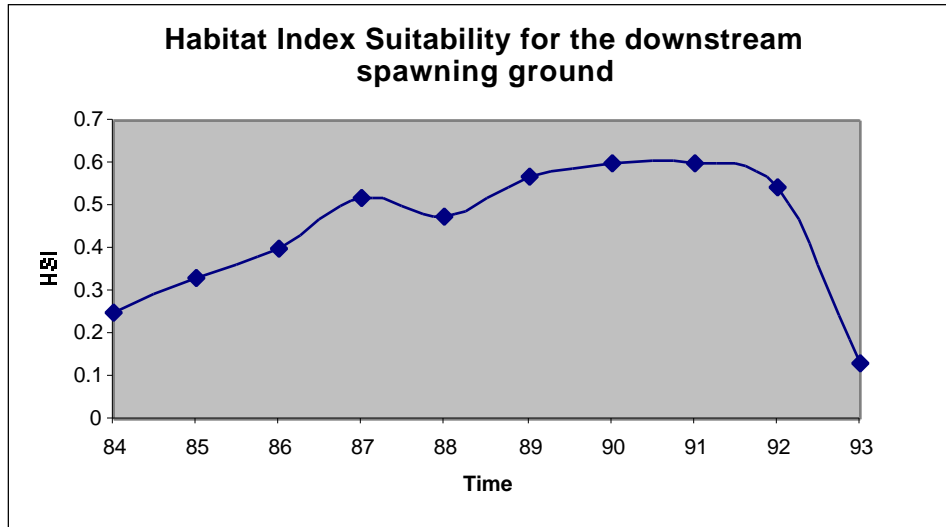


Figure 5. Downstream Habitat Suitability Index (HSI) for 1984 – 1993.

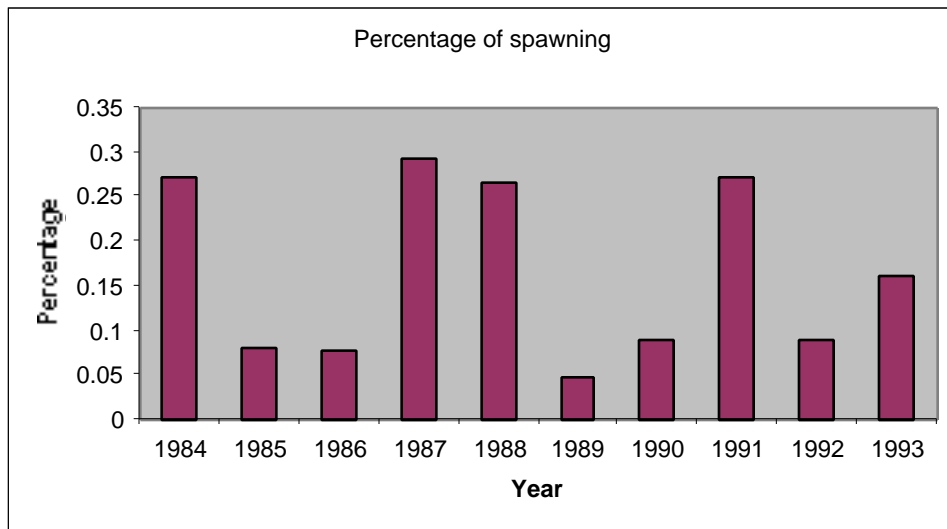


Figure 6. Percentage of spawning for 1984-1993.

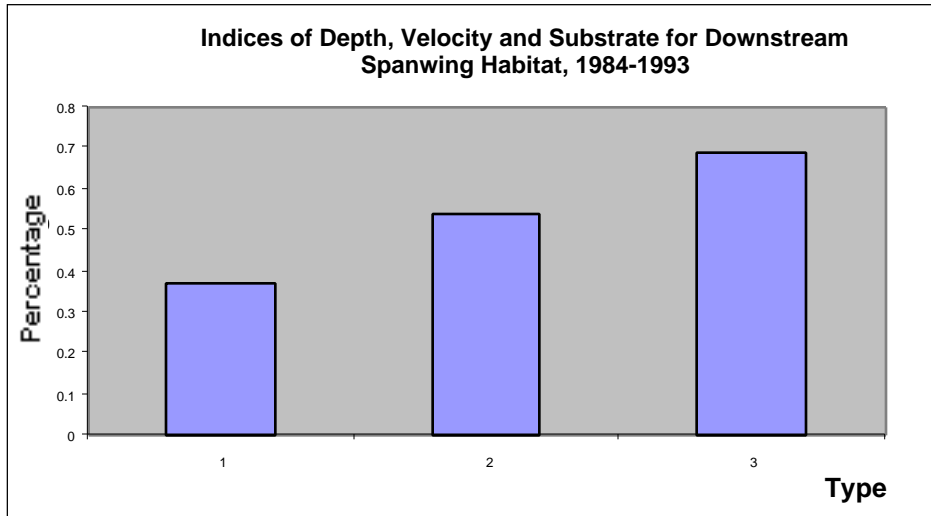


Figure 7. Relative contribution of: 1) I_D ; 2) I_S ; and 3) I_V where 1 = Index for Depth, 2 = Index for Substrate, and 3 = Index for Velocity

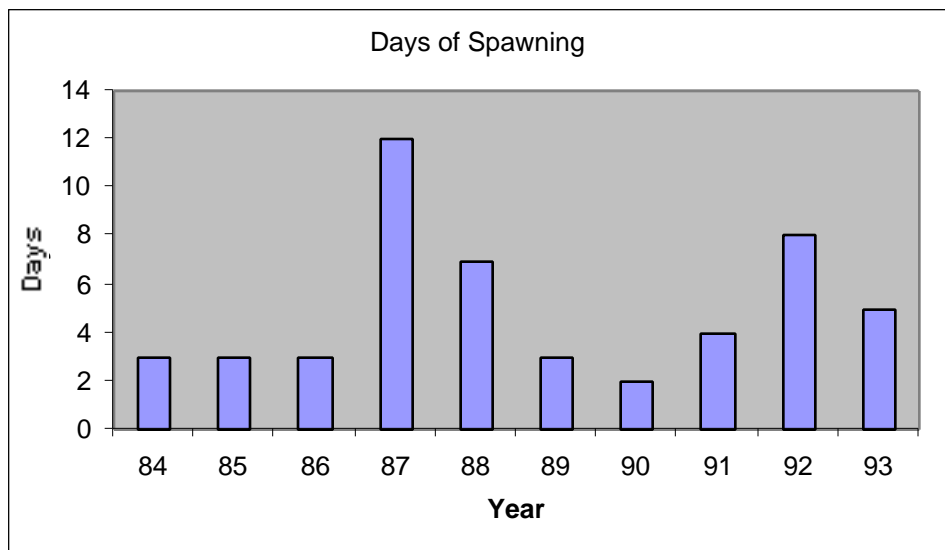


Figure 8. Distribution of spawning days for 1984-1993.

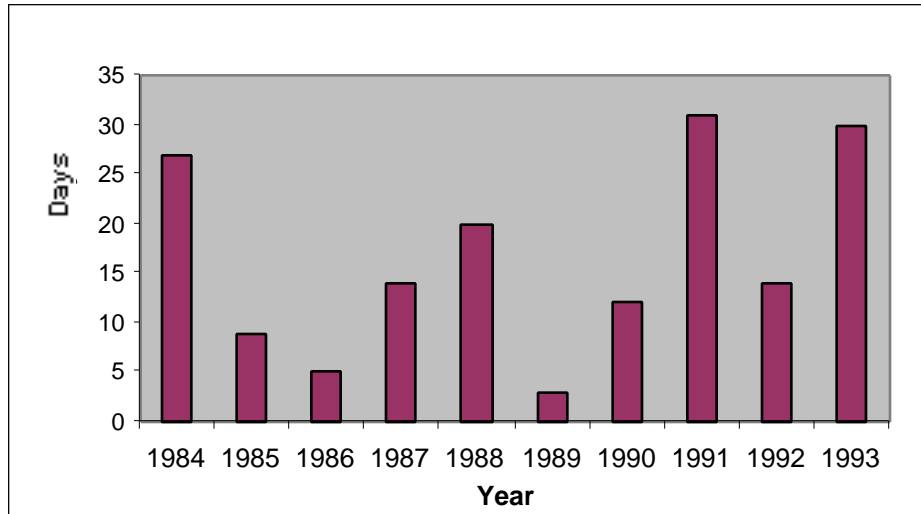


Figure 9. Period with egg density less than the maximum for before dam removal, 1984-1993

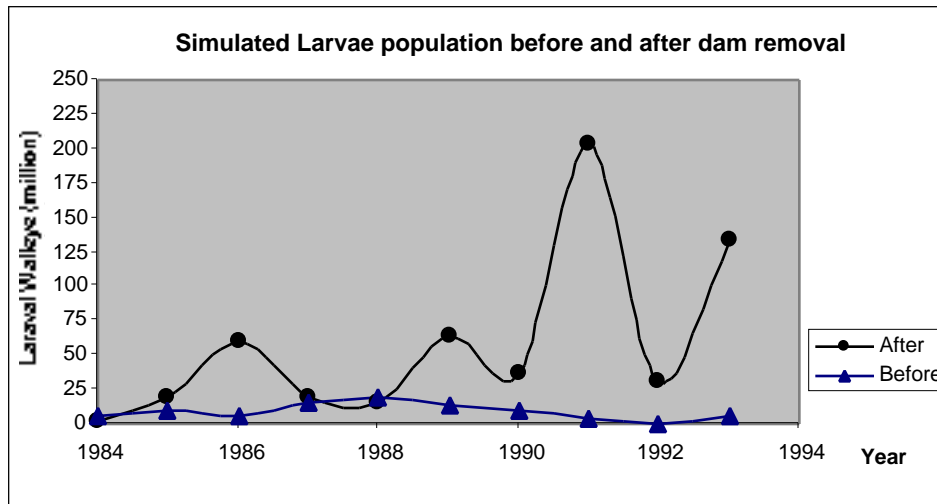


Figure 11. Simulated larval walleye population before and after dam removal for 1984-1993

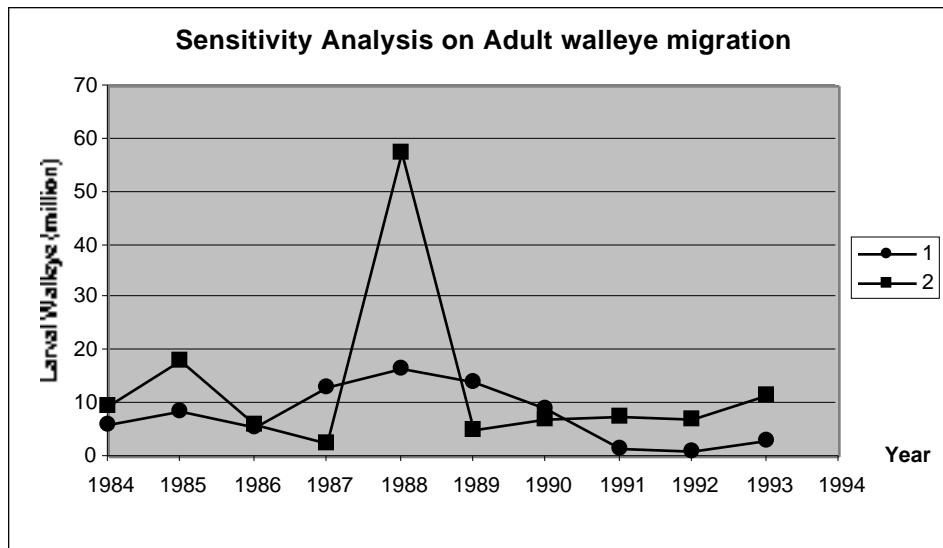


Figure 12. Sensitivity Analysis on Adult Walleye Migration for: 1 = a constant number of adult walleye migrating each day and 2) a normally distributed number fish migrating each season.

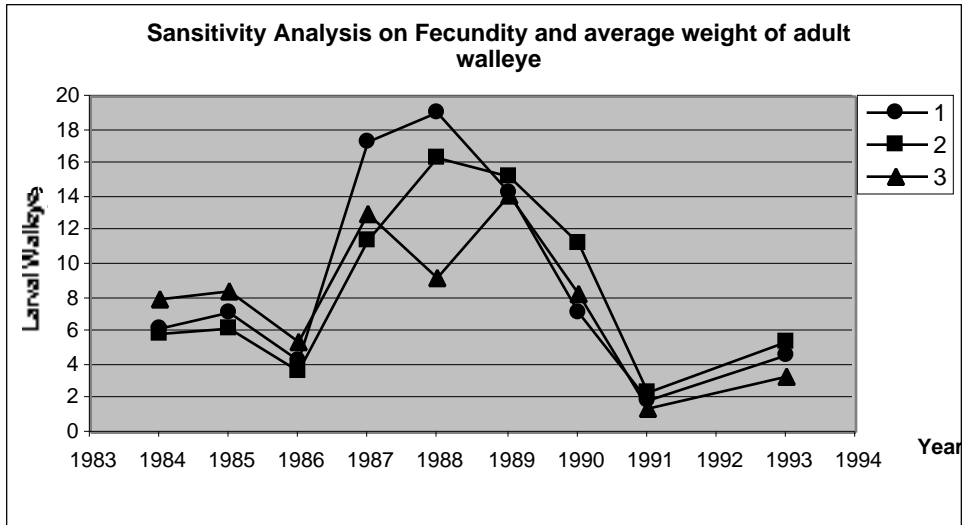


Figure 13. Sensitivity Analysis for Fecundity and Average Weight of Adult Walleye. 1: H = 770g, W = 61.3/g; 2: H = 882g, W = 74/g; 3: H = 1292g, W = 82.69/g;

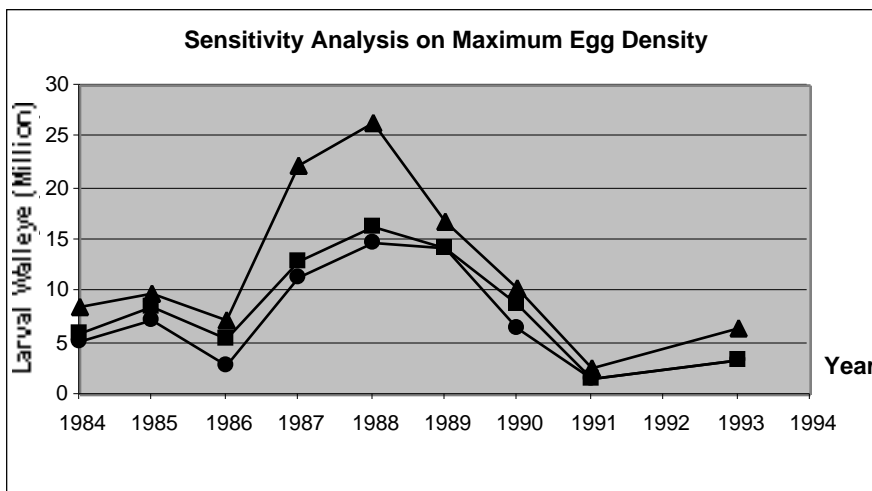


Figure 14. Sensitivity Analysis on Maximum Egg Density. Legend the same as Figure 14.

Significance

Dam removal is currently one of the major interests in river restoration in the U.S., so the model should be valuable to many coastal watersheds nationwide. In Ohio this work is of interest to the Ohio Department of Natural Resources, Wildlife Division who can use simulation as a way project the effects of and to promote dam removal. The results of this study have stimulated new collaborations in watershed modeling. In one recent proposal to Sea Grant we will add a GIS module to cover the entire watershed and will work with other researchers to add Lake habitat and an landscape change modules. In another effort will expand the model to predict floods and graded sediment distributions will a economist's model of wildlife and recreational river value.

Basic Information

Title:	Sonochemical Remediation of Polychlorinated Biphenyl Contaminated Sediments
Project Number:	G-05
Start Date:	9/1/1998
End Date:	12/31/2000
Research Category:	Water Quality
Focus Category:	Toxic Substances, Sediments, Treatment
Descriptors:	Contaminated Sediment, Remediation, Surface Water Quality, Oxidation, Toxic Substances
Lead Institute:	Ohio State University
Principal Investigators:	Linda K. Weavers, Yu-Ping Chin

Publication

1. Lu, Yifang and Linda K. Weavers, 2001, "Sonochemical Desorption and Destruction of 4-Chlorobiphenyl from Synthetic Sediments," submitted to Environmental Science and Technology. (submitted 2/7/01)
2. Lu, Yifang and Linda K. Weavers, 2000, "Sonochemical Remediation of PCB Contaminated Sediments," in 220th National Meeting of the American Chemical Society, Division of Environmental Chemistry, Washington, DC, p. 678-681.
3. Lu, Yifang, 2000, "Sonochemical Desorption and Destruction of 4-Chlorobiphenyl from Synthetic Sediments," M.S. Thesis, The Ohio State University, College of Engineering, Department of Civil and Environmental Engineering and Geodetic Science, Columbus, Ohio, 83 p.
4. Chang, Shuh-Kuen, Y. Lu, and L. K. Weavers, 2001, "The role of humic acid in the combined sonochemical desorption and transformation of contaminants from sediments." in The Second Annual Symposium on Natural Organic Matter in Soils and Water, North Central Region, Columbus, OH.

FINAL REPORT

PROJECT NUMBER: G-05

Start: 9/1/98

End: 12/31/00

TITLE: Sonochemical Remediation of PCB Contaminated Sediments

INVESTIGATORS:

Lead P.I.: Linda K. Weavers, The Ohio State University

Co-Investigator: Yu-Ping Chin, The Ohio State University

FUNDING: FEDERAL: \$66,431 **NON-FEDERAL:** \$137,322

CONGRESSIONAL DISTRICT: Fifteenth

FOCUS CATEGORIES: TRT, SED, TS

DESCRIPTORS: Contaminated Sediment, Remediation, Surface Water Quality, Oxidation, Toxic Substances

PROBLEM AND RESEARCH OBJECTIVES:

In December 1997, EPA released the report, "The Incidence and Severity of Sediment Contamination in Surface Waters of the United States" documenting the severity of sediment contamination. Of the 96 Areas of Probable Concern, 39 are located within nine states in the North Central Region, many contaminated with polychlorinated biphenyls (PCBs) (US EPA, 1997b). For example, the Ottawa River in Ohio has a fish consumption advisory in effect due to PCB levels more than 30 times the USFDA health standard for fish filets. Moreover, the EPA estimates that in the United States approximately 10% of the sediment underlying surface waters is sufficiently contaminated to pose risks to fish, humans, and wildlife (Bolattino and Tuchman, 1993). It is difficult to treat sediments or soils because the sorbed hydrophobic contaminants are less accessible. Currently, capping the sediments in place or extraction and removal to a hazardous waste landfill is the most common method of treatment. However, the contaminants are not destroyed and pose a potential future risk. Moreover, episodic events such as storms and ships may compromise the capping material (by re-suspension) which could potentially mobilize the contaminants.

One of the EPA's four goals for managing contaminated sediment is to better understand the fundamental processes involving contaminated sediment and to develop solutions (US EPA, 1998). Ultrasonic irradiation of contaminated sediments may provide an on-site treatment technology that removes the contaminant from the sediment and subsequently destroys the contaminant through sonochemical oxidation. Research into the fundamental factors affecting sonochemical remediation of contaminated sediments will increase the understanding of this potential treatment process as well as lend insight into the factors affecting desorption of contaminants from sediments.

The development of this treatment technology will provide an alternate solution to existing sediment remediation technologies. Existing treatment technologies such as capping have the limitation that the pollutants are not destroyed and pose a future risk. Incineration is also used, but is prohibitively expensive and labor intensive. Conversely, sonication of sediments can be performed on a ship, does not require dewatering, and since sonication destroys

the contaminants, the sediments can be replaced after treatment. The proposed process is potentially more energy efficient and environmentally benign than conventional sediment remediation technologies.

The purpose of this project is to investigate the application of ultrasound to sediment polluted with PCBs. PCBs are an EPA priority pollutant and persist in the environment due to their unreactive nature. They are extremely hydrophobic and tend to partition from the aqueous phase to the gas or solid phase. Ultrasound applied to polluted sediment is a two-step process. First, the physical effects of acoustic cavitation have the potential to clean the sediment surface by the jets of imploding cavitation bubbles impinging on the particles and shear forces from microstreaming near the particle surface. Then, the PCBs will preferentially partition to the cavitation bubble (due to its high octanol/water partitioning coefficient ($\log K_{ow} > 5$) and high Henry's Law constant ($H \sim 50 \text{ Pa m}^3 \text{ mol}^{-1}$)) where they will be destroyed by pyrolysis or oxidation with $\text{OH}\cdot$ radical. In this proposed remediation process, the sediment does not need to be dewatered and dried for remediation. Also, this process is transportable and has the potential to be used on a ship as dredging occurs.

Specifically, the *goals of this research were:*

- 1) *to demonstrate the ability of sonication to remove PCB from synthetic and natural sediments;*
- 2) *to show that sonochemical techniques destroy the PCB once it enters the soluble phase;*
- 3) *to characterize the role of sediment matrix parameters in sonochemical remediation; and*
- 4) *to identify key design variables in the sonochemical remediation of contaminated sediments.*

METHODOLOGY:

In this study, 4-chlorobiphenyl (4-CB) was used as a model PCB. 4-CB was purchased from Chem Service and was used without further purification. A 4-CB standard (100 mg l^{-1}) was purchased from Ultra-Scientific. Three kinds of silica particles (diameters $2 \mu\text{m}$, $60 \mu\text{m}$ and $130 \mu\text{m}$) were purchased from Fisher Scientific. Two Alumina particles (diameter $130 \mu\text{m}$) with surface areas, SA_0 , of 200 and $155 \text{ m}^2 \text{ g}^{-1}$ were purchased from Sigma-Aldrich. The median diameters of these particles were determined from manufacturer specification and confirmed in our laboratory using a Malvern Mastersizer particle size analyzer. Water used was treated in a Millipore system ($R = 18.2 \text{ M}\Omega\text{-cm}$). All solutions were initially adjusted to pH 6 and $I = 0.001 \text{ M}$ with HClO_4 and KClO_4 . Humic acid, obtained from Aldrich (Milwaukee, WI), was purified according to Onken and Traina (15). All other reagents were of highest purity available and used as received.

Quantitative analysis of 4-CB was determined with a Hewlett-Packard 6890 gas chromatograph equipped with an electron capture detector (GC-ECD). A HP-5 column ($30\text{m} \times 320 \mu\text{m} \times 0.25 \mu\text{m}$, Hewlett-Packard) was used to quantify 4-CB. In homogeneous solution experiments, a sample of 5.0 ml was extracted with 2 ml hexane. In heterogeneous experiments, a large volume of sample (20 or 25 ml) was taken. However, an extraction ratio of 2:5 between hexane and sample was maintained.

An ultrasonic probe system (Sonic Dismembrator 550, Fisher Scientific) operating at 20 kHz, was used for ultrasonic irradiation experiments. Calorimetry, the temperature increase in an insulated vessel (typically the reactor vessel without cooling water), used to measure the energy input into the reactor was $460 \text{ W l}^{-1} \pm 5\%$. An air saturated sample solution of 25 ml was sonicated in a glass rosette reactor and experiments were conducted in a closed system with minimal headspace using a Teflon collar to connect the neck of the glass reactor to the probe. The probe tip was located near the bottom of the reactor to ensure particles were well mixed throughout the reactor. The reactor was water-jacketed and the temperature was controlled at 20

°C by a circulating constant temperature cooling bath. To minimize interactions of 4-CB with surfaces, all containers and other materials used were made of either Teflon or glass. Control experiments revealed that 4-CB did not sorb to the reaction vessel over the course of the experiments. Selected experiments were run in duplicate or triplicate to verify the reproducibility of the results; however, reported errors are determined from the error of the slope of kinetic plots.

To compare the efficiency between different ultrasonic systems, another ultrasonic system, a near-field acoustic processor (NAP, model NAP-3606-HP-TC, Advanced Sonic Processing), was used. The NAP has water-cooled magneto-strictive transducers fixed to each stainless steel parallel plate operating at 16 kHz on one plate and 20 kHz on the other. The NAP system runs in a continuous circulation mode with a mechanically mixed temperature-controlled glass vessel, double diaphragm Teflon pump, and ½" PTFE Teflon tubing connecting the components. The power density of the NAP as measured by calorimetry was 53.3 W L⁻¹.

Stock solutions of 4-CB were prepared by dissolving 4-CB in water (pH = 6 for alumina, pH = 2 for silica, I = 0.001 M) and stirring for one week in a sealed volumetric flask. The purpose of adjusting the pH was to prevent coagulation of particles and to be sure the particle size measured was the diameter of a single particle. To prepare 4-CB sorbed model sediments, aliquots of 100 ml of a 40 mg l⁻¹ HA solution (pH = 6, I = 0.001 M) were mixed with 5 g alumina particles. After continually mixing for one hour, the solution was allowed to settle. During the following day, the solution was mixed occasionally. After 2 days, the solution was centrifuged and the supernatant was analyzed using a TOC analyzer (Shimadzu TOC-5000A) then discarded. Next, sorption of 4-CB occurred by adding 4-CB stock solution to the HA laden alumina resulting in a particle concentration of 25 g l⁻¹. Sorption of 4-CB to prepared HA coated particles was performed similar to HA sorption; however, the mixing time was 7 days. Again, the solutions were centrifuged and the supernatant was discarded. Following 4-CB sorption, the HA concentration of the supernatant was measured again by TOC. HA remaining on particles was determined by mass balance to be 297 mg C kg⁻¹ (organic carbon = 0.03%). The organic carbon content is significantly lower than most sediment systems; however, we only intended to investigate desorption from one well-controlled system: 4-CB sorption into monolayer organic carbon on inorganic particles. In investigating only this system we eliminated complications such as that from particle aggregates, sorption into carbonaceous particles and heterogeneous organic matter.

4-CB sorbed to particles was determined by mixing 0.5 ml acetone and 10 ml hexane to the particles and contacting for 40 minutes. The hexane was sampled and the 4-CB concentration was quantified using GC-ECD. For sonication experiments, particles (bare, HA laden, HA and 4-CB laden or no particles) were transferred to the reactor and 25 ml of MilliQ water, 6 µM 4-CB, and/or 8.5 or 60 mg l⁻¹ HA was added. Each 25 ml sample was sonicated for a different time to generate kinetic information. After sonication, a 10 ml aliquot of solution with minimal particles was transferred to a 15 ml glass centrifuge tube, the remaining 15 ml of solution was transferred to a 45 ml glass sample vial. The 10 ml solution was centrifuged for 6 minutes at 4000 rpm. After centrifugation, 5 ml of the 10 ml supernatant was extracted with 2 ml hexane to obtain the aqueous 4-CB mass in the 5 ml sample (M_{aq}). The remaining 5 ml of sample in the 10 ml aliquot was transferred to the 45 ml sample vial containing the remaining sample. 10 mL hexane was used to extract and quantify the mass of 4-CB from the remaining 20 ml aqueous solution and particles (M_{mix}). 4-CB sorbed on particles, M_{sorb}, was obtained by:

$$M_{\text{sorb}} = (M_{\text{mix}} + M_{\text{aq}}) - M_{\text{aq}} \times 5 \quad (1)$$

This extraction method was tested in control experiments. The average error in the precision of this method was found to be approximately 5 %, with a maximum error of 8%.

PRINCIPAL FINDINGS AND SIGNIFICANCE:

Initial Controls and Experiments

Preliminary experiments and controls were conducted in the first 6 months of this project. An analytical technique to remove 4-CB from particles using hexane extractions and detection on the GC-ECD was developed. In addition, a method was developed using the Mastersizer particle sizer to investigate changing particle sizes during sonication. Proper lens cleaning and sampling and stirring protocols were developed to obtain accurate and reproducible results. Various techniques were employed to sorb 4-CB to 2, 20, and 200 g/L silica and alumina solutions. These experiments resulted in essentially no sorption of 4-CB to bare particles under our specified conditions. Significant levels of sorption of 4-CB to humic acid laden particles only occurred with 200 g/L concentrations of alumina. Furthermore, in these initial experiments, particle dispersion was problematic. In an attempt to keep particles dispersed throughout the duration of a sonication experiment, a new probe reactor was designed and has been employed for all experiments.

Sonolysis of PCB in aqueous phase.

4-Chlorobiphenyl was used as a model PCB in our study. Initially the sonication of 4-CB in distilled water was conducted to determine the efficiency of ultrasound in destroying 4-CB in aqueous solution. Figure 1 shows that the degradation of 4-CB follows first-order kinetics, with a k value of $0.120 \pm 0.009 \text{ min}^{-1}$. In addition, after 20 minutes, more than 90% of the 4-CB was destroyed. Therefore, PCB is amenable to destruction by sonication.

Sonication effect on particles.

Before studying the destruction of PCB contaminated sediments, it is necessary to know the effect of sonication on particles. Changes in the surface structure and the size of particles are expected to be important factors that will affect the mechanisms of desorption of PCB from particles into the aqueous phase as well as on degradation efficiency of PCB during sonication.

For all the particles tested, compared to only hydrodynamic mixing, sonication decreases the particle size, following a first-order kinetic regime. An increasing rate of particle size reduction was observed with increasing diameter and surface area (Table 1). In control experiments to monitor the particle size change at different pH values (silica at pH 6, alumina at pH 2), no apparent difference in the rate of size reduction was found at different pH values. It seems that rate constant of reduction (k) for bigger particles is faster than that for smaller particles for the same type of particle. For the alumina particles, the larger rate constant of particle size reduction corresponds to the particle with a larger surface area. This may be due to the more porous structure of the larger surface area particles. Also, for silica and alumina with the same initial size, the size reduction rate for silica is faster than alumina in the probe system, but opposite in NAP system. This may be caused by the different structures of the particles and different reactor configurations (*i.e.*, batch vs. continuous circulation).

Efficiencies of the two sonochemical systems were compared by normalizing k in the NAP to that of the probe based on the power density measured in the reactors as follows:

$$k_{\text{normalize}} = \frac{k_{\text{soni.}}}{PD_{\text{NAP}}} * PD_{\text{probe}} \quad (1)$$

In the above equation, k is the first-order k and PD_{NAP} and PD_{probe} are the power densities in the NAP and probe reactors, respectively.

Therefore, we can use the normalized k of NAP to compare with the k_{obs} obtained from the probe system. Using the silica particle with an initial size of 60 μm as an example, we calculate a $k_{\text{normalized}}$ in NAP as 0.177 min^{-1} which is ten times the k_{obs} (0.0176 min^{-1}) in probe system. Hence, the efficiency of the NAP is much higher than the probe. Therefore, it is better to apply a NAP in the actual treatment system. Similar results have been obtained in other studies investigating the degradation of 4-nitrophenol and surfactants (Hua *et al.*, 1996; Pee *et al.*, 2000).

The structure of the particles before, during, and after sonolysis was analyzed using scanning electron microscopy (SEM). Figures 2 and 3 show the two images of silica particles (initial diameter of 60 μm) before sonication and after 60 minutes of sonication. Compared to initial and non-sonicated particles, the surface of the particles became both smoothed and pitted as a result of sonication. In addition, we found that there are many small particles formed during sonication, likely a result from the breakup of large particles.

The dissolution of alumina and silica in the aqueous phase was measured using ICP-OES. Compared to hydrodynamic mixing only, the concentration of silicon or aluminum in aqueous solution increases with increasing sonication time. The concentration for all the particles after 60 minutes of sonication and only hydrodynamic mixing are listed in Table 2. For all the particles tested, the concentration after sonication was 6-20 times that of only mixing.

Assuming that the decrease of the particle size was due entirely to the dissolution of particle and the particles are approximately spherical, the expected aqueous silica and alumina concentrations were calculated. The calculated concentrations were thousands of times higher than the actual concentration measured from ICP-OES. Therefore, it appears that the small particles are formed dominantly from the breakup of large particles.

Based on these results, it seems that two mechanisms are occurring simultaneously: microstreaming acts to smooth particle surfaces and dissolve particles and microjets imploding on the particle surfaces both shear and pit the surface of the particles.

Effect of particles on the degradation rate of 4-CB

The degradation of 4-CB was investigated in the presence of silica and alumina particles at 2, 20, and 200 g/L. Figure 4 shows the degradation of 4-CB in the presence of various concentrations of bare alumina particles ($SA_0 = 200 \text{ m}^2 \text{ g}^{-1}$). The degradation rate constant decreased compared to the degradation rate constant of 4-CB without particles. Similar results were obtained for the degradation of 4-CB in the presence of other sizes and types of particles. The degradation rate constants for 4-CB degradation in the presence of different bare particles is shown in Table 3. In the presence of 2 g l^{-1} silica particles, the rate constant decreased with increasing particle size. In addition, increasing the silica particle concentration from 2 g l^{-1} to 20 g l^{-1} , resulted in a similar trend in that the larger particle sizes corresponded to a larger reduction in the 4-CB degradation rate constant compared to 4-CB degradation without particles present. Similar to silica particles, the presence of alumina particles resulted in a lower degradation rate than that in aqueous 4-CB solutions. However, changing the particle concentration from 2 g l^{-1} to 20 g l^{-1} did not seem to affect the degradation of 4-CB. Furthermore, the degradation rates of 4-CB for the same sized alumina particles with differing surface area were within experimental error. However, the dissolution of the particles observed in the presence of sonication does correlate with the reduction in the degradation rate constant of 4-CB. Clearly, the composition of the particles is important in their interaction with the ultrasound.

Effect of humic acid on 4-CB degradation

First, purified Aldrich humic acid with an initial concentration of 60 mg l^{-1} was sonicated and the total organic carbon was measured with time. The TOC level did not change during a 1-hour period of sonication. Although no HA was oxidized to CO_2 , HA may have been transformed to a more highly oxidized species by reaction with $\bullet\text{OH}$; however, this could not be determined with TOC analysis.

Next, the degradation of $6 \text{ }\mu\text{M}$ 4-CB in HA solutions of concentrations of 8.5 mg l^{-1} and 60 mg l^{-1} were performed. Figure 5 shows the first-order degradation of 4-CB with different HA concentrations. The existence of HA decreased the degradation efficiency of 4-CB. Furthermore, increasing the HA concentration further decreases the degradation efficiency of 4-CB. Other studies investigating the influence of dissolved organic matter on degradation by photocatalysis (Minero, *et al.*, 1999 and Wang *et al.*, 1999), Fenton's reagent (Lindsey and Tarr, 2000a and 2000b) and sonication (Taylor *et al.*, 1999) also indicated that the existence of HA decreased the degradation rate of their pollutant models. Furthermore, the decay rate constant of the model compounds decreased with increasing HA concentration. HA is a strong scavenger of OH radicals; therefore, the competition for $\bullet\text{OH}$ between HA and 4-CB will affect the destruction of 4-CB. Minero *et al.* (1999) observed a 36% and 81% reduction in phenol degradation by TiO_2 photocatalysis in the presence of 5 and 50 mg l^{-1} HA, respectively. This is significantly greater than the 20% and 49% reduction observed with 4-CB for 8.5 and 60 mg l^{-1} HA, respectively.

Desorption and destruction of 4-CB

In the final set of experiments, alumina particles with an initial particle size of $130 \text{ }\mu\text{m}$ and surface area of $200 \text{ m}^2 \text{ g}^{-1}$ were chosen as the model particles. In control experiments, 4-CB was sorbed to bare alumina particles. However, no sorption was achieved during a 12-day period. Similar results were obtained for 4-CB sorption to silica particles.

Next, HA was added to enhance the adsorption of 4-CB to sediments. As in the methods described above, initially alumina particles were coated with HA. Through quantification of TOC in the aqueous phase before and after adsorption, the final HA adsorbed on particles was 297 mg C kg^{-1} (% organic carbon = 0.03%). Sorbed 4-CB was obtained by quantifying the 4-CB concentration in aqueous solution before and after sonication and by extracting 4-CB from particles. For the sonochemical system used, if all of the sorbed fraction desorbed, the equivalent concentration of 4-CB and HA in aqueous solution would be $7.9 \text{ }\mu\text{M}$ and 60 mg l^{-1} , respectively.

The samples were sonicated and analyzed as shown in Figure 6. The 4-CB aqueous concentration remained rather low, whereas the 4-CB concentration adsorbed on particles decreased. Ninety percent of the total 4-CB was degraded after 45 minutes. Similar to 4-CB degradation in aqueous solution, the total 4-CB decreased following a first-order kinetic regime with $k = 0.051 \pm 0.003 \text{ min}^{-1}$, as shown in Figure 7.

To determine if HA was desorbed, we measured the TOC level in the aqueous phase during sonication in the absence of 4-CB. The TOC in the aqueous phase corresponding to HA remained at 8.5 mg l^{-1} during the 1-hour sonication. Thus, the TOC adsorbed on particles also remained relatively constant. Although the TOC remained constant, the color of the particles changed from brown to white with increasing sonication time. This indicates that HA was likely oxidized as a result of sonication although sonication did not appear to desorb HA from the particles. Therefore, it is likely that chemical transformations may occur on the surface of particles in addition to in the aqueous phase.

To investigate whether the desorption of 4-CB was due to sonication or simply due to re-equilibration from degradation of the aqueous phase concentration, [4-CB] was measured during hydrodynamic mixing. A constant aqueous concentration of $\sim 0.5 \text{ }\mu\text{M}$ was observed over a 1

hour period. Moreover, assuming that the system reaches equilibrium rapidly and $0.5 \mu\text{M}$ is the equilibrium concentration in this system, a concentration of $1.5 \mu\text{M}$ observed in aqueous solution in Figure 6 verifies that desorption is occurring as a result of sonication. Therefore, we can conclude that sonication increased desorption of 4-CB from particles during sonication. In addition, it is plausible that during sonication, microjets and microstreaming may break weak bonds between HA and 4-CB, allowing desorption of 4-CB from particles during sonication.

Model of system

Lastly, we modeled the system to understand how combined sonochemical desorption and destruction compared to sonochemical destruction alone. Sedlak and Andren modeled the effect of sorption on the degradation of PCBs in a photo-Fenton system (Sedlak and Andren, 1994). For mono-chlorinated biphenyls, their results fit a first-order model with the desorption rate fast compared to the reaction rate. Similar to Sedlak and Andren, assuming that desorption is not a limiting step, then only two factors result in reduction of the degradation rate of 4-CB from 4-CB adsorbed particles; one is HA, the other is the presence of particles. Performing a kinetic analysis to determine the expected rate constant with both desorption and destruction, loss terms ($\sum k_{\text{loss}}$) due to HA such as $\bullet\text{OH}$ scavenging and sequestration of 4-CB by HA and particles including attenuation of sound and alteration of cavitation bubble collapses must be taken into account as follows:

$$k_{\text{expected}} = k_{\text{aq}} - \sum k_{\text{loss}} \quad (2)$$

where k_{expected} is the expected degradation rate constant, k_{aq} is the degradation rate constant observed in aqueous solution, and

$$\sum k_{\text{loss}} = k_{\text{loss-HA}} + k_{\text{loss-particles}} \quad (3)$$

$$k_{\text{loss-HA}} = k_{\text{aq}} - k_{\text{HA}} \quad (4)$$

$$k_{\text{loss-Particles}} = k_{\text{aq}} - k_{\text{Particles}} \quad (5)$$

where k_{HA} is the degradation rate constant in the presence of 8.5 mg l^{-1} HA and $k_{\text{Particles}}$ is the degradation rate constant in the presence of 200 g l^{-1} bare alumina particles (without sorption). Therefore, the expected degradation rate constant becomes:

$$k_{\text{expected}} = k_{\text{HA}} + k_{\text{Particles}} - k_{\text{aq}} \quad (6)$$

Using values from Table 4, and considering standard error, the calculated k_{expected} is equal to k_{obs} . Therefore, based on this simple model that accounts for degradation rate reduction mechanisms by HA and particles, no other factors appear to complicate the synthetic system investigated. This study demonstrates the potential for sonolysis to both desorb organic contaminants from HA laden sediments and degrade the contaminants in-situ. A higher desorbed 4-CB concentration in the presence of ultrasound verifies the hypothesized enhanced sonochemical desorption. In addition, reactions may occur on the surface of the particle as we suspected occurred with HA; however, based on our modeling with 4-CB, it appears that the main mechanism is desorption followed by degradation.

REFERENCES:

Bolattino, C. and M. Tuchman. (1993) A Summary of Contaminated Sediment Activities within the United States Great Lakes Areas of Concern.

Hua, I., R. Hochemer, and M.R. Hoffmann. (1995) *Environ. Sci. Technol.* **29**, 2790-2796.

Lindsey, M. E., M. A. Tarr. (2000a) *Environ. Sci. Technol.* **34**, 444-449.

Lindsey, M. E., M. A. Tarr. (2000b) *Chemosphere.* **41**, 409-417.

McGroddy, S. E., J. W. Farrington and P. M. Gschwend. (1996) *Environ. Sci. Technol.* **30**, 172-177.

Minero, C., E. Pelizzetti, M. Sega, S.E. Friberg, and J. Sjoblom. (1999) *J. Dispersion Sci. Technol.* **20**, 643-661.

Pee, G. Y., L. K. Weavers, and J. F. Rathman. (2000) Proceedings of the 220th National Meeting of the American Chemical Society, Division of Environmental Chemistry, "Sonochemical Degradation of Surfactants."

Sedlak, D. L., A. W. Andren. (1994) *Environ. Sci. Technol.* **28**, 1207-1215.

Taylor, E., B. B. Cook, and M. A. Tarr. (1999) *Ultrasonics Sonochemistry.* **6**, 175-183.

United States Environmental Protection Agency (1997) The Incidence and Severity of Sediment Contamination in Surface Waters of the United States Vol. 2. EPA 823-R-97-007.

United States Environmental Protection Agency (1998) Fact Sheet: Contaminated Sediment: EPA's Report to Congress. EPA-823-F-98-001.

Wang, Y., C.-S. Hong, F. Fang. (1999) *Environ. Eng. Sci.* **16**, 433-440.

REFEREED PUBLICATIONS RESULTING FROM PROJECT:

Y. Lu and L. K. Weavers, "Sonochemical Desorption and Destruction of 4-Chlorobiphenyl from Synthetic Sediments," submitted to *Environmental Science and Technology*. (submitted 2/7/01)

Y. Lu, N. Riyanto, and L. K. Weavers, "The Effects Sonolysis on Synthetic Sediment Particles" in preparation, to be submitted to *Ultrasonics Sonochemistry*.

CONFERENCE PROCEEDINGS:

Y. Lu and L. K. Weavers, August 20, 2000, 220th National Meeting of the American Chemical Society, Division of Environmental Chemistry, "Sonochemical Remediation of PCB Contaminated Sediments." (Extended abstract)

S-. K. Chang, Y. Lu, and L. K. Weavers, The Second Annual Symposium on Natural Organic Matter in Soils and Water, North Central Region, Columbus, OH, March 19-20, 2001, "The role of humic acid in the combined sonochemical desorption and transformation of contaminants from sediments." (Abstract)

L. K. Weavers and Y. Lu, 31st Annual Ultrasonic Industry Association Symposium, Atlanta, GA, October 10-12, 2001, "Sonochemical desorption and destruction of 4-chlorobiphenyl from synthetic sediments." (Abstract)

OTHER PUBLICATIONS:

Lu, Y., April 15, 2000, The 2000 Edward F. Hayes Graduate Research Forum, "Sonochemical Remediation of PCB Contaminated Sediments."

INFORMATION TRANSFER ACTIVITIES

An article was published in this research project in *News in Engineering*, The Ohio State University College of Engineering magazine in December 1999 entitled: "Dealing with a Toxic Threat." This was reprinted (with permission) in the Spring issue of *Vibrations*, the Ultrasonic Industry Association quarterly newsletter. The article discusses the problem of contaminated sediments in the United States and the research we are performing to develop a solution.

STUDENT SUPPORT:

Yifang Lu, master of science student in the Department of Civil and Environmental Engineering and Geodetic Science. She defended her M.S. thesis in September 2000.

Nicolas Riyanto, undergraduate student in the Department of Chemical Engineering. He defended his B.S. honors thesis in August 2000.

Liang-Hiong Chia, undergraduate student in the Department of Chemical Engineering

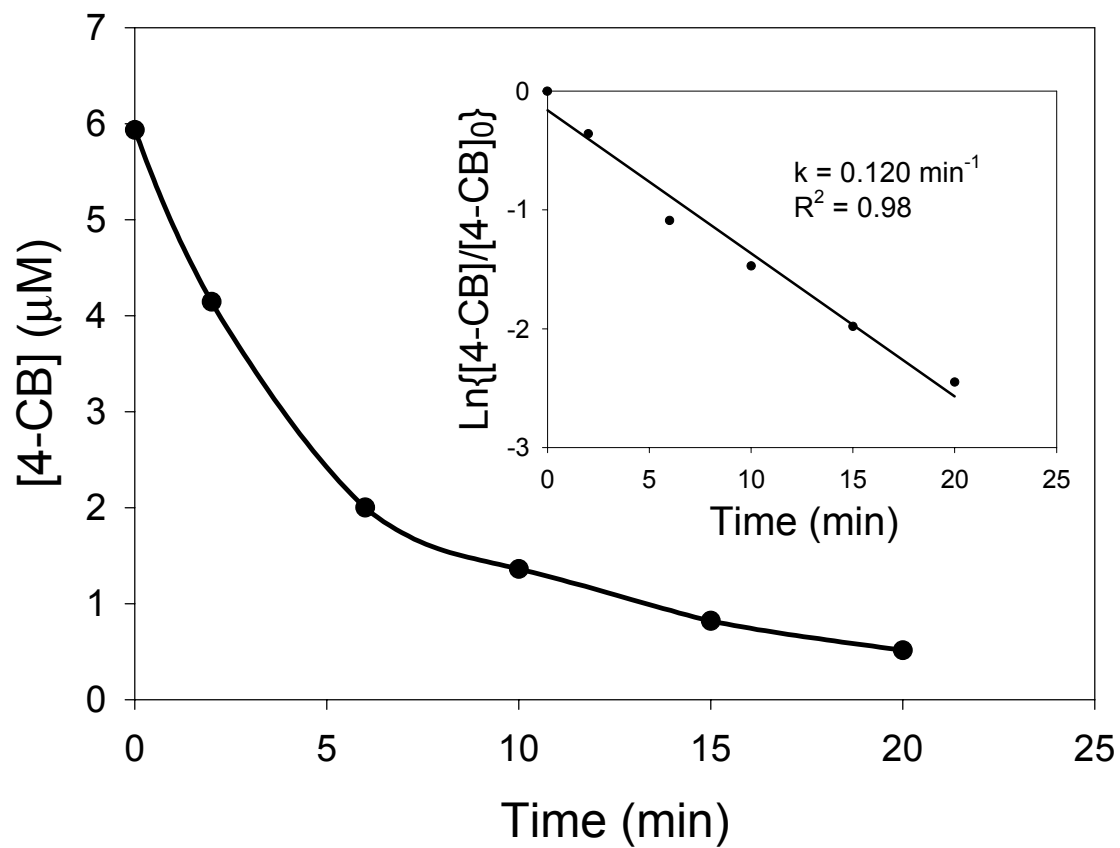


Figure 1: Sonolysis degradation plot of $6 \mu\text{M}$ 4-CB in ultra pure water.

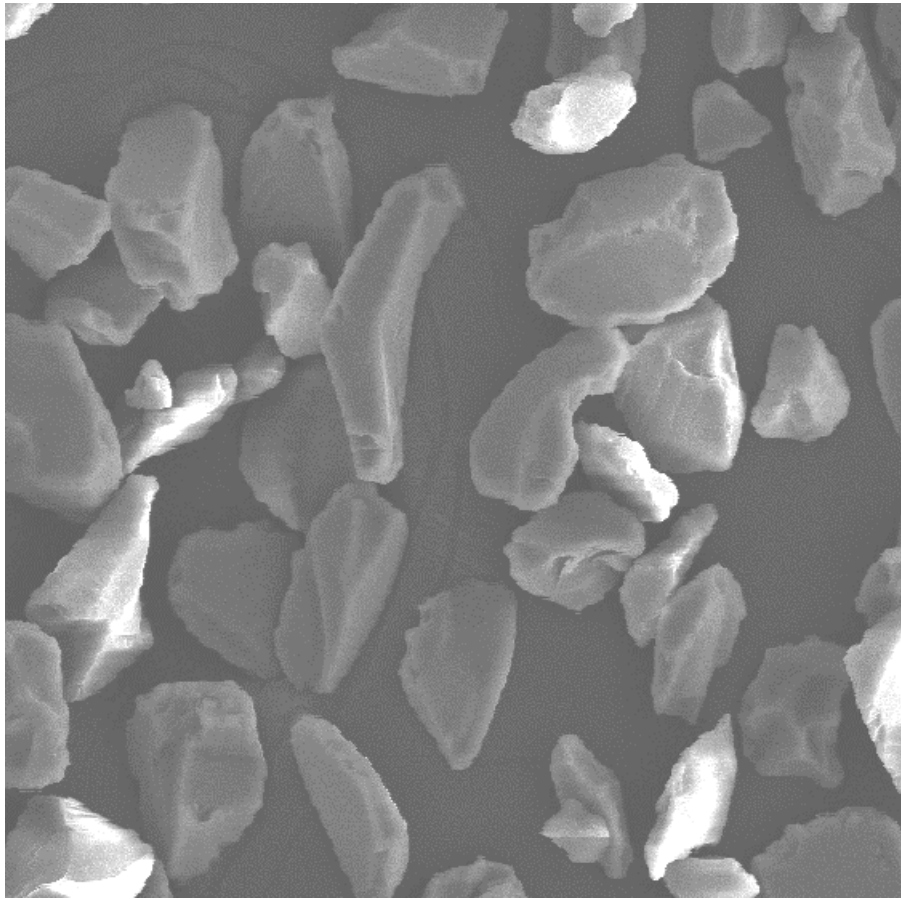


Figure 2: Initial particle structure of silica before sonication (initial size of 60 μm)

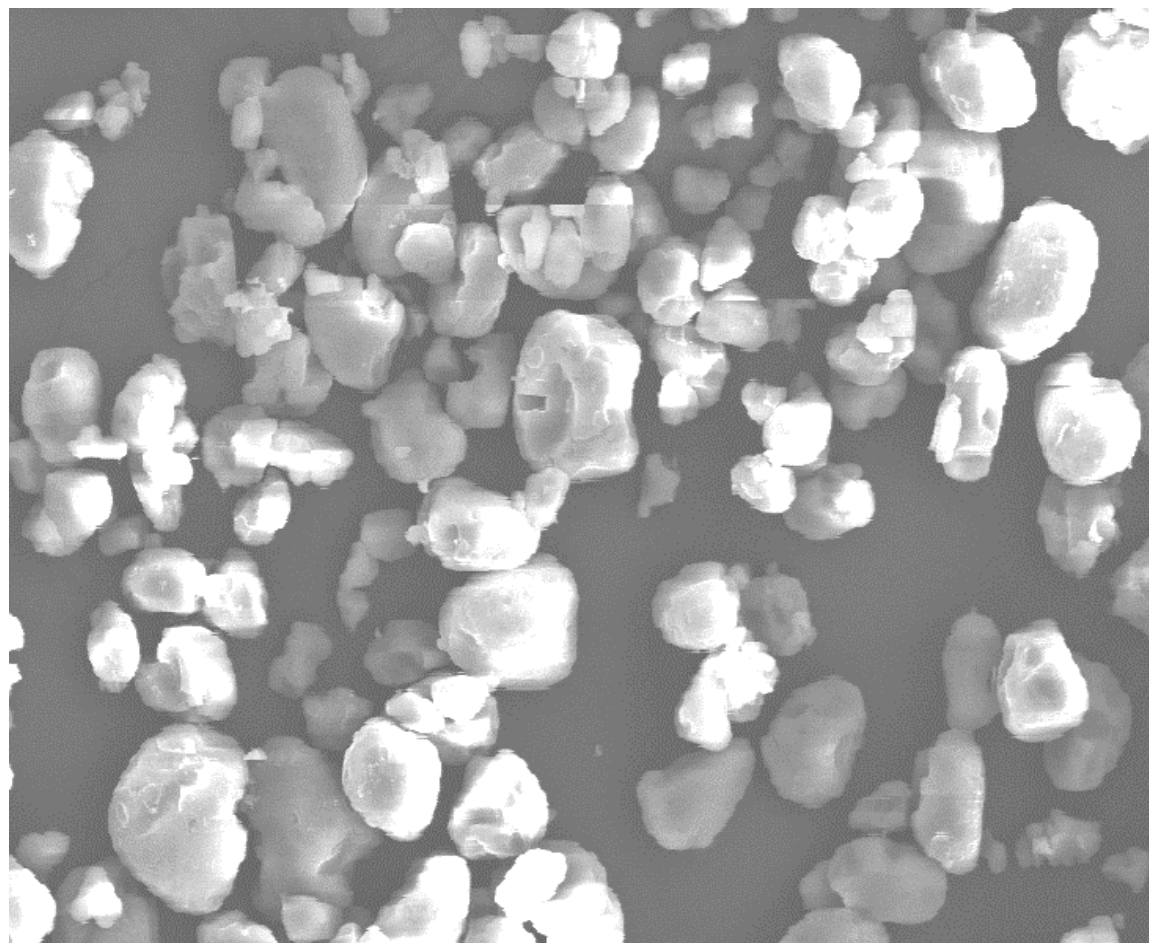


Figure 3: Silica particle structure after sonication for 60 minutes

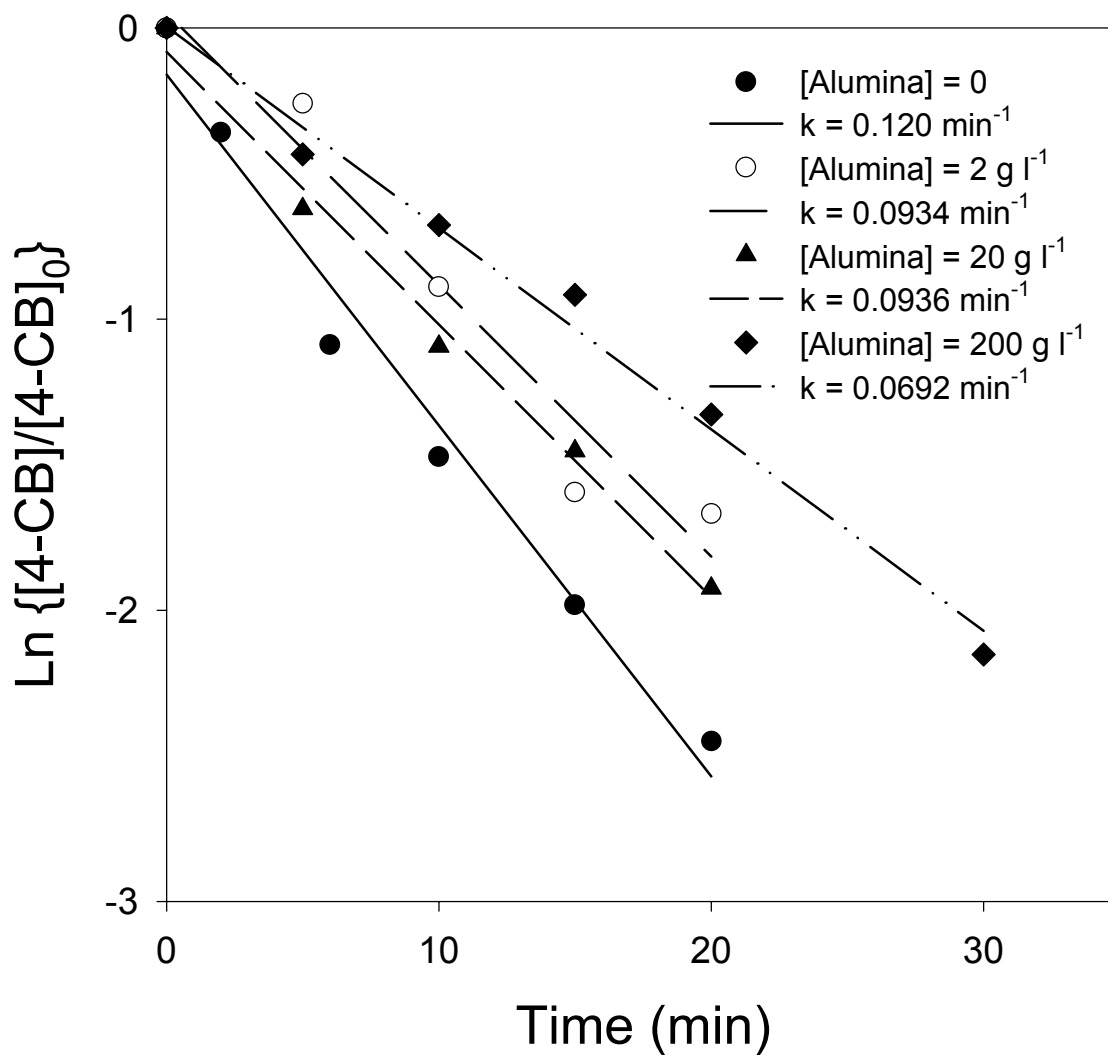


Figure 4: Sonolytic degradation of 6 μM 4-CB (pH = 6, I = 0.001 M) in the presence of different particle concentrations of alumina ($D_0 \sim 125 \mu\text{m}$, $SA_0 = 200 \text{ m}^2 \text{ g}^{-1}$).

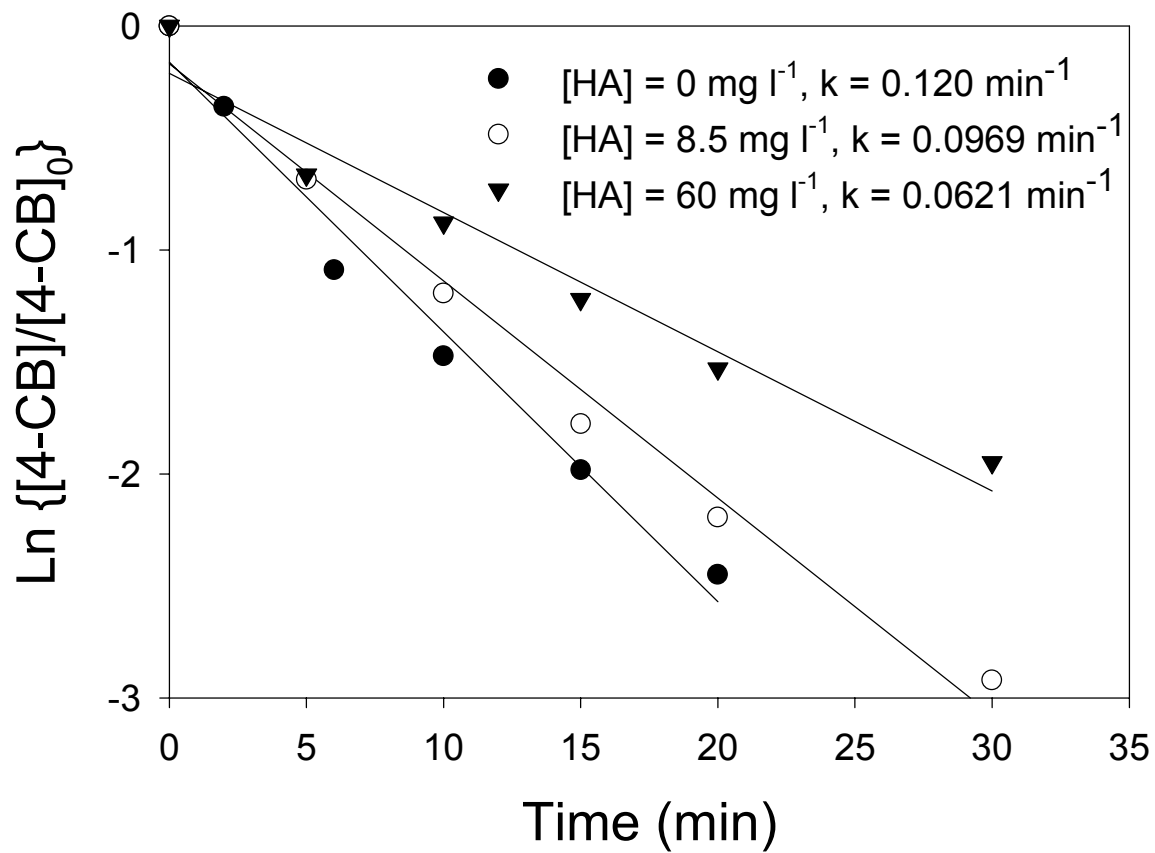


Figure 5: Sonolytic degradation of 6 μ M 4-CB in HA solution. (pH = 6, I = 0.001 M)

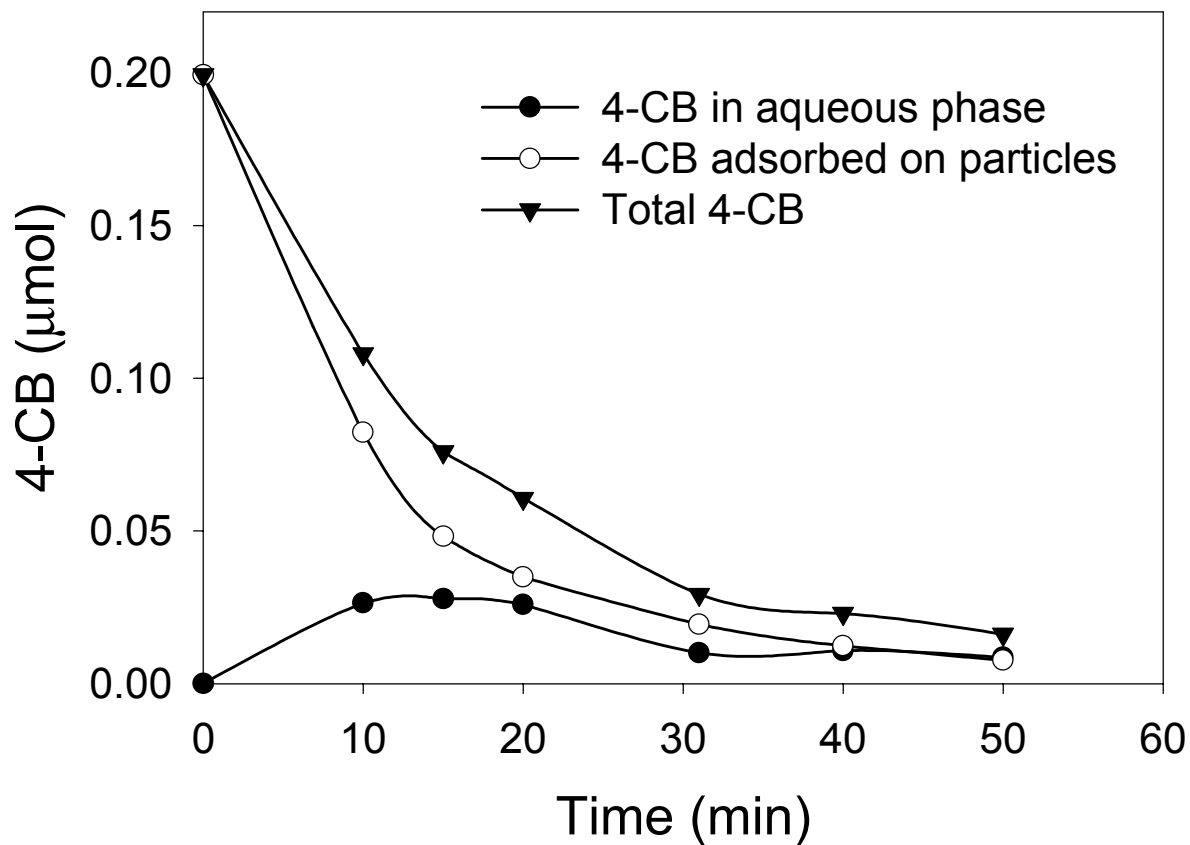


Figure 6: Sonochemical desorption and degradation of 4-CB from HA laden particles ($C_{\text{alumina}} = 200 \text{ g L}^{-1}$, $D_0 \sim 125 \text{ }\mu\text{m}$, $SA_0 = 200 \text{ m}^2 \text{ g}^{-1}$, $\text{pH} = 6$, $I = 0.001 \text{ M}$); 4-CB initial equivalent aqueous concentration = $7.9 \text{ }\mu\text{M}$; HA equivalent aqueous concentration = 60 mg L^{-1} .

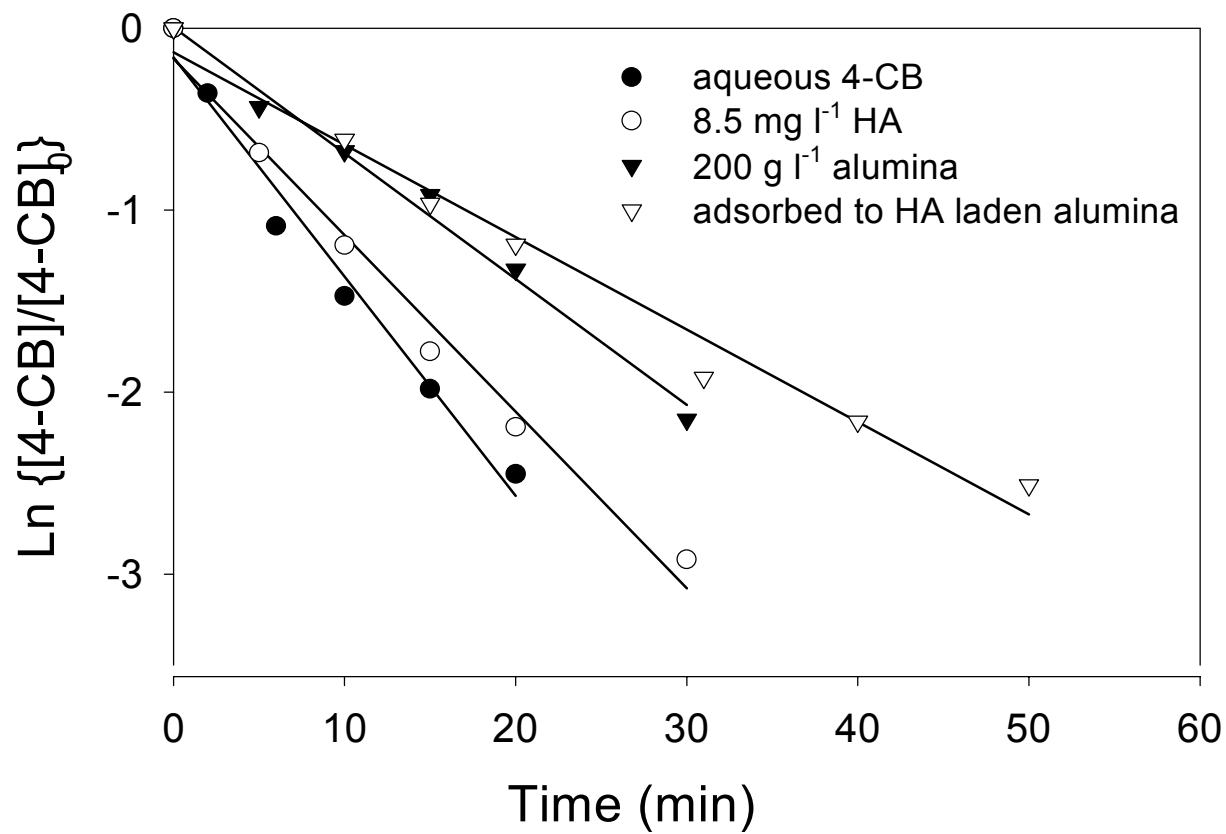


Figure 7: Particle and HA effects on sonochemical desorption and degradation of 4-CB. Conditions as in Figs. 2-4.

Table 1: The first-order rate of particle size reduction during sonication (2 g/L particle concentration)

Particle	k (probe) min ⁻¹	k (NAP) [†] min ⁻¹
Silica (with initial diameter ~ 2 μm)	0.005210±0.002138	N.R.
Silica (with initial diameter ~ 60 μm)	0.0176±0.001241	0.0207±0.000714
Silica (with initial diameter ~ 130 μm)	0.0237±0.002934	0.0568±0.00785
Alumina (surface area ~ 155 m ² /g) [‡]	0.0107±0.001686	N.R.
Alumina (surface area ~ 200 m ² /g) [‡]	0.017±0.0008709	0.1143±0.0178

[†] reported rate constants for NAP are normalized using eqn 1

[‡] Initial particle size ~55 μm

N.R. – not reported

Table 2: The concentration of silicon and aluminum in aqueous solution after sonication and with hydrodynamic mixing after 60 min and the expected concentration if dissolution of silica and alumina is the dominant mechanism of particle size reduction (2g/L particle concentration).

Particle	C (Sonication) (μM)	C (Without Sonication) (μM)	C (expected) (mM)
Silica ($d_0 \sim 2 \mu\text{m}$)	8.12	N/A	49.42
Silica ($d_0 \sim 60 \mu\text{m}$)	26.93	1.24	68.58
Silica ($d_0 \sim 130\mu\text{m}$)	16.95	2.37	70.49
Alumina ($155 \text{ m}^2/\text{g}$) [‡]	6.38	0.50	66.49
Alumina ($200 \text{ m}^2/\text{g}$) [‡]	4.18	0.36	70.56

[‡] Initial particle size $\sim 130 \mu\text{m}$

Table 3: First-order degradation rate constant of 4-CB in the presence of different particles and particle concentrations.

Particle characteristics ‡	k (2g l ⁻¹) min ⁻¹	k (20g l ⁻¹) min ⁻¹
Silica ($D_0 = 2 \mu\text{m}$)	0.098 ± 0.006	0.082 ± 0.006
Silica ($D_0 = 60 \mu\text{m}$)	0.095 ± 0.003	0.066 ± 0.005
Silica ($D_0 = 130 \mu\text{m}$)	0.086 ± 0.005	0.076 ± 0.007
Alumina ($D_0 = 130 \mu\text{m}$, $SA_0 = 155 \text{ m}^2 \text{ g}^{-1}$)	0.097 ± 0.007	0.097 ± 0.004
Alumina ($D_0 = 130 \mu\text{m}$, $SA_0 = 200 \text{ m}^2 \text{ g}^{-1}$)	0.093 ± 0.009	0.094 ± 0.005

† k (0 g l⁻¹) = $0.120 \pm 0.009 \text{ min}^{-1}$. k (200 g l⁻¹ alumina, $SA_0 = 200 \text{ m}^2 \text{ g}^{-1}$) = $0.069 \pm 0.004 \text{ min}^{-1}$.

‡ D_0 is the initial particle size as measured by particle size analysis. SA_0 is the initial surface area reported by the manufacturer.

Table 4: First-order rate constants for degradation of 4-CB under various conditions.

Reaction condition [†]	k (min ⁻¹)
aqueous solution	0.120 ± 0.009
200 g l ⁻¹ bare particles	0.069 ± 0.004
8.5 mg l ⁻¹ HA	0.097 ± 0.006
200 g l ⁻¹ HA laden particles(observed)	0.051 ± 0.003
200 g l ⁻¹ HA laden particles(expected)	0.05 ± 0.01

[†] All particles used were alumina particles with surface area of 200m² g⁻¹. [4-CB] = 6 μM except degradation in the presence of HA laden particles in which equivalent aqueous [4-CB] was 7.9 μM.

Basic Information

Title:	Enhanced Removal of DBP Precursors During Precipitative Softening Through Co-Adsorption Processes
Project Number:	G-04
Start Date:	9/1/1998
End Date:	2/28/2001
Research Category:	Engineering
Focus Category:	Treatment, Surface Water, Water Quality
Descriptors:	
Lead Institute:	Ohio State University
Principal Investigators:	, Harold Webb Walker

Publication

1. Bob, M. and H. W. Walker (2001) Enhanced Adsorption of Natural Organic Matter on Calcium Carbonate Particles Through Surface Charge Modification, Colloids and Surfaces, in press.
2. Bob, M. (expected 2002) Enhanced Removal of DBP Precursors During Lime-Soda Softening, Ph.D. Dissertation, Department of Civil and Environmental Engineering and Geodetic Science, The Ohio State University, Columbus, OH.

PROBLEM AND RESEARCH OBJECTIVES

The presence of natural organic matter (NOM) in raw water supplies is a major concern in drinking water treatment. NOM can facilitate the transport of organic and inorganic pollutants as humic complexes through water treatment facilities [1], and enhance biological growth in distribution systems [2]. NOM is also a major precursor to the formation of disinfection by products (DBPs), such as trihalomethanes and other halogenated organics [3]. Stevens et al. [4], Edzwald et al. [5] and others [2] have found that the formation of DBPs is directly proportional to the concentration of total organic carbon (TOC). DBPs are probable carcinogens and short-term exposure can lead to dizziness, headaches, as well as problems associated with the central nervous system [6]. Recent studies have also linked DBPs to increased incidence of miscarriage, rectal and bladder cancer, and neural tube birth defects [6, 7, 8]. As a result, the USEPA has proposed new maximum contaminant levels (MCLs) of 40 and 30 $\mu\text{g/L}$ in finished drinking water for THMs and HAAs, respectively [9].

To help meet these new MCLs, water treatment plants utilizing lime softening will be required to remove 20-30% of the NOM present in their source water [10]. Lime softening is employed in drinking water treatment primarily for the removal of polyvalent metallic ions, principally calcium and magnesium. The addition of lime in the softening process converts these species into calcium carbonate (CaCO_3) and magnesium hydroxide ($\text{Mg}(\text{OH})_2$) precipitates [1]. Previous studies indicate, however, that NOM removal during lime softening is limited [11, 12, 13, 14]. Randtke [11] has shown that calcium carbonate is precipitated as a dense crystalline solid with very low surface area, which results in minimal sites for natural organic matter adsorption. Electrostatic

repulsion arising from the high negative charge density of humic substances and CaCO_3 surfaces at high pH also leads to low levels of NOM adsorption. While the formation of $\text{Mg}(\text{OH})_2$ during softening can aid in removing natural organic matter, the precipitation of magnesium occurs only at high pH, a condition uncommon in practice [11]. One approach to improve NOM removal is to use “enhanced precipitative softening” in which the amount of added lime is increased substantially. However, this approach leads to higher chemical costs and greater production of waste sludge.

In this research, a new approach to increase the removal of DBP precursors during the lime softening process was investigated. In particular, experiments were carried out to examine whether the modification of the surface of calcium carbonate particles by adsorption of synthetic polyelectrolytes could be used to improve NOM removal during softening. Previous studies using colloidal silica [15], as well as other model surfaces [16], have revealed that multilayers of oppositely charged polymers can be formed through the sequential addition of cationic and anionic polyelectrolytes. These past studies suggest that NOM removal during water treatment could be enhanced through the formation of anionic humic acid-cationic polymer multilayers on particle floc surfaces. Although this may be a promising approach, no studies have been conducted looking at how coating calcium carbonate particles with synthetic polymer may influence NOM adsorption.

To elucidate whether polyelectrolytes can be used to modify floc surface properties and enhance NOM removal, the adsorption of negatively charged humic acid on polyacrylamide-coated calcium carbonate particles was examined. The surface of calcium carbonate particles was modified using cationic polyacrylamides of various size

and charge density. The electrophoretic mobility of the coated particles was examined by electrophoretic light scattering to gain insight into the mechanisms controlling humic acid adsorption on these surfaces. This work provides important new insight into the role of synthetic polymers in controlling NOM removal during lime softening, as well as new fundamental information on the mechanisms important in the sequential adsorption of multiple polymeric species on solid surfaces.

METHODOLOGY

Materials

Calcium carbonate particles were provided by Specialty Minerals (Bethlehem, PA). Particle size distributions were determined by the manufacturer using a Micromeritics Sedigraph 5100 and showed that the particles had a mean diameter (D_{50}) of 0.83 μm , D_{20} of 0.57 μm , and D_{90} of 1.47 μm . The particles had a specific surface area of 5.9 m^2/g as determined by the manufacturer.

Humic acid used in this study was obtained from Aldrich Chemical Company (Milwaukee, WI). This humic acid has a reported molecular weight of 4100 g/mol [17]. Aldrich humic acid was prepared by the base extraction of coal by the manufacturer and was not isolated from natural waters. However, a number of previous studies have utilized this material, and therefore, it represents a good model humic substance. Prior to use, Aldrich humic acid solutions were filtered using 0.22 μm filters (Millipore, Bedford, MA) and stored at 4 °C. Cationic polyacrylamides (CPAM) with different charge densities and molecular weights were supplied by Polydyne Inc. (Riceboro, GA). These cationic polyacrylamides have low and high molecular weights with degree of cation substitution varying from 5% to 55%. A degree of cation substitution of 5% indicates that

5% of the monomer units have positively charged functional groups. High molecular weight CPAM has a molecular weight in the range of 5 to 10 million Daltons and low molecular weight CPAM has a molecular weight in the range 1 to 2 million Daltons, as determined by the manufacturer. All solutions were prepared in MilliQ water using only analytical grade reagents.

Humic Acid Adsorption onto Calcium Carbonate Particles

The adsorption of humic acid onto calcium carbonate particles was determined spectrophotometrically using a UV-VIS 2401PC double beam spectrophotometer. (Shimadzu Corporation, MD). Adsorption measurements were carried out at a temperature of 25 °C and different pH values (7.5 and 9.5). To carry out a humic acid adsorption experiment, humic acid was prepared in carbonate buffer at a desired salt concentration (0.001 M KCl). An aliquot of well-mixed calcium carbonate particles was then added to a series of humic acid solutions at varying concentrations (5-70 mg/L). The final solution was adjusted to the desired pH using 0.2 N HCl or 0.2 N NaOH. The mixture was then incubated for at least two hours, after which time the pH of the solution was again measured. The samples were then filtered with 0.22 µm filters (Millipore, Bedford, MA) and the equilibrium concentration of the supernatant measured using the spectrophotometer. The amount of humic acid adsorbed was determined based on the measured depletion in solution. Control experiments were carried out and showed virtually no humic acid was lost by filtration or to the surface of reaction vessels. The final pH of the solution was measured to verify no significant changes in solution conditions during the course of an adsorption experiment. For all experiments, the

change in pH was less than 0.2 pH units. In addition, turbidity measurements indicated that a 0.22 μm filter removed over 99.9% of the particles, and hence, the fraction of particles that escaped through the filter was negligible.

Cationic Polymer Adsorption onto Calcium Carbonate Particles

The adsorption of cationic polyacrylamides onto calcium carbonate particles was determined using a total organic carbon analyzer (TOC 5000A, Shimadzu Corporation, MD). The cationic polymer solution was prepared in carbonate buffer at the desired salt concentration (0.001 M KCl). As in the case of humic acid, an aliquot of well-mixed calcium carbonate particles was added to different concentrations of the polymer and the final pH adjusted using HCl or NaOH. The mixture was incubated for at least two hours and then the pH was again measured. Next, samples were centrifuged and the concentration of polymer in the supernatant was measured using the TOC analyzer. Preliminary experiments showed that CPAM adsorbed significantly to filter surfaces, and thus centrifugation was employed to separate solid particles from polymer in solution. Control experiments showed that centrifugation removed 99.9% of the particles, and therefore, the mass of particles left in the supernatant was negligible.

Humic Acid Adsorption onto Polymer-Coated Calcium Carbonate Particles

To examine the adsorption of humic acid on cationic polymer-coated particles, polyacrylamide was prepared at 100 mg/L using carbonate buffer. Next, 200 μL of a 20 g/L well-mixed calcium carbonate solution was added to 5 ml of the cationic polymer solution and the mixture was incubated for at least two hours. Following this incubation

period, the suspension was centrifuged for at least two hours in order to separate the particles from any cationic polymer remaining in solution. The particles were then resuspended in humic acid solution and the pH adjusted using NaOH or HCl. This mixture was incubated for an additional two hours, after which time, the pH of the solution was again checked. The coated particles were separated from humic acid by filtration through 0.22 μm pore size Millex-GV disposable filters (Millipore, Bedford, MA). The depletion of humic acid in solution was monitored spectrophotometrically. Control tubes containing humic acid and no particles were treated in identical manner to ensure that there was no adsorption onto the filter surface. The adsorption of UV light by the polymer was negligible, and therefore, the concentration measured by this spectrophotometric technique represented only humic acid in solution. Furthermore, control experiments verified no measurable desorption of polymer occurred following resuspension of the coated particles. It was not possible, however, to determine whether humic acid adsorption facilitated the release of CPAM, due to the inability to distinguish CPAM from humic acid in solution using total organic carbon measurements.

Electrophoretic Mobility Measurements

The electrophoretic mobility of calcium carbonate particles, both in the presence and absence of CPAM, was determined using an electrophoretic light scattering instrument (ZetaPlus, Brookhaven Instruments Corp., NY). All mobility measurements were carried out at 25 $^{\circ}\text{C}$ and a salt concentration of 0.001 M KCl. The pH of the solutions was adjusted by adding varying amounts of either 0.1 M NaOH or 0.1 M HCl. For the mobility measurements of the polymer-coated particles, calcium carbonate

particles were first saturated with the cationic polymer and then the mobility was measured using the ZetaPlus. Each calculated mobility value represents the average of at least 10 independent measurements.

PRINCIPAL FINDINGS AND SIGNIFICANCE

Initial experiments focused on examining the affinity of humic acid for the surface of bare calcium carbonate particles at different pH values (7.5 and 9.5) at a salt concentration of 0.001 M KCl. These data are shown in panel A of Figure 1. As can be seen, the amount of humic acid adsorbed on to the surface of calcium carbonate particles varied with the pH value. The maximum surface density of humic acid increased from approximately 20 mg/g at pH 9.5 (open circles) to 120 mg/g at pH 7.5 (filled circles). For both pH values, a plateau was observed at high equilibrium concentrations suggesting monolayer coverage on the calcium carbonate surface.

Electrostatic interactions likely play a role in controlling the amount of humic acids adsorbed on the calcium carbonate surface at these different pH values. Humic acid is known to be fully protonated, i.e. has a degree of ionization, $\alpha = 0$ at pH 3 [18], and thus is negatively charged above this pH value. Electrophoretic mobility measurements were carried out to elucidate the electrostatic character of the bare calcium carbonate particles. These data are shown in panel B of Figure 1. As can be seen, the isoelectric point (IEP) for these particles was around pH 8.1, which is within the range reported by other researchers [19, 20]. At pH 7.5, the calcium carbonate particles were uncharged or slightly positively charged, and high adsorption affinity of the negatively charged humic acid was observed. At pH 9.5, on the other hand, the particles were negatively charged

and had an electrophoretic mobility value of $-1.5 \text{ (}\mu\text{m/s)/}(V/\text{cm})$. Under these conditions, electrostatic interactions between the particles and humic acid were repulsive, and subsequently, adsorption was low.

In addition to electrostatic forces, the dependence of humic acid adsorption on pH seen in our experiments may also depend on specific or non-specific chemical interactions between humic acid and the CaCO_3 surface. For example, previous studies have shown that humic acid can reverse the surface charge of synthetic calcite particles at low pH, from a net positive charge to a net negative charge [21]. This suggests that humic acid does not adsorb to calcite by a simple charge neutralization mechanism. However, further work, perhaps utilizing spectroscopic techniques, is needed in order to elucidate the specific mechanisms controlling the binding of humic acid at the calcite-water interface. Another factor that may influence humic acid adsorption is the conformation of this polymer at different pH values. Cornel and co-workers have shown that the diffusion coefficient of humic acid in solution decreases as a function of pH, even at relatively high pH values between 6.4 and 10 [22]. The more coiled humic conformation at lower pH values likely facilitates greater adsorption as compared to an uncoiled conformation under high pH conditions.

In one of the few studies looking at the adsorption of humic acid on calcium carbonate particles (calcite, in particular), Petrovic et al. [23] also observed a decrease in the amount of adsorption with increasing pH. However, in this previous study experiments were conducted over a lower pH range (roughly 3-8). Although no direct evidence was provided, Petrovic et al. speculated that the dependence of humic acid adsorption on pH was influenced by electrostatic interactions as well as a ligand

exchange mechanism, as is seen for humic acid adsorption on metal oxyhydroxide surfaces [24]. Petrovic et al. point out that complexation reactions between humic acid and surface hydroxyl groups such as CaOH and CaOH_2^+ are pH dependent. As pH increases, these surface functional groups become deprotonated, and therefore, they suggested the potential for surface complexation decreases. Our experiments were carried out at higher pH values (7.5 to 9.5), and therefore, ligand exchange was perhaps less important. It should also be noted, however, that humic acid can form complexes with dissolved calcium [25]. But again, this process is perhaps more important at low pH values where the solubility of calcium is higher.

To examine how the modification of the calcium carbonate surface might influence humic acid adsorption, the affinity of a well-known cationic polymer (polyacrylamide) for calcium carbonate particles was first examined. Figure 2 shows the adsorption of high molecular weight CPAMs with various charge densities on the surface of calcium carbonate particles at pH 9.5 and a salt concentration of 0.001 M KCl. The amount of CPAM adsorbed varied from about 20 mg/g for 5% charge density CPAM to close to 70 mg/g for 55% charge density CPAM. Previous studies have shown that electrostatic interactions are important in controlling the adsorption of CPAM on polystyrene latex [26] as well as clay [27]. The fact that the amount of CPAM adsorbed on calcium carbonate increased with increasing CPAM charge density suggests, however, that both electrostatic and non-electrostatic interactions may be important in this system. If the process were solely electrostatic in nature, high charge density CPAM molecules would more effectively neutralize the negative surface charge of calcium carbonate, and subsequently, adsorption would decrease with increasing charge density.

Next, adsorption measurements of humic acid onto CPAM-coated calcium carbonate particles were carried out. Figure 3 shows the adsorption of humic acid onto calcium carbonate particles coated with high molecular weight CPAMs having various charge densities, at pH 9.5 and 0.001M KCl. The adsorption of humic acid onto bare calcium carbonate particles (filled circles) are reproduced from Figure 1 for comparison. As can be seen, coating the particles with low charge density CPAM (5%) had little effect on the amount of humic acid adsorbed (open circles). When particles were coated with 20% charge density CPAM (filled triangles), the amount of humic acid adsorbed was only slightly greater than the adsorption onto bare particles. However, when calcium carbonate particles were coated with 35% (open triangles) and 55% (filled squares) charge density CPAM, the amount of humic acid adsorbed significantly increased. For both high charge density CPAMs (35% and 55%), the maximum humic acid surface density was about 60 mg/g, which was three times greater than the bare particle maximum surface density. The 55% charge density polymer improved adsorption slightly more than the 35% charge density polymer.

A number of mechanisms may influence the adsorption of humic acid onto polymer-coated calcium carbonate particles. Coating calcium carbonate particles with cationic polymer will influence both specific chemical and electrostatic interactions between humic acid and the calcium carbonate surface. To gain better insight into the role of electrostatic interactions in controlling humic acid adsorption onto polymer-coated particles, electrophoretic mobility measurements of CPAM-coated calcium carbonate particles were carried out as a function of pH at 0.001 M KCl. These data are shown in Figure 4. Electrophoretic mobility data for the bare calcium carbonate particles (filled

circles) are reproduced from panel B of Figure 1 for comparison. As can be seen, the presence of cationic polymer with 55% charge density and high molecular weight (filled triangles) resulted in a positive electrophoretic mobility at all measured pH values, but the mobility decreased slightly with increasing pH. At pH 9.5 the coated particles had a mobility of 2.7 ($\mu\text{m/s}/(\text{V/cm})$) while the bare particles had a mobility of about -1.5 ($\mu\text{m/s}/(\text{V/cm})$). Thus, coating the particles with high charge density CPAM reversed the charge of the particles, and thus, facilitated the attachment of humic acid to positively charged polymer segments or sites on the coated particles.

The mobility of calcium carbonate particles when coated with 5% charge density, high molecular weight CPAM is also shown in Figure 4 (open circles). As can be seen, the presence of this low charge density polymer also influenced the mobility of the particles. The net mobility of the particles was positive at a pH value of 8.7, but significantly decreased with increasing pH. Overall, the mobility values in this case were much less than the 55% charge density polymer-coated particles. It is interesting to note that humic acid adsorption onto particles coated with 5% charge density polymer was similar to levels observed on the bare particles, despite the slight charge reversal caused by this polymer at pH 9.5. This result suggests that humic acid adsorption was influenced both by electrostatic interactions as well as specific or non-specific chemical interactions between humic acid and adsorbed polymer chains. Adsorption of the 5% charge density polymer was low, and therefore, this allowed for few chemical interactions between humic acid and adsorbed polymer molecules. For the 55% charge density polymer, on the other hand, the particles had a high positive charge density and

there was high polymer adsorption density, both of which appear to have facilitated humic acid adsorption.

To examine if the molecular weight of CPAM is important, adsorption measurements on calcium carbonate particles coated with low molecular weight cationic polyacrylamides were also carried out. These measurements were conducted at a salt concentration of 0.001M KCl and pH 9.5. Panel A of Figure 5 shows the maximum amount of low molecular weight CPAM (filled triangles) adsorbed onto the calcium carbonate particles as a function of polymer charge density. The data for high molecular weight CPAM (open circles) are shown for comparison. As was seen for high molecular weight CPAM, the amount of low molecular weight CPAM adsorbed varied significantly with the charge density (from about 15 mg/g for 5% charge density to close to 160 mg/g for 55% charge density). In general, the maximum surface density of the low molecular weight CPAMs was higher than that for high molecular weight CPAMs. A possible explanation for this is based on the conformation of CPAM on the calcium carbonate particle surface. High molecular weight CPAM may occupy more area per monomer unit as a result of less lateral conformational freedom on the particle surface compared to low molecular weight CPAM.

The amount of humic acid adsorbed on calcium carbonate when coated with low molecular weight CPAM (filled triangles) is shown in panel B of Figure 5. Adsorption data for humic acid on bare and high molecular weight CPAM-coated particles are shown for comparison. In general, the amount of humic acid adsorbed had the same trend with charge density as in the case of high molecular weight CPAM (open circles), but the maximum surface density was lower. The amount of humic acid adsorbed on particles

coated with 55% charge density, low molecular weight CPAM was 50 mg/g compared to 60 mg/g for the equivalent high molecular weight polymer. This result again suggests that electrostatic interactions are not the only important factor controlling humic acid adsorption on CPAM-coated particles. If the process were controlled solely by electrostatic interactions, we would expect the low molecular weight CPAM to facilitate a greater amount of humic acid adsorption as a result of the greater CPAM surface density. However, just the opposite trend was observed. Perhaps the more compact conformation of low molecular weight CPAM on the calcium carbonate surface blocks sites on the particles available for humic acid adsorption.

To explore the role of pH in controlling humic acid adsorption on CPAM-coated particles, adsorption experiments were carried out at a pH value of 7.5. The results of humic acid adsorption onto calcium carbonate particles coated with low and high molecular weight CPAMs at 0.001 M KCl and pH 7.5 are shown in Figure 6. Data are presented for 5% and 55% charge density, low and high molecular weight polymers. The adsorption of humic acid onto bare calcium carbonate particles (filled circles) are reproduced from Figure 1 for comparison. At pH 7.5, coating the particles with 5% charge density CPAM resulted in lower humic acid adsorption than for the bare calcium carbonate particles, for both low and high molecular weight polymers. Under these conditions, the bare particles were positively charged and therefore conditions were highly favorable for humic acid adsorption. Although the adsorption of 5% charge density polymer was low (data not shown), the presence of small amounts of this polymer on the surface may have blocked sites on particles that were otherwise favorable for humic acid adsorption. When the particles were coated with 55% charge density

polymer, the amount of humic acid adsorbed was slightly higher than on the bare particles. We suspect that these high charge density polymers had a more significant effect on the surface charge characteristics of the particles and this resulted in the slightly higher amount of humic acid adsorption. It should be noted that adsorption of humic acid onto CaCO_3 is high at pH 7.5 without the addition of polymer. However, this pH value is much lower than the pH encountered in the softening process. At low pH, hardness cations may not be effectively removed, and therefore, pH adjustment alone may not be an effective approach to improve NOM removal during softening.

Summary

The data presented in this research suggest that one way to improve the removal of NOM during lime softening is to modify the surface characteristics of calcium carbonate precipitates. Coating calcium carbonate particles with CPAM significantly increased adsorption of humic acid at pH 9.5. The adsorption of CPAM converted negatively charged calcium carbonate to positively charged particles, which induced electrostatic attraction between humic acid molecules and coated particle surfaces. The amount of humic acid adsorbed increased with the charge density of CPAM, and high molecular weight CPAM was more effective at improving humic acid adsorption than low molecular weight CPAM. Although humic acid adsorption increased upon coating the particles with CPAM, the amount of humic acid adsorbed was not directly related to the CPAM adsorption density. This suggests non-electrostatic interactions also play a role in controlling the adsorption process. These data indicate that coating calcium carbonate

precipitates with cationic polymer may provide an effective approach for enhancing NOM removal during the lime softening process.

ARTICLES IN REFEREED JOURNALS

- Bob, M. and H. W. Walker, “Enhanced Adsorption of Natural Organic Matter on Calcium Carbonate Particles Through Surface Charge Modification”, *Colloids and Surfaces*, in press.

DISSERTATIONS

- Bob, M. “Enhanced Removal of DBP Precursors During Lime-Soda Softening,” Department of Civil and Environmental Engineering and Geodetic Science, The Ohio State University, expected 6/15/2002.

OTHER PUBLICATIONS

- Bob, M., “Enhanced Adsorption of Natural Organic Matter on Calcium Carbonate Particles Through Surface Charge Modification”; abstract published in the American Water Works Association, Ohio section Newsletter, Spring 2001.

PRESENTATIONS

- Bob, Mustafa, and H. W. Walker, “Enhanced Removal of DBP Precursors During Precipitative Softening through Co-Adsorption Processes”, presented at the 74th American Chemical Society (ACS) Colloid and Surface Science Symposium, Lehigh University, Bethlehem, PA, June 19-21, 2000.

- Bob, Mustafa, “Enhanced Removal of DBP Precursors During Precipitative Softening through Co-Adsorption Processes”, presented at the Ohio Section, American Water Works Association Annual Conference, Dayton, OH, August 2000.

AWARDS

- This research was awarded first place in the 2000 Ohio Section American Water Work Association Student Paper Competition.
- The PI was awarded the Ohio State University College of Engineering Lumley Research Award partially based on the results of this research.

REFERENCES

- [1] American Water Works Association, Water Quality and Treatment, 4th edition. F. W. Pontius, Ed. (1990) McGraw-Hill, Inc.
- [2] P. C. Singer, Water Sci. Technol. 40 (1999) 25.
- [3] J. J. Hook, Water Treatment and Examination 23 (1974) 234.
- [4] A. A. Stevens, C. J. Slocum, D. R. Seeger, G. G. Robeck, J. Am. Water Works Assoc. 68 (1976) 615.
- [5] J. K. Edzwald, W. C. Becker, K. L. Wattier, J. Am. Water Works Assoc. 77 (1985) 122.
- [6] K. Waller, S. H. Swan, G. Delorenze, B. Hopkins, Epidemiology 9 (1998) 134.
- [7] M. E. Hildesheim, K. P. Cantor, C. F. Lynch, M. Dosemeci, J. Lubin, M. Alavanja, G. Craunl, Epidemiology 9 (1997) 29.
- [8] K. P. Cantor, C. F. Lynch, M. E. Hildesheim, M. Dosemeci, J. Lubin, M. Alavanja, G. Craunl, Epidemiology 9 (1997) 21.
- [9] USEPA. Disinfection and disinfection by products: final rule. Federal Register, 63 (241), 69478.
- [10] USEPA, Guidance Manual for Enhanced Coagulation and Enhanced Precipitative Softening, Washington D.C., September, 1993.
- [11] S. J. Randtke, J. Am. Water Works Assoc. 80 (1988) 40.
- [12] S. J. Randtke, C. E. Thiel, M. Y. Liao, C. N. Yamaya, J. Am. Water Works Assoc. 74 (1982) 192.
- [13] M. J. Semmens, A. B. Staples, J. Am. Water Works Assoc. 78 (1986) 76.
- [14] A. P. Black, R. F. Christman, J. Am. Water Works Assoc. 53 (1961) 737.

-
- [15] N. G. Hoogeveen, M. A. Cohen Stuart, G. J. Fleer, and M. R. Bohmer, *Langmuir*, 12 (1996) 3675.
- [16] E. Donath, D. Walther, V. N. Shilov, E. Knippel, A. Budde, K. Lowack, C. A. Helm, and H. Mohwald, *Langmuir*, 13 (1997) 5294.
- [17] Y. P. Chin, G. Aiken, E. O'Loughlin, *Environ. Sci. Technol.* 28 (1994) 1853.
- [18] G. Newcombe, C. Donati, M. Drikas, R. Hayes, *Water Supply* 14 (1994) 129.
- [19] P. Somasundaran, G. E. Agar. *J. Colloid Interface Sci.* 24 (1967) 433.
- [20] D. W. Thompson, P. G. Pownall, *J. Colloid Interface Sci.* 131 (1989) 74.
- [21] V. Neda and J. Biscan, *Colloids Surf.* 137 (1998) 7.
- [22] R. M. Cornel, R. S. Summers, and P. V. Roberts, *J. Colloid Interface Sci.* 110 (1986) 149.
- [23] M. Petrovic, M. Kastelan-Macan, and J. M. Horvat, *Water, Air, and Soil Pollution.* 111 (1999) 41.
- [24] B. Gu, J. Schmitt, Z. Chen, L. Liang, and J. F. McCarthy, *Environ. Sci. Technol.* 28 (1994) 38.
- [25] J. Hering and F. M. M. Morel, *Environ. Sci. Technol.* 22 (1988) 1234.
- [26] H. Tanaka, A. Swerin, L. Odberg, S. B. Park, *J. Pulp Paper Sci.* 25 (1999) 283.
- [27] G. Durand-Piana, F. Lafuma, R. Audebert, *J. Colloid Interface Sci.* 119 (1987) 474.

Figure Legends

Figure 1. (Panel A) Adsorption of humic acid on calcium carbonate particles at a salt concentration of 0.001 M KCl and two pH values; pH 9.5 (○) and pH 7.5 (●). (Panel B) Electrophoretic mobility of bare calcium carbonate particles at 0.001M KCl as a function of pH.

Figure 2. Adsorption of high molecular weight CPAM on calcium carbonate particles at 0.001M KCl and pH 9.5. Experiments were carried out with 5% charge density CPAM (●), 20% charge density CPAM (○), and 55% charge density CPAM (▼).

Figure 3. Adsorption of humic acid on bare (●) and CPAM-coated calcium carbonate particles at 0.001M KCl and pH 9.5. Particles were coated with high molecular weight CPAM at 5% charge density (○), 20% charge density (▼), 35% charge density (▽) and 55% charge density (■).

Figure 4. Electrophoretic mobility of bare (●) and CPAM-coated calcium carbonate particles at 0.001M KCl. Particles were coated with high molecular weight CPAM at 5% charge density (○) and 55% charge density (▼).

Figure 5. (Panel A) Adsorption of low molecular weight (▼) and high molecular weight (○) CPAM of various charge densities onto calcium carbonate particles at pH 9.5 and 0.001M KCl. (Panel B) Humic acid adsorption on calcium carbonate particles coated with low molecular weight (▼) and high molecular weight (○) CPAM of various charge density at pH 9.5 and 0.001 M KCl. Adsorption of humic acid on the bare particles is shown as a solid line for comparison.

Figure 6. Adsorption of humic acid on bare (●) and CPAM-coated calcium carbonate particles at 0.001M KCl and pH 7.5. Particles were coated with high molecular weight CPAM at 5% charge density (○), high molecular weight CPAM at 55% charge density (▼), low molecular weight CPAM at 5% charge density (▽) and low molecular weight CPAM at 55% charge density (■).

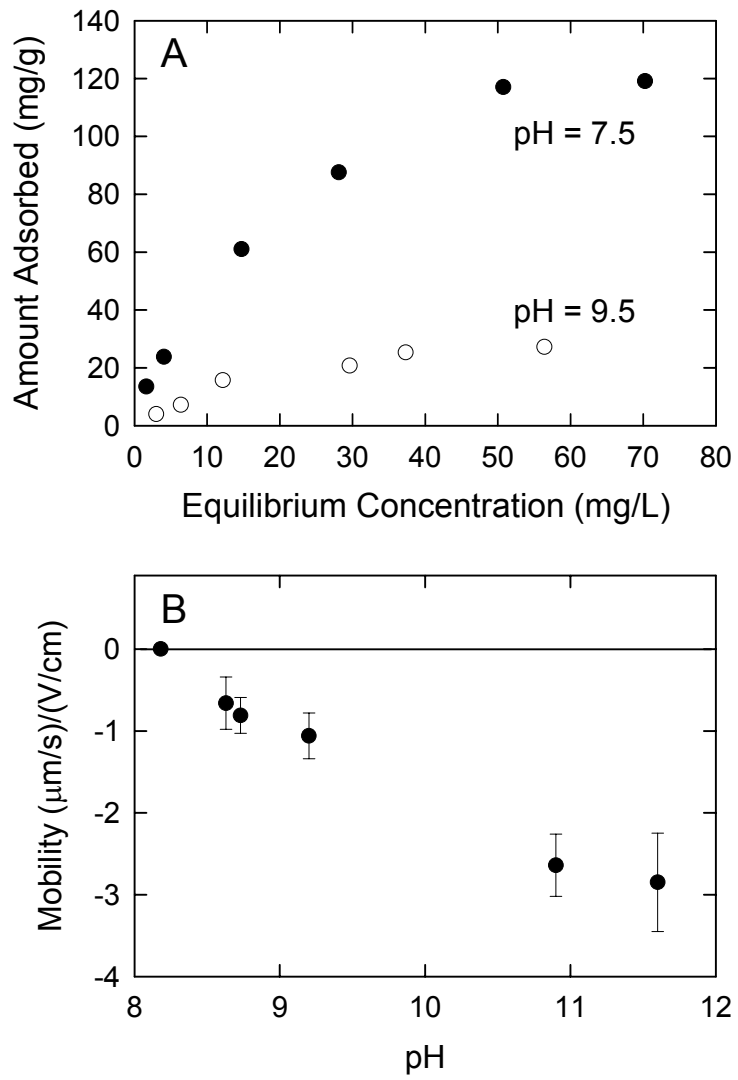


Figure 1. Bob and Walker

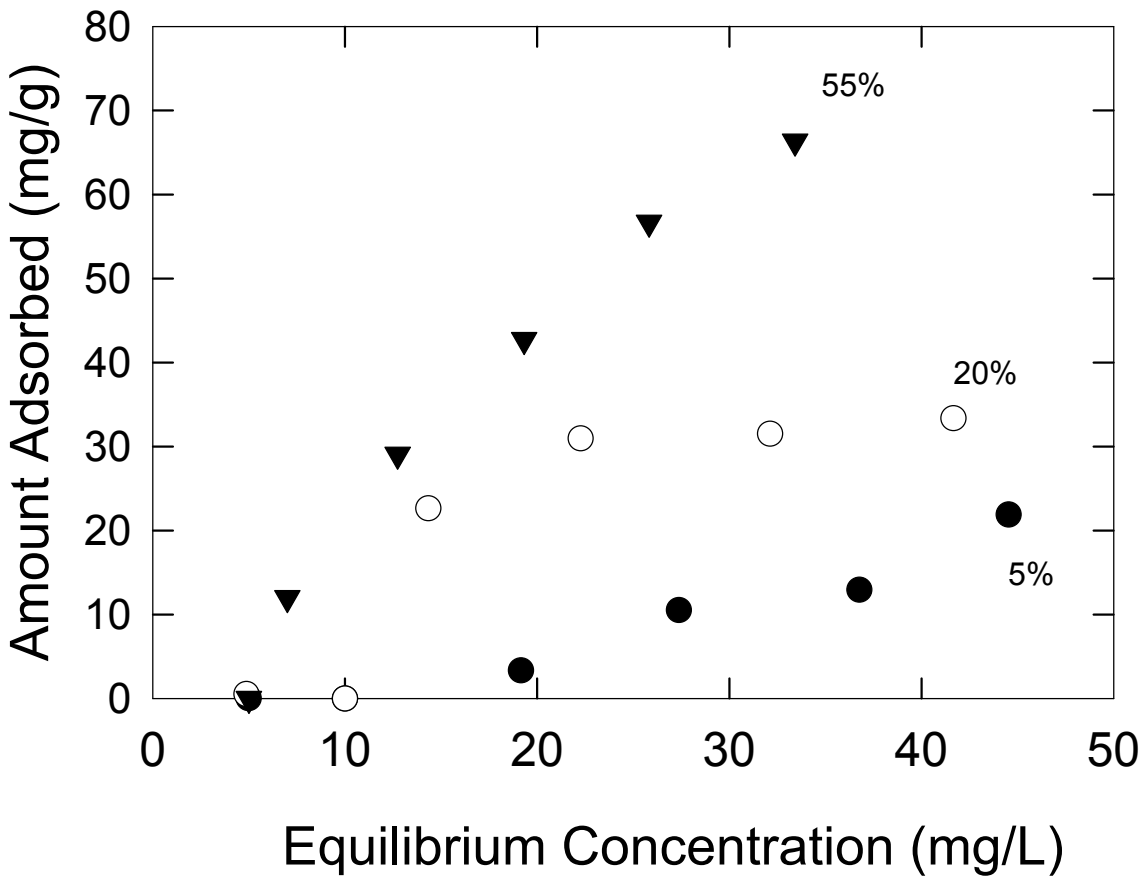


Figure 2. Bob and Walker

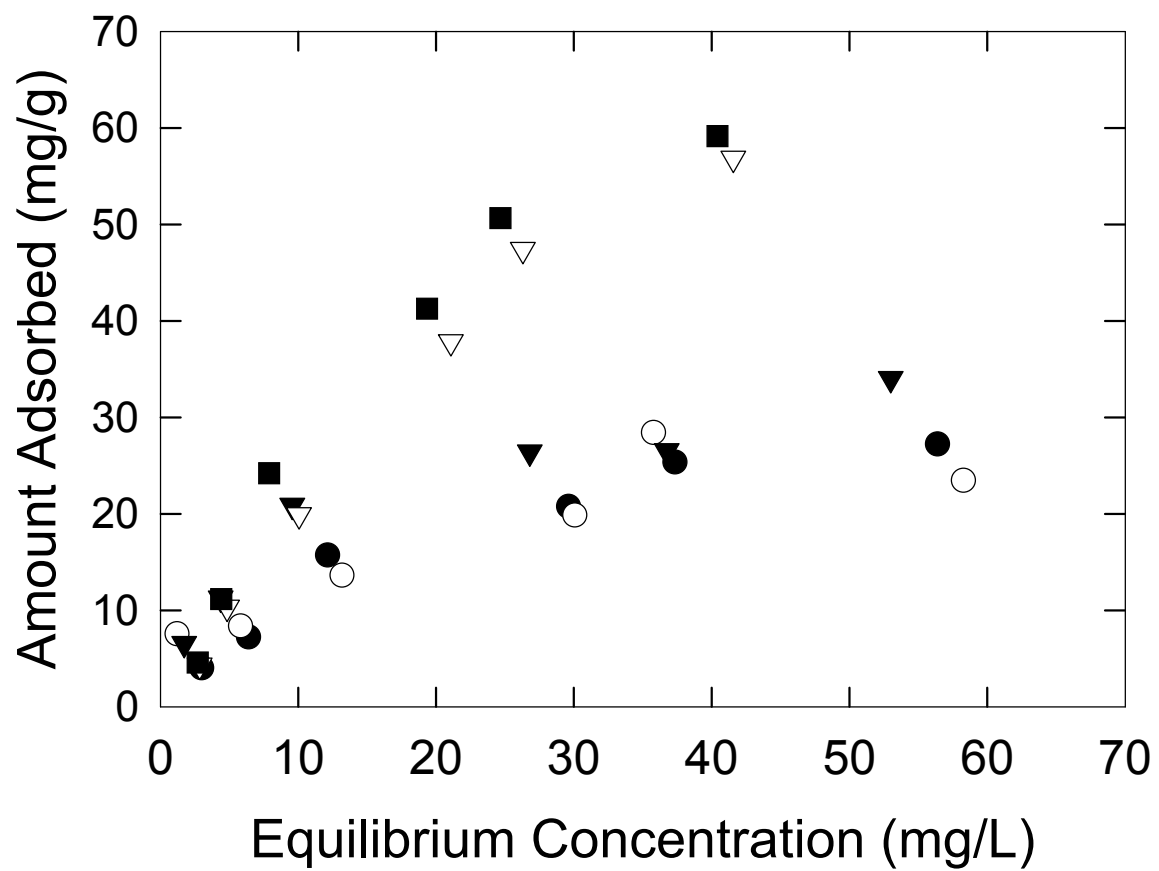


Figure 3. Bob and Walker

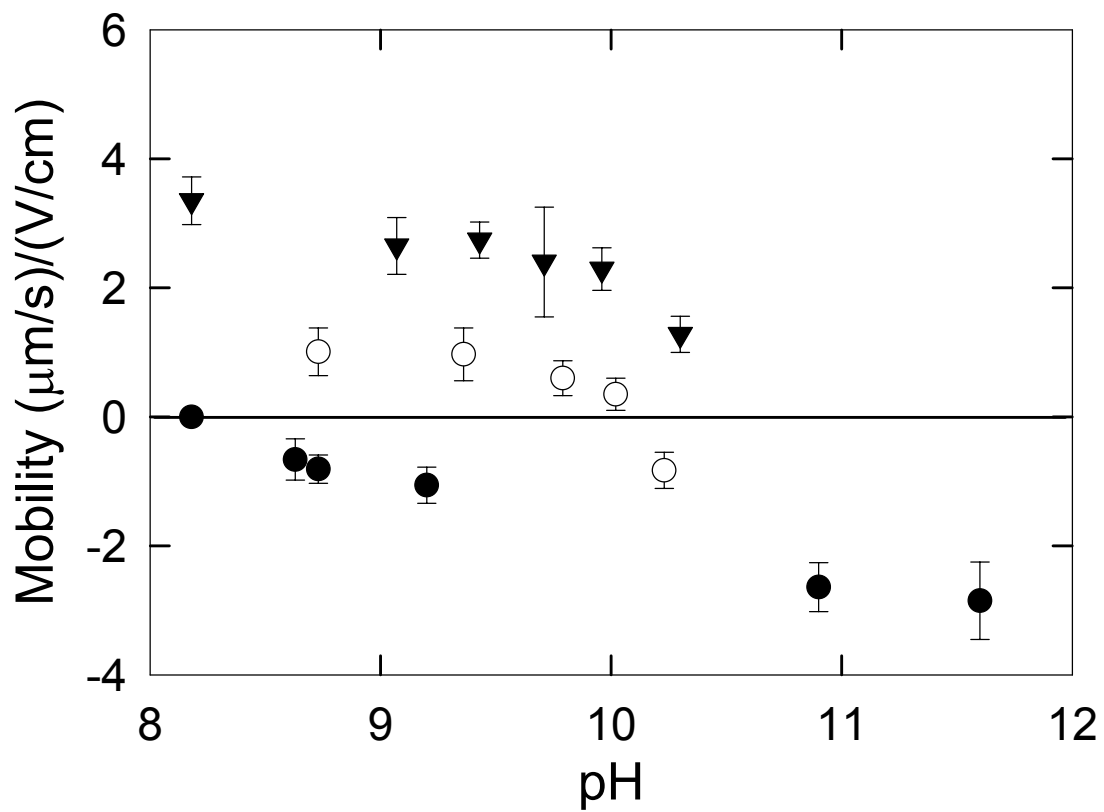


Figure 4. Bob and Walker

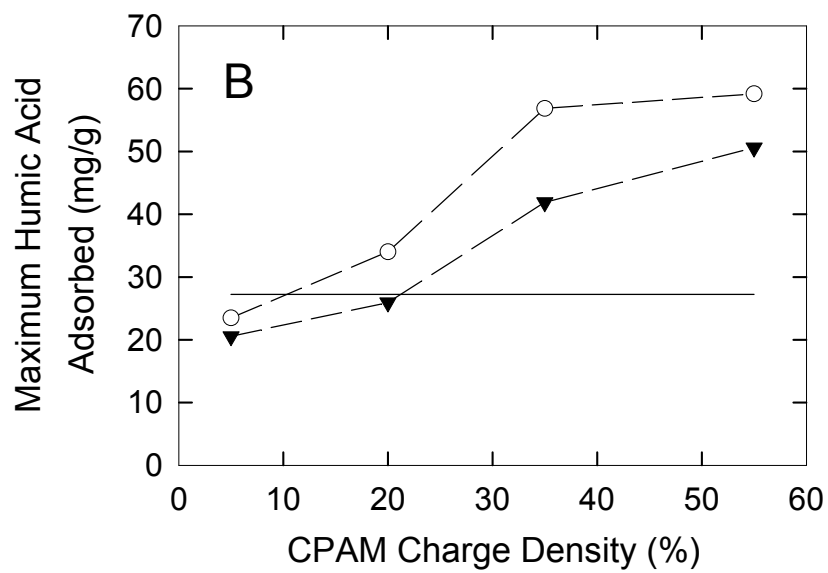
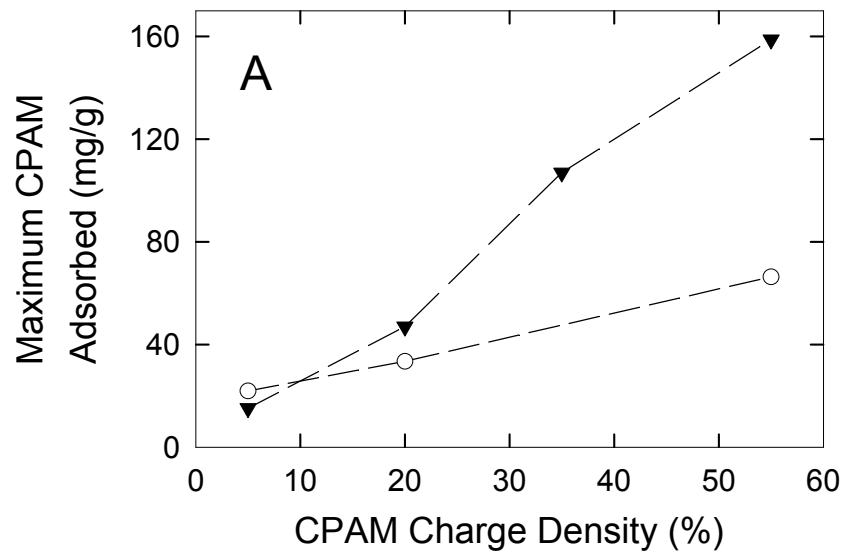


Figure 5. Bob and Walker

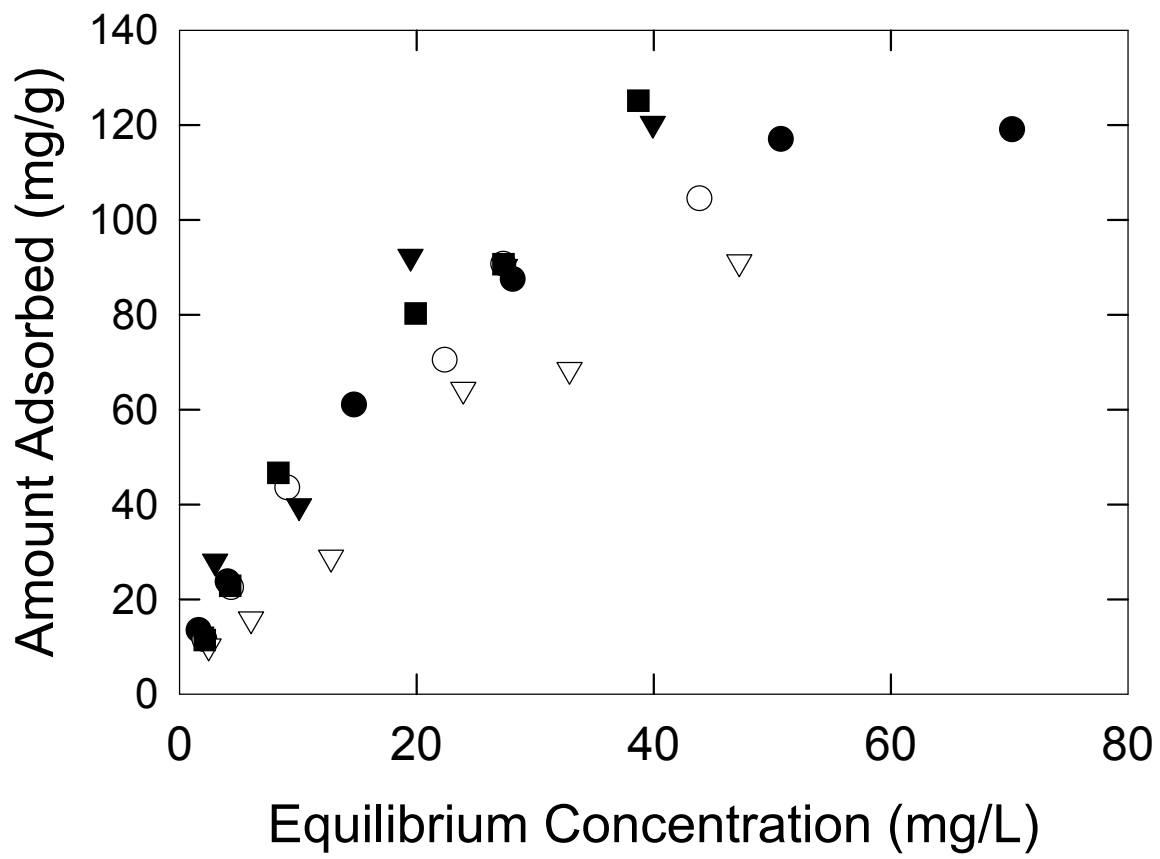


Figure 6. Bob and Walker

Basic Information

Title:	Ultrasonic cleaning of fouled membranes during drinking water treatment
Project Number:	B-05
Start Date:	3/1/1999
End Date:	2/28/2001
Research Category:	Engineering
Focus Category:	Treatment, Water Supply, Water Use
Descriptors:	
Lead Institute:	Ohio State University
Principal Investigators:	Harold Webb Walker, Linda K. Weavers

Publication

1. Lamminen, M. O. (expected 2003). Ultrasonic Cleaning of Fouled Membranes During Drinking Water Treatment [dissertation]. Department of Civil and Environmental Engineering and Geodetic Science, The Ohio State University, Columbus, Ohio.
2. Lamminen M. O, Walker H. W., Weavers L. K. 2000. Sonochemical cleaning of humic acid fouled membranes [abstract]. In : Pacifichem 2000; Dec 14-19; Honolulu, HI.

Final Report

Ultrasonic Cleaning of Fouled Membranes During Drinking Water Treatment

Focus Categories: TRT, WS, WU

Project Duration: Mar. 1 1999 to Feb. 28, 2001

Total Federal Funds: \$50,000

Total Non-Federal Funds: \$100,000

Congressional District: 15th Congressional District

Harold W. Walker

Department of Civil and Environmental Engineering and Geodetic Science
The Ohio State University
Columbus, Ohio 43210

[phone] (614) 292-8263
[fax] (614) 292-3780
[email] walker.455@osu.edu

Linda K. Weavers

Department of Civil and Environmental Engineering and Geodetic Science
The Ohio State University
Columbus, Ohio 43210

[phone] (614) 292-4061
[fax] (614) 292-3780
[email] weavers.1@osu.edu

Problem and Research Objectives

The presence of pathogens in surface water poses a serious threat to the safety of public drinking water supplies. For example, in 1993 Milwaukee Wisconsin experienced the largest single outbreak of waterborne disease in U.S. history [1]. The outbreak, which occurred due to the presence of *Cryptosporidium parvum* in drinking water obtained from Lake Michigan, resulted in over 400,000 confirmed cases of gastrointestinal disease.

Other confirmed etiological agents involved in waterborne outbreaks of gastrointestinal disease include *Giardia lamblia*, *Shigella sp.*, and *Escherichia coli* 0157:H7 [2]. As a result of the health effects associated with microbial pathogens and other drinking water contaminants, nearly 40% of water treatment plants in the United States will have to upgrade their systems by 2001 at an estimated cost of \$10 billion [3]. It is estimated that 80% of water treatment facilities will have to make changes to meet regulatory requirements by the year 2005 [3].

The United States Environmental Protection Agency (USEPA) Surface Water Treatment Rule (SWTR) mandates specific removal requirements during drinking water treatment for pathogens such as *Giardia* (99.9% removal) and viruses (99.99%) [4]. These removal requirements apply to all water treatment plants utilizing surface water, or groundwater under the direct influence of surface water, and serving greater than 10,000 people. The Enhanced Surface Water Treatment Rule (ESWTR) broadens these requirements and specifies that utilities must also demonstrate 99.0% removal for the pathogen *Cryptosporidium* [5]. The Long Term ESWTR will specify that small systems serving less than 10,000 people also meet the removal requirements of the SWTR and ESWTR.

Membrane processes will likely play a major role in meeting upcoming removal requirements for drinking water treatment. Presently, a number of large-scale membrane filtration plants (0.6 to 37 million gallons per day) have been constructed for treating drinking water [6]. Membranes are gaining increased acceptance for use in drinking water applications. They are especially attractive for small systems because of their

ability to meet multiple water treatment requirements. For example, membrane filtration is effective at removing particulates and pathogens, as well as organic molecules that contribute to the formation of disinfection by-products. Membrane filtration is currently listed as a USEPA compliance technology for small systems to meet the SWTR [7].

Although membrane systems are versatile, they can be prone to fouling which reduces flux and decreases productivity. The cleaning processes used to restore productivity can be broadly characterized as being physical, chemical or electrical techniques. Physical processes to increase permeate water flux include low and high frequency backwashing [8,9,10,11,12], cross-flow shearing [13], and bubbling [14]. Chemical processes are the commonly used techniques in practice and include acid/base treatment [15] and the use of surfactants. Both of these process types are limited in that they are labor intensive and require significant downtime. There may also be a limitation to the effectiveness with which the membrane can be restored using these techniques [15]. Electrical processes are relatively new and involve either applying a direct or alternating current to the membrane surface to remove deposited particles [16,17,18]. This technique is attractive in that it requires little or no downtime. However, application of an electric field can result in a change of water pH and electrolysis at the electrode surface. In addition, electrical cleaning processes can result in electro-coating of membrane surfaces for solutions with high hardness or metal contents.

In this research, a new approach for decreasing membrane fouling during drinking water treatment was investigated. In particular, systematic experiments were carried out to look at possible ultrasonic cleaning mechanisms and quantify their effect on the

cleaning of membrane surfaces. Ultrasound has many benefits, which have been documented by other researchers in previous research [19,20,21,22,23,24]. Previous studies have shown that ultrasound can be used for cleaning or maintaining membranes in bench scale water treatment systems [19,20,23,24,] and there have been several studies on the use of ultrasound for membrane distillation [21,22], but none have looked at the mechanisms controlling the removal of foulants. Ultrasound has been shown to improve the filtration rates of flat sheet systems operating in cross-flow mode [19,20,23,24]. Most systems have used a cross flow system with the entire cell submerged in a sonicating bath while one researcher subjected a small portion of the membrane surface to ultrasound [24]. It was found that ultrasound could remove the cake or gel layer relatively easily, while it was more difficult to remove the contaminants lodged within the pores of the membrane [23].

These studies suggest that ultrasound may be a viable alternative to current membrane cleaning processes. Although these previous studies show promising results, the ultrasonic mechanisms affecting the removal of fouling materials from the membrane surface are still unknown. In order to know what factors in a real-world system are most important, and to design the most effective ultrasonic cleaning systems, it is essential to know which mechanisms control the cleaning process.

The application of results generated from this research in drinking water treatment will lead to a number of practical benefits. Benefits that may accrue include a more reliable and less costly treatment approach for small systems and lower chemical costs for large plants utilizing membrane processes. In addition, application of this research

may lead to a decrease in the negative health effects associated with microbial pathogens by facilitating the widespread application of membrane technology.

Methodology

All experiments were carried out using Anodisc gamma alumina ceramic membranes (25 mm diameter) manufactured by Whatman (NJ). The pore size of the membranes used was 0.2 μm , while the membrane thickness was approximately 60 μm . This material was selected for its resistance to high temperatures, to limit the possibility of high temperature alteration as cavitation bubbles created at certain frequencies collapse near or on the membrane surface. A number of previous studies have utilized these membranes, so they are well characterized [25,26,27,28]. Alumina is also a good sound reflecting material and thus offers the potential of facile cleaning by ultrasound [29]. Membrane pores are large enough to allow for clear imaging using SEM, and therefore, can be visually inspected for any defects or damage as a result of ultrasonic treatment.

The filtration apparatus, which was used for all experiments, was an Amicon Ultra Filtration (Bedford, MA) 10 mL small stirred cell. This cell operates in dead end mode with all of the solution being forced through the membrane. This cell was fed from a larger Nalgene polypropylene 4L mixing vessel. The driving force for the system was an ultra high purity nitrogen gas cylinder pressurizing the mixing vessel to a pressure of 10 psig. All system components were rigorously cleaned following each run.

The particles that were chosen to foul the membranes were sulfate latex particles obtained from Interfacial Dynamics Corporation (Portland, OR). The particles were negatively charged as stated by the manufacturer and confirmed by zeta potential

measurements using a ZetaPlus (Brookhaven Instruments Corp, Brookhaven, NY). The particles used for all of the experiments had a diameter of 0.5 μm . These nearly spherical particles were selected because of their monodisperse size distribution and due to the availability of different sizes and charges from the manufacturer for future experiments. The sulfate latex particles attach to the surface of the positively charged membrane quite strongly and cannot be removed with simple agitation or washing. Also, these particles were very effectively examined using SEM.

Following fouling of the membrane, the membrane was removed and cleaned in a glass vessel attached to an ultrasonic transducer manufactured by L3 Communications Elac Nautik (Kiel, Germany). The membrane was held in place using several sheets of Mylar[®] which were then clamped to a stainless steel stand. Mylar[®] was used because it was found to be acoustically invisible and did not affect the acoustic energy of the system [30]. The stainless steel stand holding the membrane was suspended a fixed distance of 10.5 cm away from the transducer. The ultrasonic unit used in these experiments has several different frequencies: 1062 kHz, 620 kHz, 340 kHz and 205.5 kHz. The power was manipulated using the controls on the generator from 1-100W. Calorimetry was performed on the system to measure the accuracy of the generator and the measured value was within 5-10% of the displayed value.

The following procedure was used to determine the effectiveness of ultrasonic cleaning. The membrane was initially weighed using a Fisher Scientific (Springfield, NJ) balance with a readability of 0.1 mg. The membrane was then placed into the filtration cell and filled with 8ml of Milli-Q water (Bedford, MA). All solutions were prepared using Milli-Q water with a resistivity of 18.2 M Ωcm with a total organic carbon

concentration of less than 5-10 $\mu\text{g/L}$. The initial flux was measured using a solution of 1 mM potassium chloride that had been pH adjusted to 7.00 with 0.1 N sodium hydroxide solution. This flux measurement was done over a period of five minutes. The potassium chloride salt solution acts as a swamping electrolyte.

The membrane was then removed and inspected visually and placed back into the filtration cell. Using the same procedure as was used for the clean solution, the fouling latex solution was then passed through the membrane. The solution consisted of 10 mg/L sulfate latex, with 1 mM potassium chloride and a pH that was adjusted to 7.00 with 0.1 N sodium hydroxide. The membrane was fouled until the flux was about 20% of the original flux measured in the absence of sulfate latex particles.

The fouled membrane was removed from the filtration cell and placed between several sheets manufactured from Mylar[®] (Surplus Sales, NE). These sheets were clamped onto a stainless steel stand. This stand was then placed into a glass sonication vessel, open to the atmosphere, which was filled with 500 ml of Milli-Q water for every experiment. The temperature was maintained at 15°C by a Neslab constant temperature bath. The orientation of the fouled membrane to the transducer surface, the power of the ultrasound, the duration of treatment and the frequency was varied using this system.

Once the membrane had been exposed to ultrasound, the flux was measured using the filtration cell with the potassium chloride pH adjusted solution. The sample was allowed to air dry and prepared for SEM. The “cleaning efficiency” was calculated by dividing the clean membrane flux by the original flux and multiplying by 100%.

Principal Findings and Significance:

Initial experiments showed that ultrasonic cleaning of particles from the surface was very effective. As shown in Figure 1, the initial clean water flux through the clean membrane was approximately 0.21 ml/sec-cm². When sulfate latex particles were added to the feed, the flux rapidly declined reaching approximately 20% of the clean water flux after about 3000 seconds. The membrane was then exposed to ultrasound and the clean water flux again measured. As can be seen in Figure 1, the flux was restored to nearly the original value using ultrasound (99.6% cleaning efficiency).

A number of mechanisms may play a role in the removal of particles from the surfaces of membranes using ultrasound. A list of possible mechanisms include:

Acoustic streaming – the adsorption of acoustic energy which results in the flow of a fluid [31]. This removal mechanism may be more likely to be prevalent near surfaces with loosely attached particles or with surfaces that can dissolve with increased contact of solvent [29].

Microstreaming – A time independent circulation of fluid which occurs near small imperfections. These are localized to regions very close to the imperfections. There are relatively significant shear forces that accompany these movements resulting in a significant affect on the system overall [31].

Cavitation Microstreamers – In a cloud of cavitation bubbles there may be instabilities where a bubble is ejected from the cloud and makes its own way through the fluid at relatively high velocity. This could potentially scour particles from a surface [31].

Shock Waves – A pressure pulse emitted into the surrounding liquid when a cavity collapses. The emitted shock wave may have an amplitude of up to 1 GPa. These shocks

may cause the collapse of other bubbles in the vicinity and initiate a cloud of cavitation, which can result in a much larger effective area [31].

Vibration – Particles may absorb some of the acoustic energy from the wave especially if they are composed of a reflecting material and begin to vibrate.

Microjets – These are formed when a cavitation bubble collapses on a surface. There is an asymmetric collapse of a bubble onto itself followed by an impact of a strong jet of water estimated to flow with a velocity of 100-200 m/s [31].

Turbulence / Acoustic Streaming

To evaluate whether mixing or turbulence could remove particles from the surface, a mixer was introduced to the system to direct water flow directly at the membrane surface. Although this mechanism was not expected to have much effect on the attached particles, it was used as a baseline against which to compare the ultrasonic methods. The mixer may not have subjected the membrane to the same effects as acoustic streaming, although the velocities generated were much more than the 10 cm/sec seen by Starritt et al. [32]. There was virtually no recovery in flux when compared to a sample with no treatment. Figure 2 is an image taken by SEM of the surface of the membrane. It is still completely coated with latex particles, with a thickness of the coating being on the order of a thousand latex spheres.

Because the mixer was not a true representation of ultrasonically generated water flow, the next experiment attempted to observe the difference in behavior of fouled membrane surfaces facing the transducer and facing away from the transducer. In both cases there was a Mylar support underneath so no flow would be allowed to pass through

the membrane, only acoustic energy from the transducer. Since there should be relatively few losses through the Mylar sheet, the differences could most likely be attributed to turbulence-aided cleaning. Through visual observation, there was much more turbulence in the region closest to the transducer than there was in the region above the stainless steel stand. This water movement may not all be attributable to acoustic streaming, and therefore, it will be defined simply as turbulence. For a couple of different power settings it was noticed that there was a large difference in cleaning efficiency. Using 620 kHz and five seconds of treatment with power setting of 10W, the cleaning efficiency was 98% with the fouled surface facing the transducer and 81% with it facing away. Because effective cleaning was observed for both membrane orientations suggests that turbulence was not the primary mechanisms controlling removal of deposited particles.

While turbulence was likely not the primary mechanism removing particles from the surface, it may act to facilitate removal of loosened particles. Scanning electron microscopy (see Figures 3 and 4) showed that the surfaces of the two membranes facing the transducer had far fewer particles still attached and had areas of membrane surface exposed, while the surfaces not facing the transducer were still heavily coated with particles.

Cavitation mechanisms

The next series of experiments examined the relationship of cleaning efficiency with respect to power. An increase in power should lead to an increase in the number of cavitation bubbles formed without decreasing the violence of the collapse. Figure 5 illustrates an increase in cleaning efficiency versus power as well as a decrease in the

amount of latex remaining on the surface. These runs were all done with the membrane facing away from the transducer at 620 kHz with a sonication time of 5 seconds. A clear trend can be seen that with increasing power there is increased particle removal, suggesting cavitation is an important particle removal mechanism.

The next series of experiments examined the cleaning efficiencies for four different frequencies. With increasing frequency, there are generally more cavitation bubbles [31], although they tend to collapse less violently, with lower temperatures and pressures. There was very little difference in the cleaning efficiency of the lower frequencies, 620, 354 and 205 kHz, with cleaning efficiencies all being near 90%. The cleaning efficiency of the highest frequency, 1054 kHz, was much lower with a value of less than 45%. This lower cleaning efficiency may have been due to less violent cavitation at this higher frequency. Less violent cavitation results in lower energy release, which may inhibit detachment of particles from the surface.

SEM of membranes

SEM of the membranes showed very interesting formations developing during sonication of the fouled surfaces, and provided additional information on important mechanisms controlling particle removal. There were 3 major types of formations that appeared on virtually all of the membranes, regardless of frequency, power of the generator, or time of treatment. The first type of formation was a small indentation, which appeared to be a small spherical impression on the surface of the latex cake layer. This is seen in Figure 6. The indentations did not sink very deeply into the latex cake layer and did not disturb the latex particles adjacent to the formation. The average diameter

of these cavities was about 18 μm with a standard deviation of about 6 μm . This was very similar in shape and size to the damage caused by microjets on metal surfaces, although the metal requires much more irradiation [33]. The latex material was not quite as sturdy as the metal, but because the latex surface is porous there is an escape route for the water once it has impacted the surface whereas in metal there is no escape for water flow.

The second type of formation was a large patch of removal of varying shape, with an average diameter of about 2.30 mm and a standard deviation of 0.67 mm. This is seen in Figure 7. This patch appeared almost as soon as ultrasound began, with the number of patches increasing with time until finally the entire surface was void of large cake formations of latex particles. This appeared to be the main source of particle removal. This removal is speculated to be due to microstreaming since most of the literature on this topic attributes the cause for most surface cleaning to microstreaming. Whether other mechanisms can play a role initiating this large removal or create nuclei for microstreaming to act upon is still not determined.

On the edges of these large patches of removed particles, there were channels as long as a millimeter in length where particles have been scoured. These channels can be seen in Figure 8. These may be from cavitation microstreamers, which are simply cavitation bubbles that are ejected from the bubble cloud. They may scour out the paths possibly making it easier for removal by microjets and microstreaming to develop. Another possibility is that the channels arise from water flow to and from the microstreaming that is taking place in the center of the large patch of removal.

Evidence as to ultrasonic induced damage to the membrane surface:

There has been no evidence, neither with extensive SEM images of the membrane surface, nor with measurement of aluminum concentrations in the cavitating solution using an ICP-OES, of any damage to the membrane surface as a result of ultrasonic treatment. This may be a result of the resistance of the membrane material to the high temperatures and pressures or a result of the short treatment times used for cleaning. Membranes were also subjected to ultrasound for periods of over an hour and no damaging effects on the membrane were found.

Summary

The results of this research have shown that it is possible to effectively clean fouled membranes using ultrasound. Increasing the power of irradiation produces higher cleaning efficiencies up until a certain power after which very small gains are made for large increases in power. Experiments using different frequencies also showed that there was very little difference in cleaning efficiencies except with the highest frequency (1062 kHz). This frequency produced very little cleaning of the membrane surface most likely as a result of soft cavitation. No damage to the membranes due to ultrasound was observed.

Several mechanisms are important in the removal of particles from the surface of membranes. The most significant mechanism appears to be microstreaming. Evidence of microjets and cavitation microstreamers were present on the surface of the fouled membranes as well, but not to the same extent as microstreaming. Turbulence or acoustic streaming was found to be a mechanism which aids in the cleaning process, but it is not the primary removal mechanism.

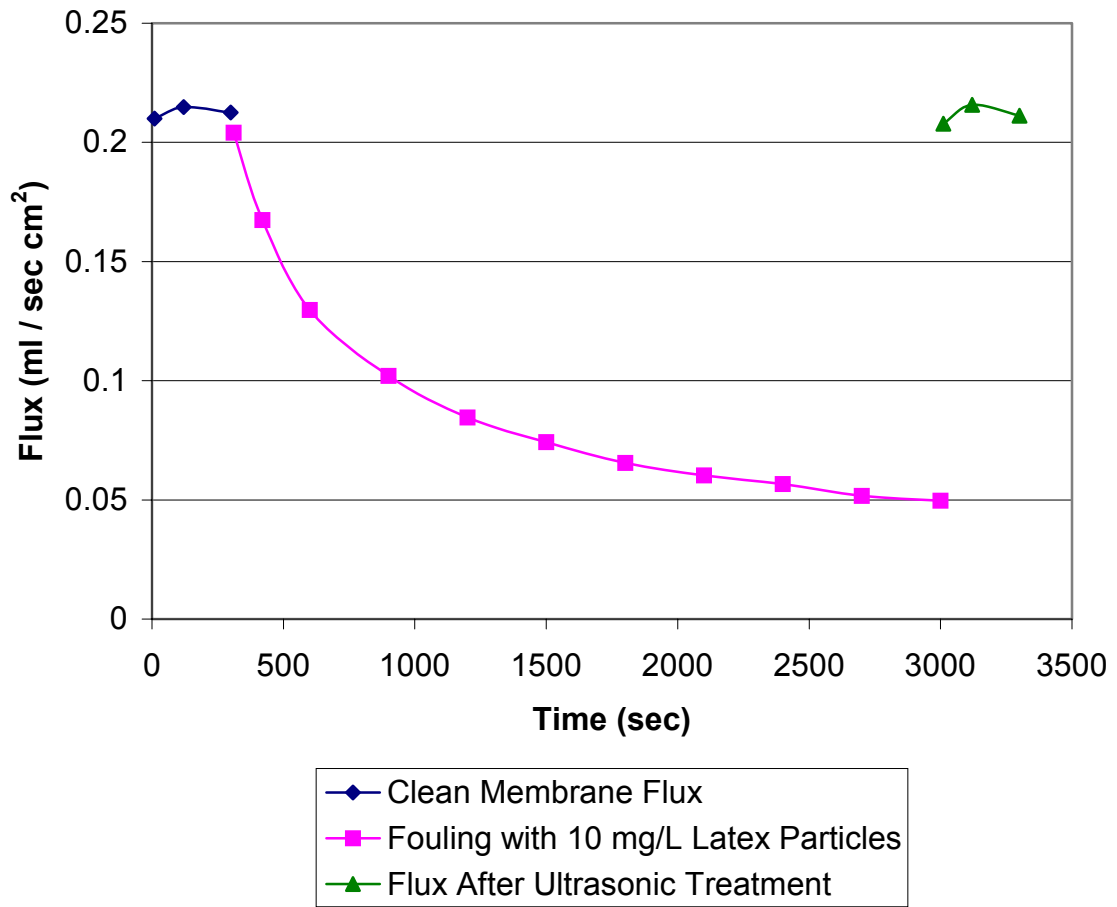


Figure 1. Flux of membrane before and after fouling with 10 mg/L sulfate latex particles. The frequency used was 205.5 kHz at 50 W with the fouled surface of the membrane facing the transducer for a duration of 5 minutes.

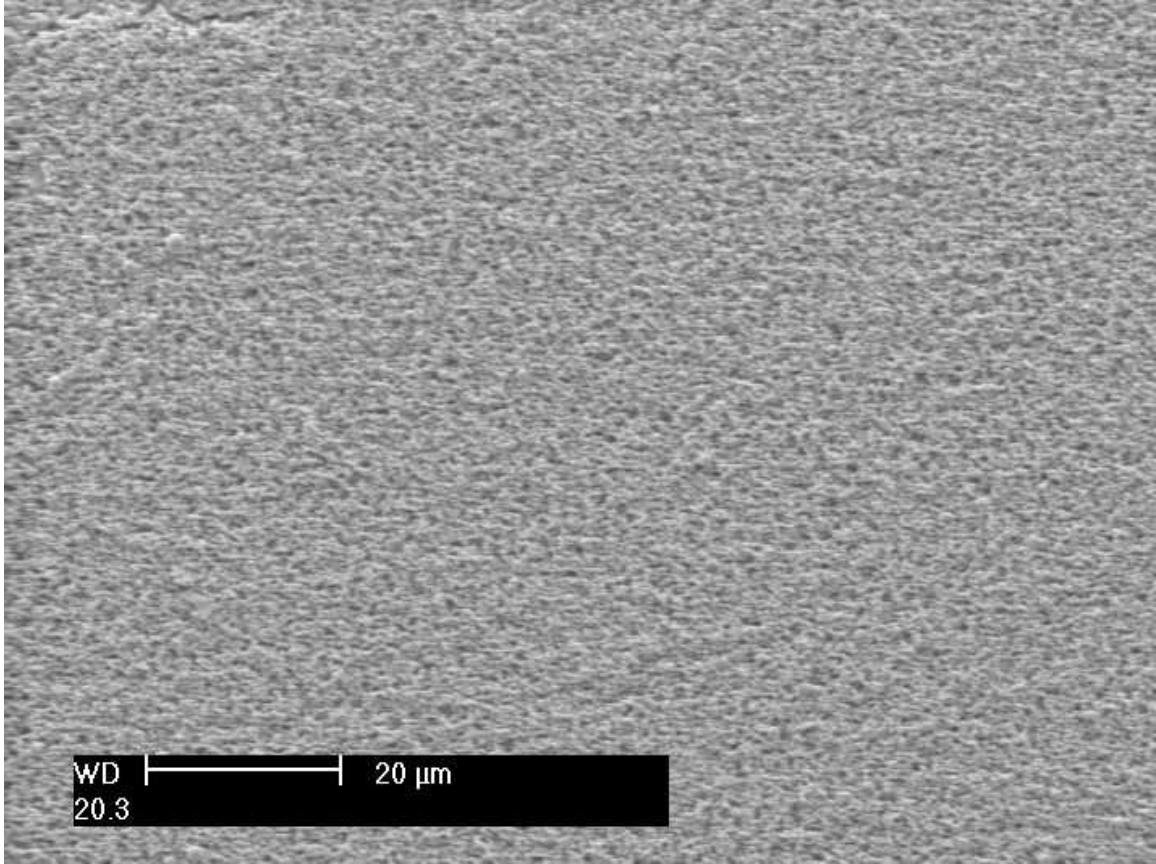


Figure 2. SEM image of the surface of a membrane treated only with a mixer which generates turbulence.

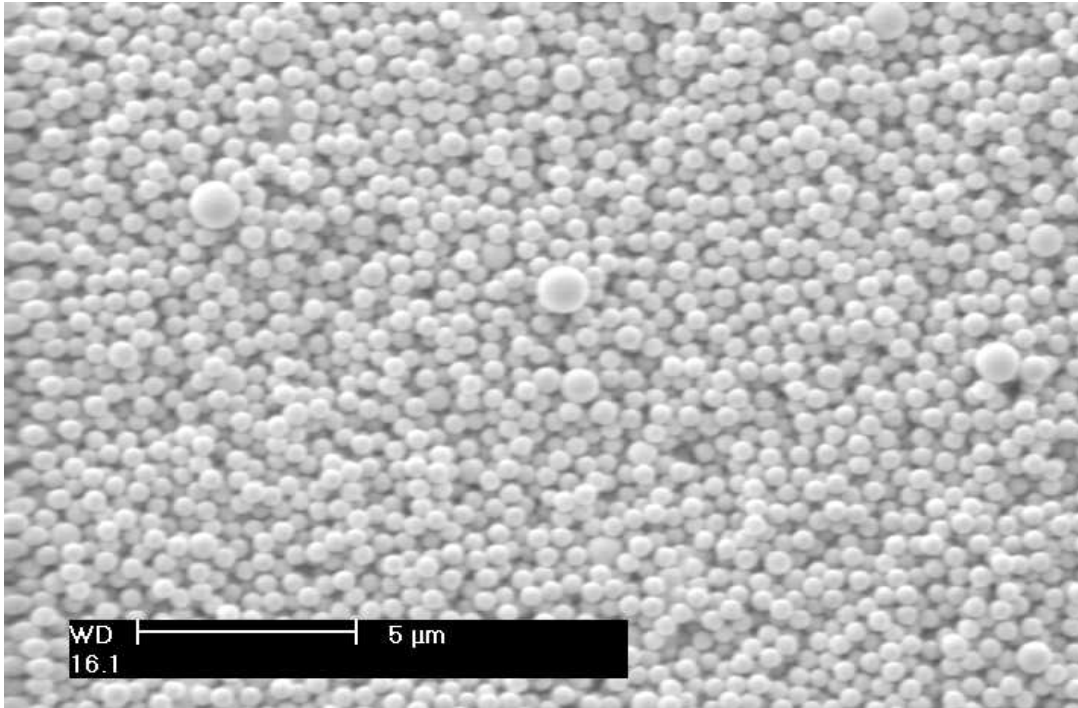
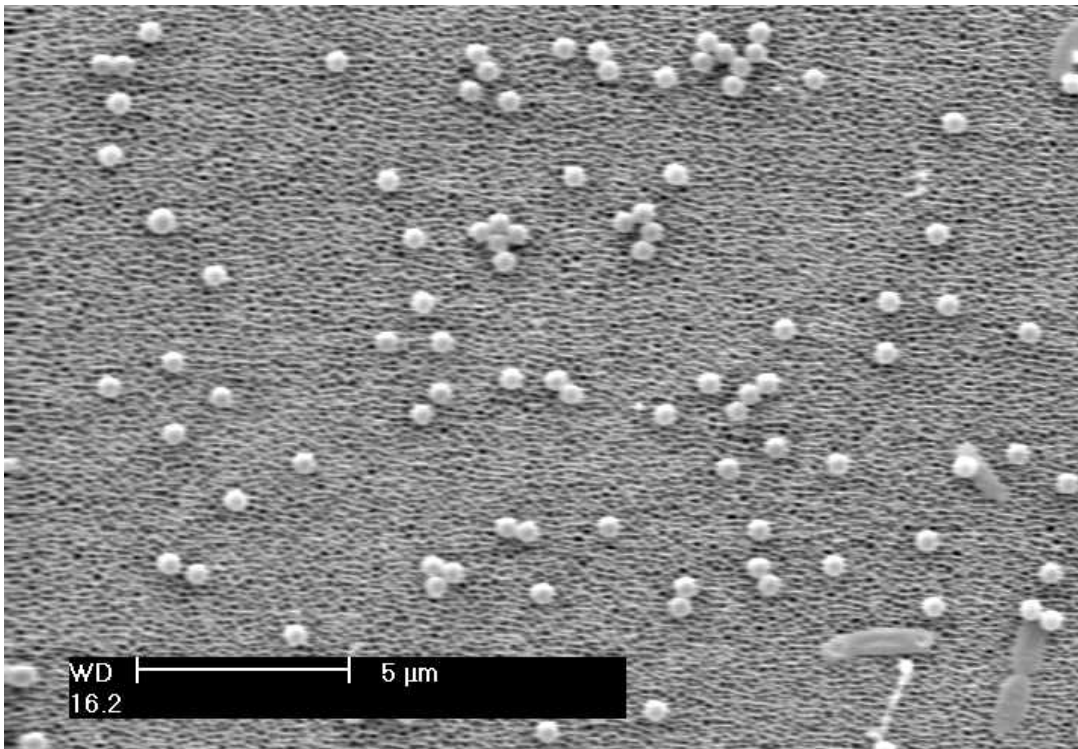


Figure 3. SEM of a membrane in which the fouled surface was not facing the transducer. 620 kHz, 10 W with 5 seconds of treatment time.



Figures 4. SEM of a membrane in which the fouled surface was facing the transducer. 620 kHz, 10 W with 5 seconds of treatment time.

Cleaning efficiency vs. Power

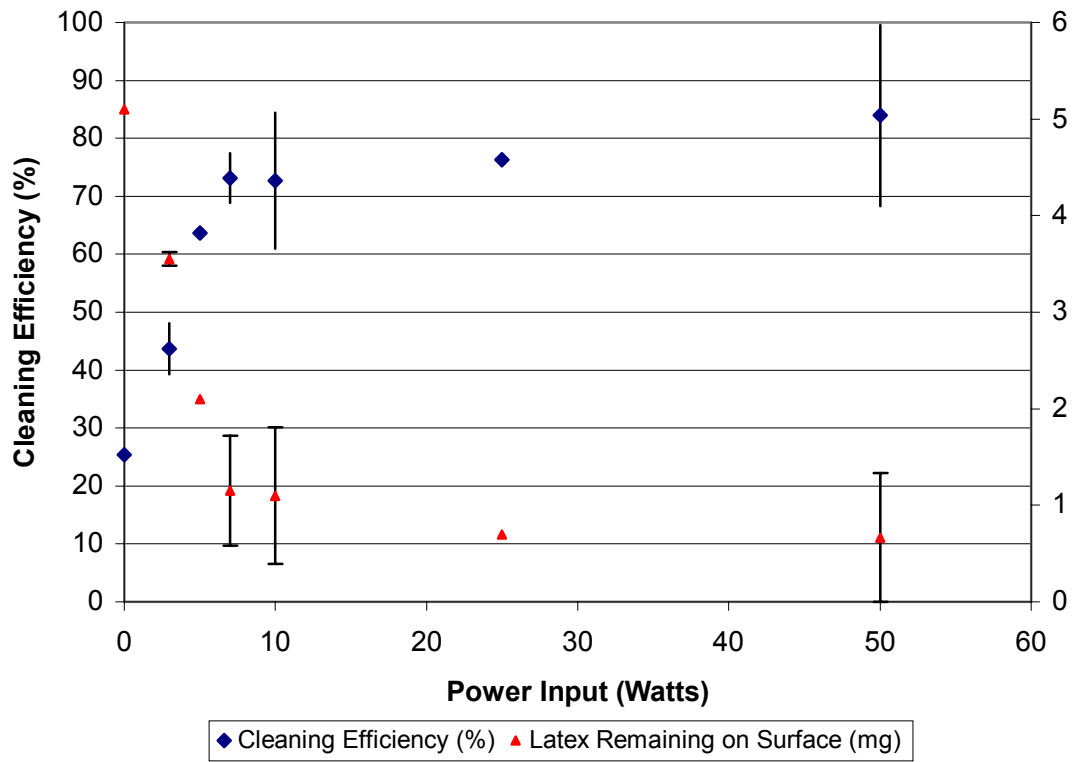


Figure 5. Cleaning efficiency of ultrasonic system at 620 KHz, with 5 seconds of treatment and differing powers.

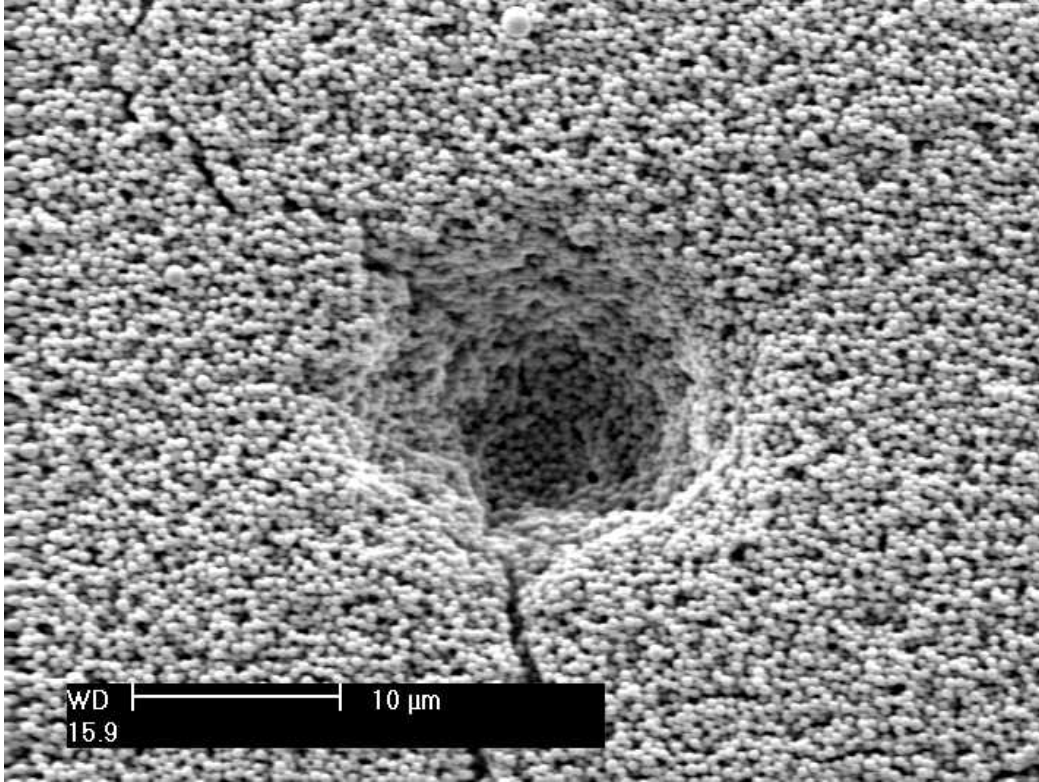


Figure 6. Image of a indentation made by a microjet

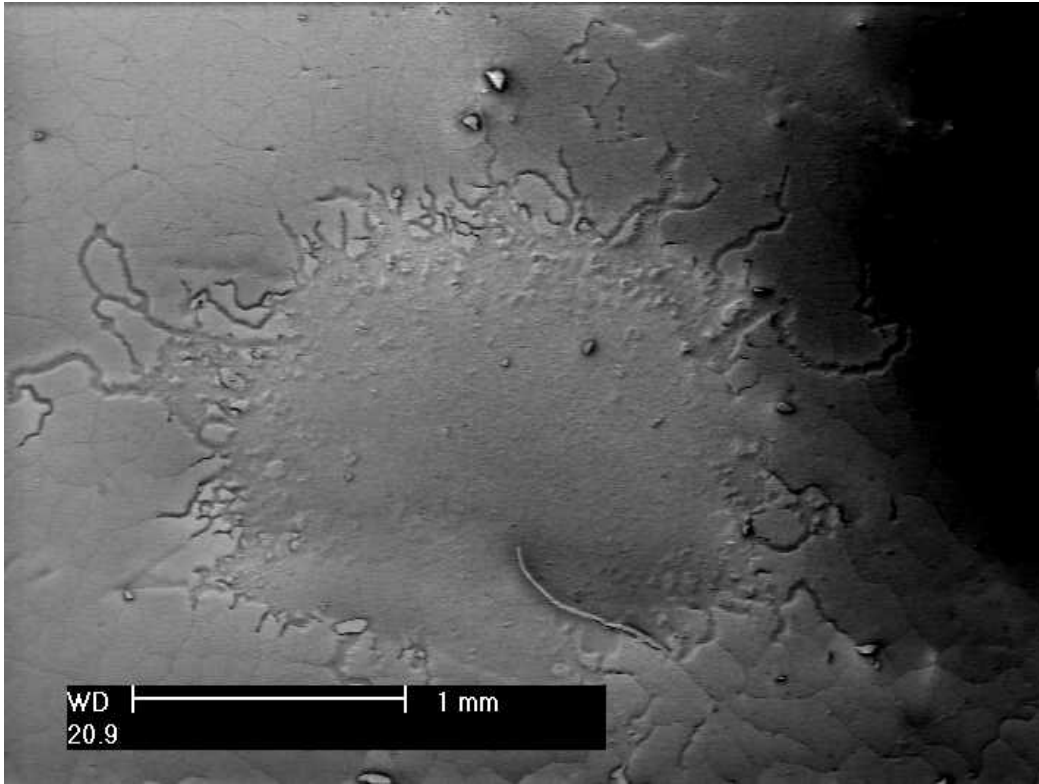


Figure 7. Image of a large patch of removal attributed to microstreaming.

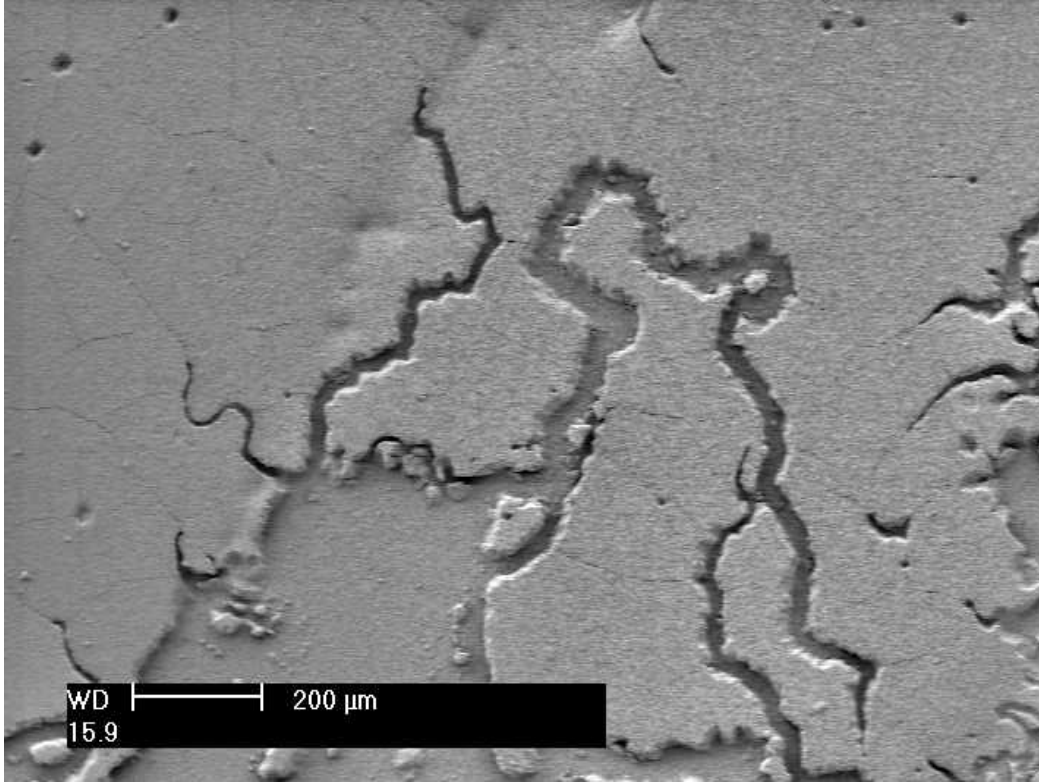


Figure 8. Image of channels extending from the large patches of removal, which may be caused by cavitation microstreamers.

DISSERTATIONS

Lamminen, M. O. (expected 2003). Ultrasonic Cleaning of Fouled Membranes During Drinking Water Treatment [dissertation]. Department of Civil and Environmental Engineering and Geodetic Science, The Ohio State University, Columbus, Ohio.

OTHER PUBLICATIONS

Lamminen M. O, Walker H. W., Weavers L. K. 2000. Sonochemical cleaning of humic acid fouled membranes [abstract]. In : Pacifichem 2000; Dec 14-19; Honolulu, HI.

PRESENTATIONS

Lamminen M. O., Walker H. W., Weavers L. K. 2000. Sonochemical cleaning of humic acid fouled membranes [presentation]. In : Pacifichem 2000; Dec 18; Honolulu, HI.

References

1. W.R. McKenzie et al., *New England Journal of Medicine*, 331, pp.161-194, 1994.
2. M.H. Kramer, et al., *Waterborne Disease:1993 and 1994*, *Journal of AWWA*, 88(3), pp. 66-80, 1996.
3. Anonymous, *Civil Engineering Magazine*, page 8, 1998
4. *Surface Water Treatment Rule*, *Federal Register*, 1989.
5. *Enhanced Surface Water Treatment Rule*, *Federal Register*, 1994.
6. N.M. Zeilig, *Large scale plants show promise*, *J. AWWA*, 89(10), p 39, 1997.
7. *Small system compliance technology list for the surface water treatment rule and total coliform rule*, *United States Environmental Protection Agency*, 1998.
8. A.G. Fane, J.C.D. Fell, *Desalination*, 62, pp. 117-136, 1987.
9. M.H.V. Mulder, *Membrane Separation Technology- Principles and Applications*, Elsevier: Amsterdam, 1995.
10. H.V. Baeyer, *Trans. ASAIIO*, 24, p. 739, 1983.
11. G. Belfort, T.F. Baltutis, and W.F. Blatt, *Polym. Sci. Technol.*, 13, p. 439, 1980.
12. V.G.J. Rodgers, *AICHE Journal*, 37(10), pp. 1517-1528, 1991.
13. M.X. Porter, *handbook of Industrial Membrane Technology*, Noyes: Park Ridge, NJ, 1990.
14. C.K. Lee, Y.G. Chang, Y.H. Lee, *Biotechnol. Bioengin.*, 41, pp. 525-530, 1993.
15. A. Braghetta, et al., *J. AWWA*, 89(1), pp.90-101, 1997.
16. S.P. Moilik, F.C. Cooper, M. Bier, *J. Colloid and Interface Sci.*, 24, pp. 427-432, 1967.

17. P.V. Zumbusch, W. Kulcke, G. Brunner, *Journal of Membrane Science*, 142, pp. 75-86, 1998.
18. C.W. Robinson, et al., *Journal of Membrane Science*, 80, pp.209-220, 1993.
19. T. Kobayashi, X. Chai, N. Fujii, Ultrasound enhanced cross-flow membrane filtration, *Separation and Purification Technology*, 17, pp 31-40, 1999.
20. X. Chai, T. Kobayashi, N. Fujii, Ultrasound-associated cleaning of polymeric membranes for water treatment, *Separation and Purification Technology*, 15, pp. 139-146, 1999.
21. C. Zhu, G. Liu, Modelling of ultrasonic enhancement on membrane distillation, *Journal of Membrane Science*, 176, pp. 31-41, 2000.
22. C. Zhu, G.L. Liu, C.S. Cheung, C.W., Leung, Z.C. Zhu, Ultrasonic stimulation on enhancement of air gap membrane distillation, *Journal of Membrane Science*, 161, pp. 85-93, 1999.
23. T. Kokugan, Kaseno, S. Fujiwara and M. Shimizu, Ultrasonic Effect on Ultrafiltration Properties of Ceramic Membrane, *Membrane*, 20 (3), 213-223 (1995).
24. X. Chai, T. Kobayashi, N. Fujii, Ultrasound effect on cross-flow filtration of polyacrylonitrile ultrafiltration membranes, *Journal of Membrane Science*, 148, pp. 129-135 (1998).
25. H. Li, A.G. Fane, H.G.L. Coster, S. Vigneswaran, Direct Observation of particle deposition on the membrane surface during crossflow microfiltration, *Journal of Membrane Science*, 149, pp. 83-97, 1998.

26. T.J. Su, J.R. Lu, Z.F. Cui, R.K. Thomas, R.K. Heenan, Application of Small Angle Neutron Scattering to the in Situ Study of Protein Fouling on Ceramic Membranes, *Langmuir*, 14, pp. 5517-5520, 1998.
27. N.J. Marston, B. Vincent, Adsorption kinetics of polymers in membranes: change of layer thickness with solvency, *Colloids and Surfaces A: Physicochemical and Engineering Aspects*, 141, pp. 73-79, 1998.
28. D.R. Pesiri, R.C. Snow, N. Elliott, C. Maggiore, R.C. Dye, The characterization of asymmetric alumina membranes by Rutherford backscattering spectrometry, *Journal of Membrane Science*, 176, pp. 209-221, 2000.
29. K.S. Suslick, *Ultrasound Its Chemical, Physical, and Biological Effects*, VCH Publishers, Inc., New York, New York, 1988.
30. S.I. Madanshetty, *Acoustic Dosimetry for Sonochemistry*, Sonochemistry and Sonoluminescence, L.A. Crum et al. (editors), Kluwer Academic Publishers, Netherlands, 1999.
31. T.G. Leighton, *The Acoustic Bubble*, Academic Press, Inc., San Diego, CA, 1994.
32. H.C. Starritt, F.A. Duck, V.F. Humphrey, An experimental investigation of streaming in pulsed ultrasound fields, *Phys Med Biol*, 36, pp 1465-1474, 1991.
33. H.C. Man, C.T. Kwok, T.M. Yue, Cavitation erosion and corrosion behaviour of laser surface alloyed MMC of SiC and Si₃N₄ on Al alloy AA6061, *Surface and Coatings Technology*, (132), pp. 11-20, 2000.

Basic Information

Title:	In-Situ Destruction of Solvents by Permanganate Oxidation
Project Number:	RF 736453
Start Date:	9/1/1998
End Date:	9/1/2000
Research Category:	Ground-water Flow and Transport
Focus Category:	Groundwater, Toxic Substances, Hydrogeochemistry
Descriptors:	ground water, DNAPL, in-situ remediation, oxidation, potassium permanganate
Lead Institute:	Ohio State University
Principal Investigators:	Frank Schwartz

Publication

Project No: RF 736453; US Geological Survey 1434-HQ-96-GR-02691

Duration: 9/98-9/00 (6 mo. extension granted)

Title: In-Situ Destruction of Solvents by Permanganate Oxidation

Investigator:

Dr. F.W. Schwartz,
Department of Geological Sciences,
The Ohio State University

Congressional District: Ohio 15th

Focus Categories: GW, TS, HYDGEO

Descriptors: ground water, DNAPL, in-situ remediation, oxidation, potassium permanganate

Problem and Research Objectives

The contamination problems posed by chlorinated solvents, like PCE, TCE, and DCE are well known. When dissolved in contaminant plumes or present as DNAPLs, solvents pose an extremely difficult challenge in cleanup. For the past six years, our research group has undertaken fundamental studies to explore reaction pathways, and the kinetics of reactions of oxidation reactions involving MnO_4^- . This study takes the next logical step in moving from small-scale batch and column tests to large-tank tests. The objectives of the study are:

- (i) to undertake proof-of-concept studies to determine the efficacy of DNAPL removal in large-scale flooding schemes,
- (ii) to elucidate how the efficiency of DNAPL removal is influenced by flow bypassing due to multiphase effects and the presence of reaction products, CO_2 and MnO_2 , and
- (iii) to develop further promising electrical and optical monitoring schemes.

Methodology

To meet the objectives of the study, we constructed a large plastic flow tank, 6 ft long, 2 ft wide, and 3 ft deep (Figure 1). Initially, there were problems with leakage around the bottom joints in that necessitated the installation of a tank liner. The tank was instrumented with a line of multi-level samplers down gradient from the emplaced TCE source. These mini-sampling wells consisted of filter points connected to 1/8 in o.d. Teflon tubing and supported by a thin dowel. In addition, we modified the electrical/optical monitoring system developed by Gheith and Schwartz (1998) for use with TCE. Briefly, this system lets us look through the narrow diameter glass-walled

casing into the tank using a CCD camera, and make resistivity measurements with an emplaced system of electrodes installed on the glass column (Figure 1). The modifications involved the addition of gold-coated wire as an electrode, and wires with non-reactive coatings. The wires from each electrode were plugged into a switch box that lets us select an appropriate combination of electrodes to provide a Wenner arrangement for resistivity measurements.

The monitoring system required significant further enhancement before it could be used. The multilevel sampling points in the tank provided water samples that were analyzed for dissolved TCE, Cl^- , and MnO_4^- . The MnO_4^- in particular is useful for tracking the overall reaction. The large number of samples coming out of a tank experiment necessitated the development of rapid sampling approaches.

In this experiment the tank was filled with flint sand. Inlet and outlet chambers are provided at the upstream and downstream ends of the tank for flow control. Water and MnO_4^- solution were pumped into and out of the tank using Ismatec peristaltic pumps (Cole Palmer Instrument Company, Chicago, Illinois). The actual flow-tank experiment involved the emplacement of a zone of residually saturated DNAPL (500 mL TCE) in a zone ($L \times W \times H = 30 \times 16 \times 36$ cm).

To date we have conducted one large flow-tank experiment. The results are now being analyzed in detail. Preliminary details are presented in this report.



Figure 1. Tank experiment for TCE removal with permanganate oxidation. As well as chemical and electrical measurements, monitoring is made possible by 5 sampling ports and 9 glass tubes wired with electrodes.

Down-hole Optical Monitoring System

In order to describe the fluid mixing pattern and TCE removal from the aquifer, an optical monitoring scheme is designed. Nine glass tubes are arranged as a network in the tank and serve as windows to the aquifer. A prototype system was designed in previous studies (Gheith and Schwartz, 1998). These narrow-diameter glass tubes are

sealed at the bottom and have an inside diameter of 16 mm. A 7mm-diameter color CCD camera (ELMO Canada) was sent down in the glass tube to observe the pattern of MnO_4^- spreading and the distribution of MnO_2 . Illumination was provided by a small light bulb positioned below the camera. A 90-degree mirror is attached to the camera to view the aquifer through the wall of glass tube. Images were recorded and stored using an S-VHS video recorder.

In a typical measurement, CCD Camera was lowered down to the bottom of the glass tube and gradually raised up, while recording. Images were taken every day in the first two weeks of the experiment and then every other day for the next two weeks; once for four days for the next two weeks, and once a week for the last two weeks. The recording time for each well in a single observation was on average about three minutes. A set of 19 snapshots was taken from each recording for further still image processing. Each snapshot was analyzed and classified into different categories of chemical reactions.

The visual monitoring system enabled us to define various zones in the tank. Let's first examine how the oxidation of TCE by MnO_4^- is indicated in the visual observations. The oxidation of dissolved TCE (colorless, aqueous) by potassium permanganate (purple, aqueous) produces manganese dioxide (black, solid), chloride ion (colorless, aqueous), and carbon dioxide (colorless, gas). These color patterns can be classified as four zones: (1) a non-reacted purple permanganate solution zone; (2) a black manganese dioxide deposits zone; (3) an oxidation reaction zone; and (4) a non-reacted dissolved TCE zone (Figure 2).

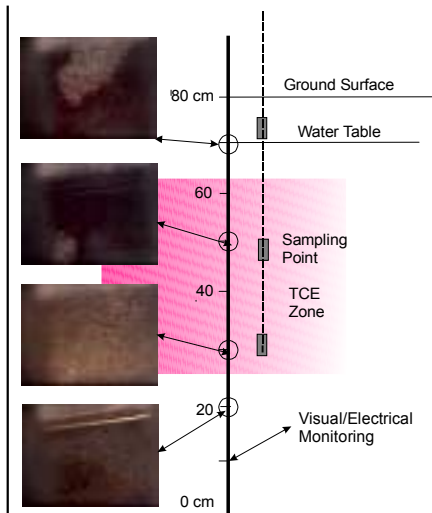


Figure 2. TCE distribution in the tank. From the source zone located left side of tank, the dissolved TCE plume moves with the flow. At the same time, as permanganate reaction progress, the size of TCE plume slowly shrinks.

Electrical Conductivity Monitoring System

Electrical monitoring schemes usually depend on measuring the change in the electrical resistivity over time. Here we utilized a Wenner array configuration involving a set of vertically emplaced electrodes. For an array of current electrodes, A and B , and potential electrodes, M and N inside the current electrodes, the resistivity, ρ , is expressed by the equation

$$\rho = \frac{2\pi}{\frac{1}{AM} - \frac{1}{BM} - \frac{1}{AN} + \frac{1}{BN}} \frac{\Delta V}{I}$$

where I is the current introduced into the earth, and ΔV is the potential difference between the potential electrodes.

Total dissolved solids (TDS) are found to be proportional to electrical conductivity, which is the reciprocal of resistivity. The monitoring scheme uses the relationship between electrical conductivity and total dissolved solids (TDS). Because potassium permanganate (KMnO_4) is very soluble in ground water, as well as one of the products chloride ions (Cl^-), while trichloroethylene (TCE) is sparingly soluble ($\sim 1100\mu\text{g/L}$), measurements of electrical conductivity are useful in monitoring how the KMnO_4^- is being consumed.

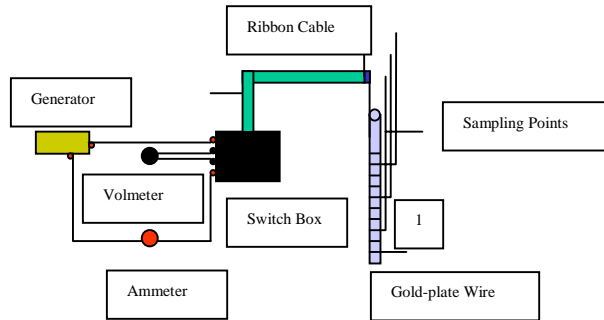


Figure 3. Glass tube (Probe) design and connections of the electrical devices.

Electrodes were equally spaced along a 1.6x89(cm) (DxL) glass tube (Figure 3). The electrodes were made from gold-plate wires wrapped around the surface of the glass tube and equally spaced along the tube at 3.8 (cm) intervals from the bottom. Each electrode was connected to a colored-ribbon cable. Each glass tube has 20 nodes, which creates 17 readings of current and voltage difference. The ribbon cable was plugged into a switch box that determined the appropriate combination of electrodes to provide the resistivity measurements. The voltage difference ΔV was measured between two

successive nodes while the current I is generated between the two outside nodes. This arrangement yielded the average apparent resistivity between the two inner nodes. A direct current, with a low frequency of 60Hz, was generated by arbitrary waveform generator made by The Ohio State Geological Sciences Electrical Shop. The use of low frequency current helped in reducing the polarization at the source and sink nodes and preventing electrolysis. Current and voltage were measured using 6-digit HP Multimeters (HP 34401A). (Figure 4)

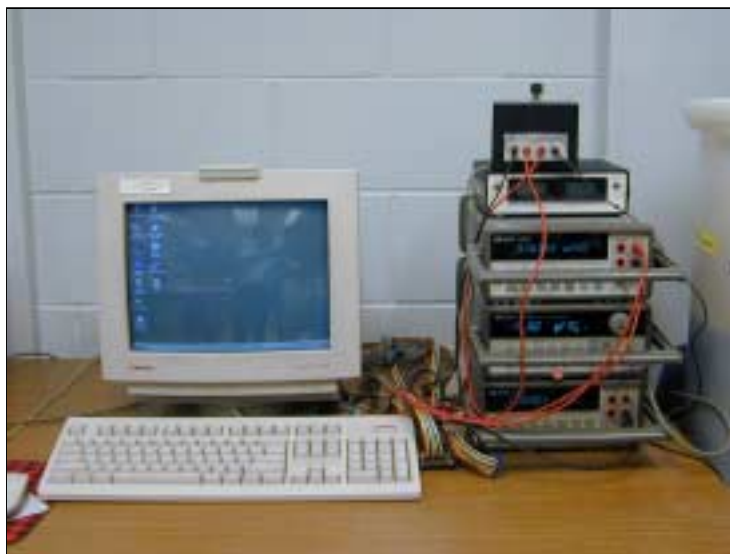


Figure 4. Electrical resistivity measurement devices

Water Sample Chemical Analysis

A line of small sampling wells was emplaced along the centerline of the tank for water sampling. Three sampling points were set at each of the location. Diffusing stones were attached to the end of tubing to filter out any possible solids or sands during sampling. Teflon tubes connected the sampling points to the surface. 1 mL of samples of water were diluted five times for permanganate, chloride and TCE analyses. MnO_4^- is analyzed using Varian Cary 1 UV-visible spectrophotometer at wavelengths ranging from 400 to 700 nm. Cl^- activity was measured with a Labconco Digital Chloridometer (Labconco, Kansas City, Missouri).

3 mL of the diluted sample was collected for UV-vis analysis immediately after each sample was taken. 0.2 mL of Hydrazine Hydrate solution was added to the remaining sample to quench the reaction. 0.1 mL of the quenched sample was then taken for the chloride titration. 1 mL of the remaining sample was transferred to a vial and 4 mL of pentane was added to the vial. The vial was shaken for 1 minute and stored for 20 minutes to enable the sample to reach equilibrium. The upper layer of the prepared sample was extracted for GC analysis.

Samples were taken every other day for the first two weeks; once for four days for the next four weeks, and once a week for the last two weeks. For each round of sampling, we tried to finish the analysis within two hours to keep the results of the experiment consistent. The electrical/optical measurements could not be taken on the same day as the chemical analysis for logistical reasons. Therefore, dates of the graphs shown here have slight time differences.

Flow Control

Background flow was provided with the help of input and output chambers on the upstream and downstream ends of the tank (Figure 5). The input and output chambers were separated from sand by rigid screens with 1.3 cm mesh size. The screens were covered with non-reactive porous material to prevent the sand from entering the chambers. The tank is filled with sands (U.S. Silica, Ottawa, Illinois). This setup provides an ambient flow across the tank.

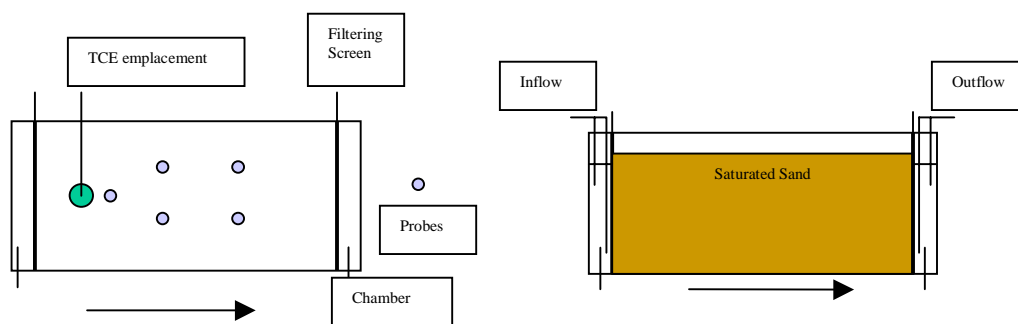


Figure 5. Diagrams of large-scale plastic tank used in the experiment: top view (left) and side view (right). Not all the electrode probes and sampling wells are shown here.

Water was pumped into inflow chamber at a number of locations to create a uniform flow to the upstream end of the tank. The outflow was controlled in the same manner. The source zone ($L \times W \times H = 30 \times 16 \times 36 \text{ cm}$) containing 500 mL of residually saturated TCE was installed near the upstream end of the tank. After the installation of the TCE contaminated zone, the MnO_4^- solution (1250 mg/L) was pumped into and out of the tank using Ismatec peristaltic pumps (Cole Palmer Instrument Company, Chicago, Illinois). Ambient flow rates were controlled at a commonly observed velocity of 25 cm/day, which is created by sending approximately 55 liters of fluid into the tank every day. It would take about 7 days for the solution to flow across the tank at this flow rate.

Results and Discussions

The sand tank was flushed with de-ionized water for two weeks before installing the emplaced TCE. The water table was lowered below the bottom of the designated contaminant zone during the installation of contaminant zone. Then water table was raised to normal position and KMnO_4^- solution (1250mg/L) was pumped constantly at about 55L/day instead of de-ionized water. Total running time of the experiment is sixty-five days. Here we discuss the preliminary results of the experiments for three different stages.

(1) Early Stage

in the early stage of the experiment, MnO_4^- began to displace the original de-ionized water used to saturate the tank. Resistivity was most useful as the experiment started. The resistivity of flint silica sand saturated with de-ionized water was greater than 300 ohm-m, which filled most of the tank in the beginning. Thus fluid was gradually displaced as permanganate solution was added to the tank. Figure 6(a) shows that the UV-vis analysis of permanganate after 2 days of experiment.

Products and reactants in the oxidation reaction in our system include Cl^- and MnO_4^- ; dissolved TCE, manganese dioxide and carbon dioxide. Generally, we monitored quantitatively and semi-quantitatively for all constituents except CO_2 . Figure 7(a) shows the concentration profiles of Cl^- after 2 days.

The upstream zone where TCE was present as a pure product was where the MnO_4^- front and dissolved TCE reacted initially. One of the products in the reaction is chloride, which contributes electrical conductivity in the porous media. Figure 8(a) shows the dissolved TCE distribution in the tank after 2 days. This figure indicates some tendency of dispersive mixing as a function of transport.

Figure 9(a) shows the resistivity distribution after 3 days of the experiment. As can be seen in the figure, the area with low resistivity is where concentrations of chloride are high.

Here are a few snapshots taken from the video streams along the glass tube observation wells after 3 days (Figure 11). These photos gave us a clear picture of the situation in the medium. A small number of sampling points are limited in their ability to reveal the progress of the oxidation reaction. That's why these video images can be of enormous benefits in monitoring the experiment. There were several patterns being categorized when analyzing these video images. The first one is the purple zone, which represents non-reacted permanganate; the second one is a black zone where the MnO_2 precipitated after the oxidation reaction; the third one is the brown zone where the oxidation reaction took place; the fourth one is the white zone with non-reacted dissolved TCE plume.

(2) Intermediate Stage

This section describes results at about 35 days after the experiment began. An interesting pattern was discovered when comparing the concentration profiles of MnO_4^- and dissolved TCE. The concentration distributions all provide a similar pattern. Figure 6(b) and figure 8(b) show the concentration distribution of permanganate and dissolved TCE, respectively. As expected, the dissolved TCE plume is not mixing well with MnO_4^- above and below. Comparison of figures 6(b) and 8(b) shows that MnO_4^- is moving above and below the dissolved TCE plume. The dissolved TCE plume continued to migrate in the direction of the ambient flow towards the output chamber with only minor dispersive mixing.

We also noticed that the zone of low resistivity (figure 8(b)) coincides with a zone of elevated Cl^- cone (figure 9(b)). The porous media thus is more electrically conductive. The zone of elevated Cl^- (Figure 7(b)) also matched the zone of high dissolved TCE (Figure 8(b)). One explanation is that when permanganate front met the upstream of the source zone, the oxidation reaction started, which created MnO_2 and CO_2 , as well as Cl^- . Manganese dioxide is solid, along with carbon dioxide (gas), lowered the hydraulic conductivity around the area, which later probably caused the permanganate to bypass the reaction zone. The other product Cl^- is mobile, though was transported downstream with flow through the reaction zone.

The MnO_2 and CO_2 made the porous medium more complicated and heterogeneous, which likely resulted in different flow rates between background permanganate flow and the dissolved TCE. It is also likely that the permanganate couldn't react with dissolved TCE efficiently because downstream of the source may have formed a weak seal around the dissolved TCE plume. During the experiment, we took sample from the outlet and detected TCE in the drainage. Dissolved TCE was also pumped out from the outlet chamber and did not have enough residence time for reaction with pumped-out permanganate. Because of dissolved TCE in the effluent, it was necessary to provide a treatment system before fluids being sent down the drain (Figure 10).

We observed similar patterns in glass tube wells 2 through 8 as compiled from snapshot images during the experiment. There is a symmetrical pattern in every well: starting from bottom up, the non-reacted purple permanganate zone, black MnO_2 zone, brown reaction zone, non-reaction white dissolved TCE zone, brown reaction zone again, black MnO_2 zone, and finally non-reacted purple permanganate zone near the top. Clearly, the dissolved TCE plume is been surrounded by these manganese dioxide precipitates near upstream, on top and below bottom, as well as at sides.

(3) Final Stage

Figure 9(c) shows the resistivity distribution after 64 days of experiment. It still indicates that the low resistivity area matched the distribution of chloride. Figure 7(c) and figure 8(c) show the concentration profiles of chloride and dissolved TCE after 64 days of experiment. Although dissolved TCE plume shrunk and narrowed, TCE had not been fully destroyed even after more than two months of flushing.

MnO_4^- has still to penetrate the entire tank. Figure 6(c) shows still a narrowed white band in the middle of the tank. The absence of MnO_4^- coincides well with the presence of the dissolved TCE (Figure 8(c)). This is also confirmed by the snapshot images (Figure 13).

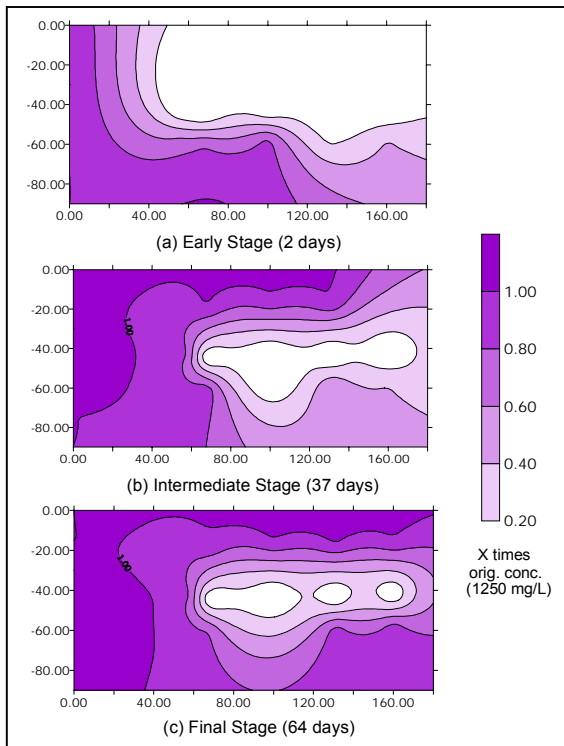


Figure 6. MnO_4^- concentration (X of 1250mg/L)

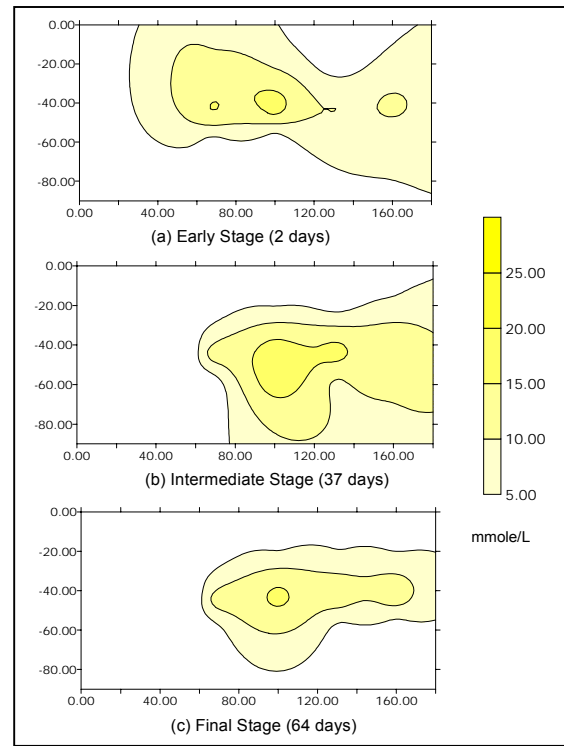


Figure 7. Chloride concentration (mmole/L)

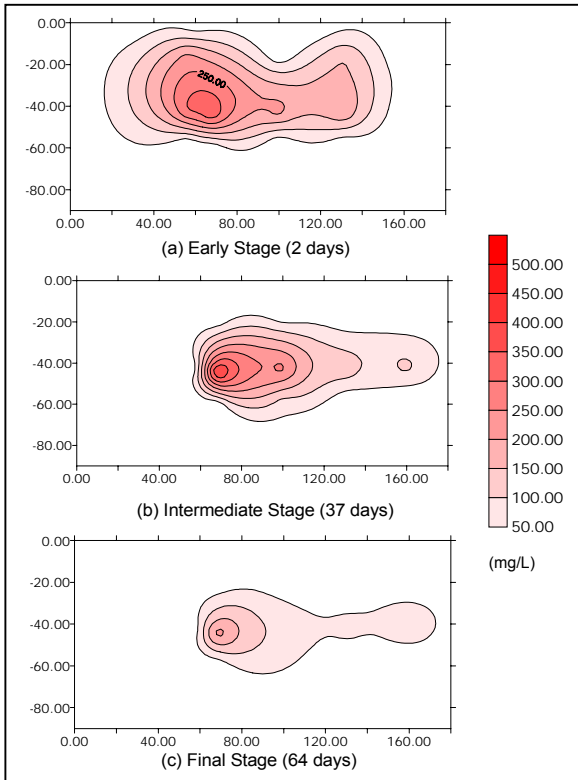


Figure 8. Dissolved TCE concentration (mg/L)

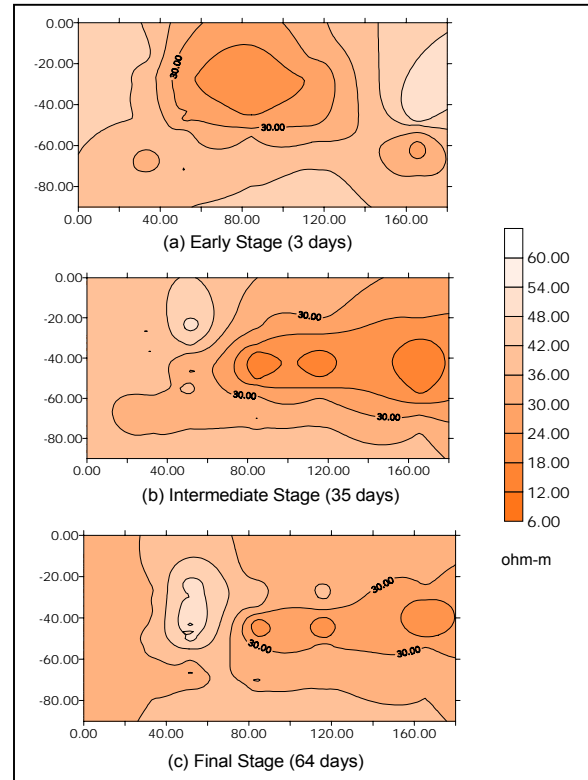


Figure 9. Electrical resistivity (ohm-m)



Figure 10. Wastewater Treatment System (creates residence time of 7 hours for additional reaction of TCE and permanganate)

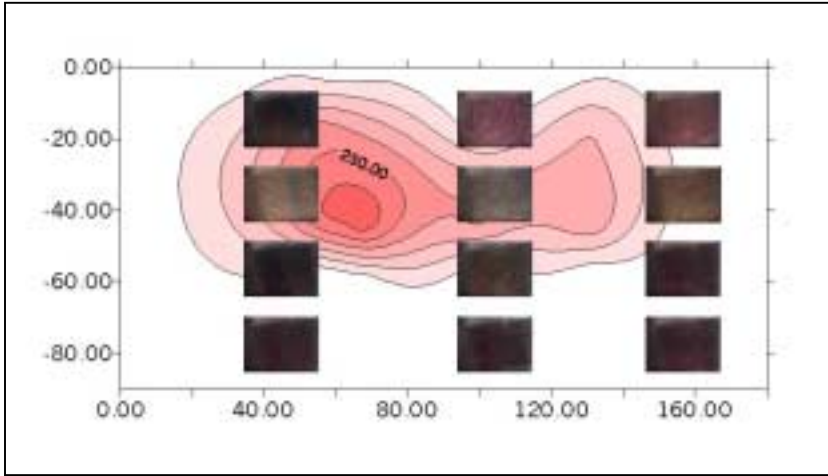


Figure 11. Snapshots images taken from video (3 days)

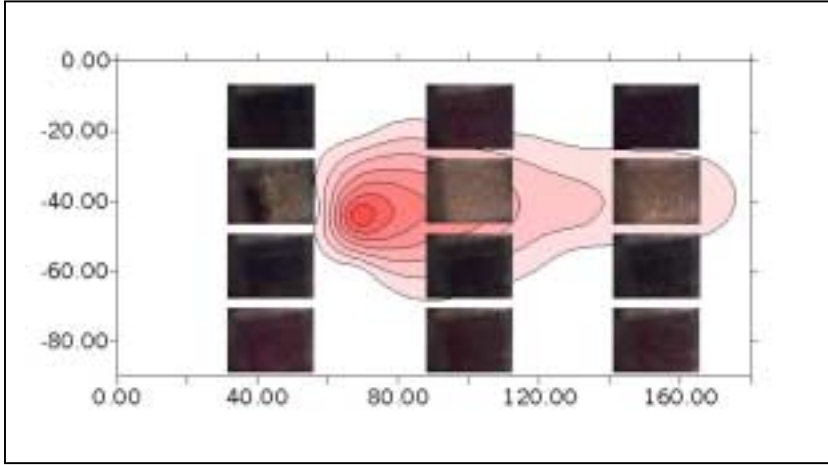


Figure 12. Snapshots images taken from video (35 days)

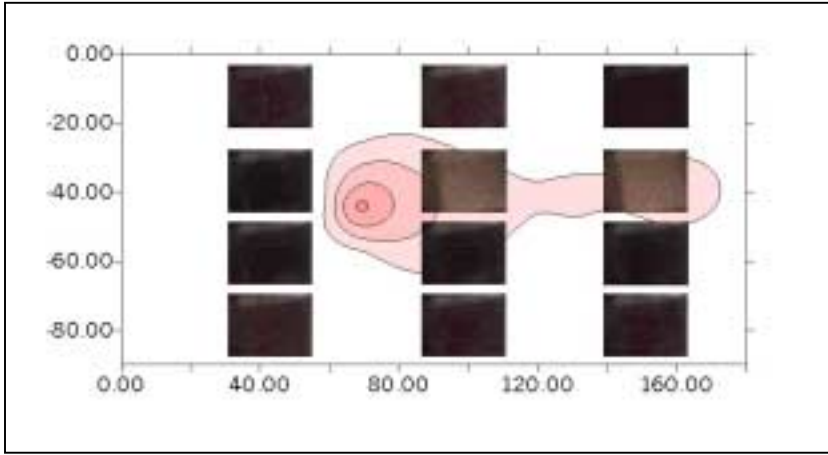


Figure 13. Snapshots images taken from video (64 days)

Conclusion

This experiment relies on a novel approach to monitoring in order to examine the in-situ destruction of TCE via oxidation. Resistivity provides the information of total dissolved solids (TDS) in the porous medium, affected by the reaction. This monitoring scheme helps us realize details of the chemical distribution in porous medium system, rather than just depending on a small number of conventional sampling points. The electrical conductivity is the reciprocal of resistivity, which is easily configured and measured by setting up simple electrical devices in the aquifer.

Video images provide a useful means of viewing processes in situ. This monitoring scheme benefits us by easily and directly understanding the spatial distribution of reactions in the aquifer. Different colors can be good indicators of different reactions taking place and modern data mining techniques can be applied to do image classification better and more efficiently.

These approaches also provide good alternatives to high-resolution chemical sampling because they avoid complexity of organic chemical analyses. Besides, with easy setup and appropriate automation, the electrical and optical monitoring schemes are rapid and time efficient.

Another important result of this experiment is that the outcome of in-situ oxidation of solvent by permanganate oxidation is not as good as expected and has its limitation. Precipitation of $\text{MnO}_2(\text{s})$ reduces the hydraulic conductivity of the medium. That would effect the efficiency of the reaction and create more wastewater (non-reacted permanganate and TCE). Several possible solutions are still being investigated by our research lab.

Reference

- Gheith,, H.M. and Schwartz, F.W., 1998, Electrical and visual monitoring small scale three-dimensional experiments, *Journal of Contaminant Hydrology*, 34, 191-205.
- Stewart, R., 1965. Oxidation by permanganate. In: KB. Wiberg (Editor), *Oxidation in organic chemistry*, part A. Academic Press, New York, NY, pp. 1068.

Basic Information

Title:	Methodology for Estimating Total Maximum Daily Load in Watersheds with Considerable Ground-Water Surface-Water Interaction
Project Number:	G-01
Start Date:	10/1/2000
End Date:	10/1/2002
Research Category:	Water Quality
Focus Category:	Hydrology, Non Point Pollution, Nutrients
Descriptors:	
Lead Institute:	Ohio State University
Principal Investigators:	Frank Schwartz, Maged Hussein

Publication

Project No: RF 740217; US Geological Survey 00HQGR0091

Duration: 9/00-9/02

Title: Methodology for Estimating Total Maximum Daily Load in Watersheds With Considerable Ground-Water Surface-Water Interaction

Investigator:

Dr. F. W. Schwartz,
Department of Geological Sciences,
The Ohio State University

Congressional District: Ohio 15th

Focus Categories: MOD, NPS, and GW

Keywords: Water Quality Modeling, Ground-Water Surface-Water Interaction, Total Maximum Daily Loads, Geographic Information Systems

Problem and Research Objectives

Significant improvements to the nation's water quality have been achieved through the implementation of point-source technology-based pollution control measures and the enforcement of the National Pollution Discharge Elimination System (NPDES). However, non-point sources (NPS) remain as major sources causing or contributing to water quality impairment because of difficulty in quantification and/or control. Section 303(d) of the Clean Water Act mandated the establishment of the Total Maximum Daily Load (TMDL) for impaired waters as a means to address the combined impact of both point and non-point source pollution (USEPA 1999a). The holistic approach for watershed protection requires consideration of water quality of the different water bodies that exist in the watershed and the interaction between them and in the development of TMDL. Ground-water surface water (GW/SW) interaction is an important factor in the transport of dissolved nutrients and pesticides and subsequent contamination of rivers and aquifers (Gardener 1999).

This study addresses an important gap in knowledge with respect to water quality impairment: the transport of contaminants from non-point sources in a coupled GW/SW system and the development of TMDL under such conditions. Its goal is to elucidate the impact of non-point source pollution on surface- and ground-water quality in large watersheds. The study has been structured around two main tasks. Task I focuses on contaminant fate and transport in ground water and the development and implementation of the TMDL concept for surface water under threat from ground water contamination. Specifically, the modeling capability of the Soil Water Assessment Tool (SWAT) will be expanded using numerical models for flow and transport in ground water. In Task II, a

comprehensive water quality model will be created for the Great Miami River Basin to demonstrate how the modeling approach can be used to develop TMDLs.

Task specific study objectives are as follows:

- Task I.1: Implementation of the Ground-Water Fate and Transport Module into SWAT.
- Task I.2: Verification and Testing of the Model and Development of the GIS Interface.
- Task II.1: Development and Calibration of a SWAT Model for the Great Miami River.
- Task II.2: Development of a Ground-Water Quality Model for the Miami Buried Valley Aquifer.
- Task II.3: Integrated Model Calibration and Verification
- Task II.4: Refinement of the Integrated Model and Interpretation of the Modeling Results.
- Task II.5: Report Preparation and Future Work.

Methodology

The proposed work is intended to address the transport of contaminants from non-point sources in a coupled GW/SW system and the development of TMDL under such conditions. Currently, most modeling efforts carried out in support of TMDL assessments rely on EPA's Better Assessment Science Integrating Point and Non-point Sources (BASINS) system in which three surface water models (QUAL2E, TOXIRoute, and NPSM) are incorporated with the SWAT model. None of the above models address the transport of pollutants through shallow ground water.

In Task I, a fate and transport module is being developed for the SWAT model. Based on the Modular Three-Dimensional Finite-Difference Ground-Water Flow Model MODFLOW, the module will be capable of simulating physical and chemical processes controlling the transport of dissolved compounds in ground water and the possible release into surface water. The model demonstration in this study will involve the 7350 mi² MIAMI-NAQWA study unit, which encompasses basins of three tributaries of the Ohio River: the Great Miami River, the Little Miami River, and Mill Creek (Figure 1).

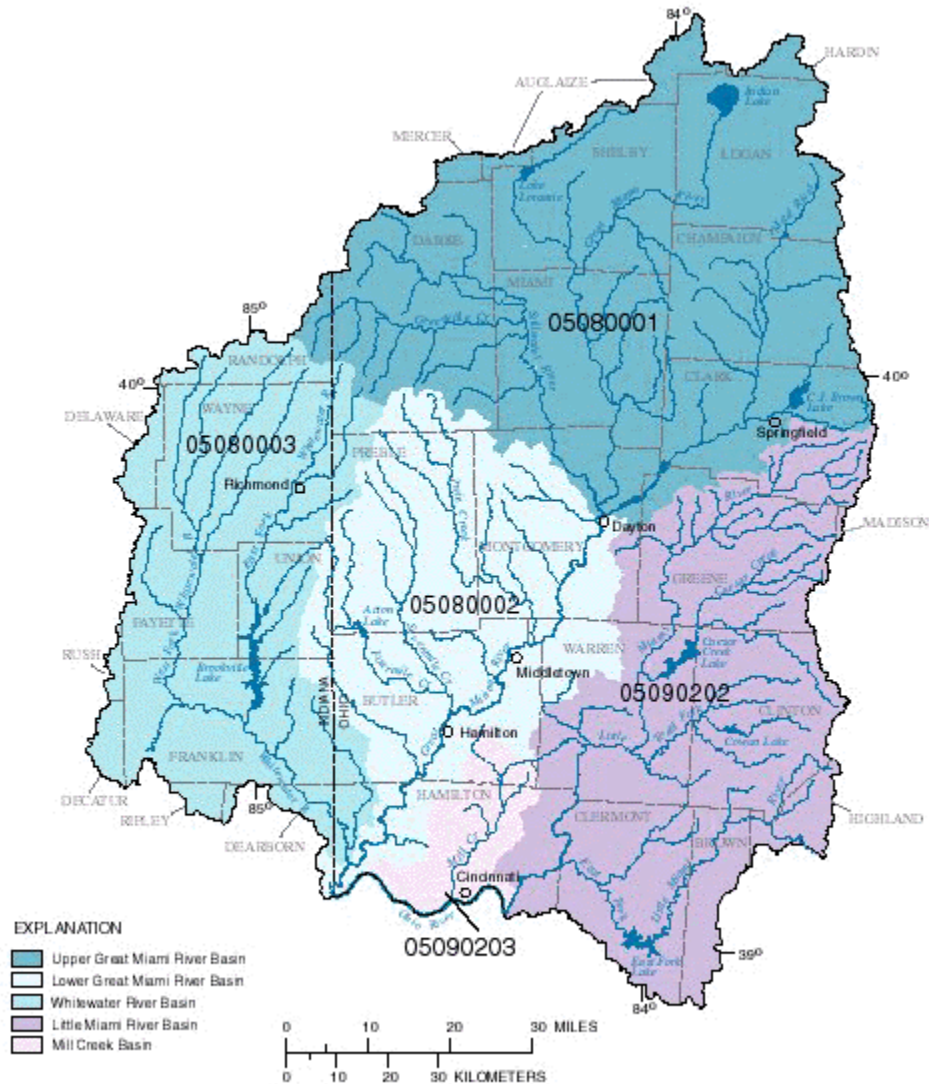


Figure 1. Location Map of the Great and Little Miami River Basins, Ohio and Indiana

To verify the fate and transport components of the developmental module, a comparison is being made against readily available models such as BASINS and WMS. The model area selected for this verification is the 656mi² Mad River sub basin of the Great Miami River Basin (Koltun 1995). Its headwaters are in Logan County and it flows south and west through Champaign, Clark, and Greene counties to its confluence with the Great Miami River in Montgomery County (Figure 2).

The Task II comprehensive water quality model that will be developed for the Great Miami River Basin will use data from the MIAMI-NAWQA study, USGS ground water models (Dumouchelle 1998), and others (Ritzi et al, 1994; IT 1993; and HydroGeoLogic 1998). Data will be compiled in a Geographic Information System (GIS) database by expanding BASINS or WMS to incorporate ground water modeling parameters.

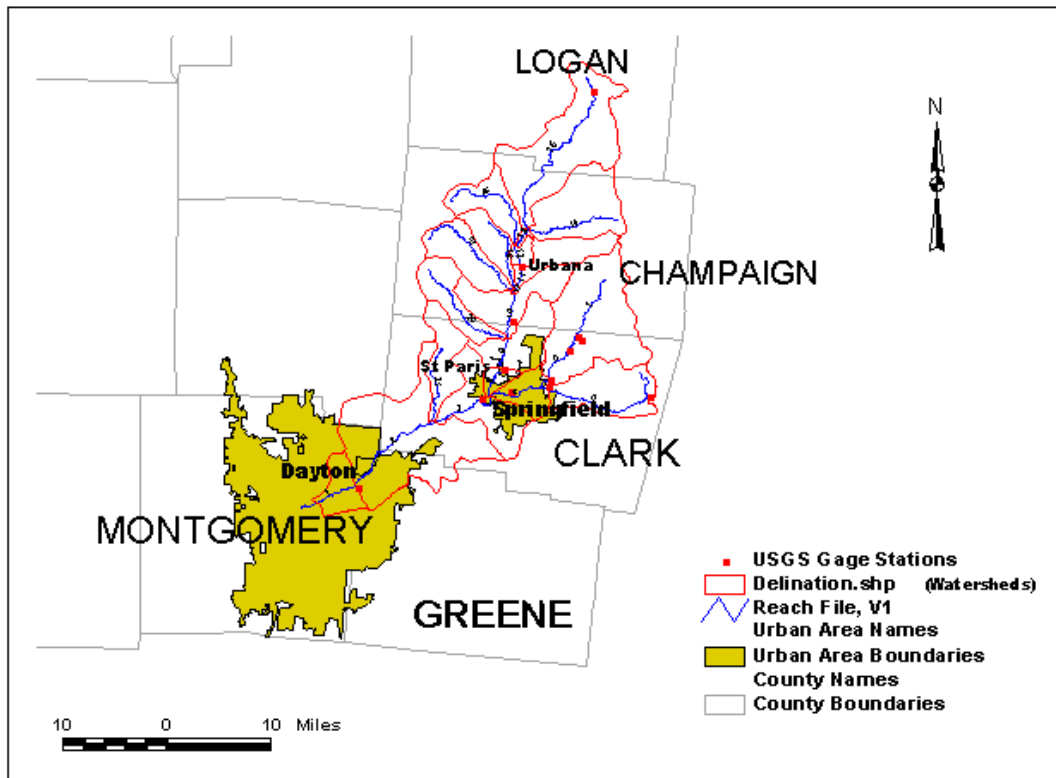


Figure 2. The Mad River Sub Basin

Principal Findings and Significance

Following the schedule timeline presented in the subject research proposal, the preponderance of project activities has focused on Task I since the September 2000 award date. Specifically, the BASINS and WMS models are being applied to the Mad River sub-basin area in preparation of the verification of ground water fate and transport components being developed for the SWAT module.

BASINS System Overview

Currently, BASINS 2.0 is being used on this project. It is a multipurpose environmental analysis system for use by regional, state, and local agencies in performing water- and water-quality-based studies (Lahlou et al, 1998). The BASINS system combines the following six components to provide the range of tools needed for performing watershed and water quality analysis:

- National Environmental Databases

- Assessment Tools
- Utilities
- Watershed Characterization Reports
- Water Quality Stream Models
- Non-Point Source Model (NPSM) and Postprocessor

The BASINS physiographic data, motoring data, and associated assessment tools are integrated in a customized geographic information system (GIS) environment, ArcView 3.2. Modeling tools include in-stream models (QUAL2E and TOXIROUTE) and NPSM, which includes the Hydrological Simulation Program – Fortran (HSPF), version 11.

The NPSM is a planning-level watershed model that is used for estimating in-stream concentrations resulting from loadings from point source and non-point sources. It is an extremely flexible tool for modeling the impact of land use associated non-point source pollution on downstream water quality (Lahlou et al, 1998). Features supported by NPSM include:

- Estimation of non-point source loadings from mixed land uses
- Estimation of the fate and transport processes in streams and one-dimensional lakes

The NPSM postprocessor facilitates the display and interpretation of output data derived from model applications.

WDMUtil is an easy to use program provided by BASINS that allows the importation of available meteorological data into WDM files and performs needed operations to create the time-series data for NPSM/HSPF (USEPA 1999b). This allows the user to add valuable local meteorological data rather relying on the limited set of meteorological data stored in BASINS. Data from the Pandora and Dayton WSO Airport, Ohio meteorological stations are used in the Mad River sub basin evaluation.

BASINS Version 3.0 is now in beta release. In addition to several new data and functions, 3.0 has added the SWAT model. The installation program installs WinHSPF, a new interface to HSPF Version 12 that is replacing NPSM from BASINS 2.0; and GenScn, a model post processing and scenario analysis tool that is used to analyze output from HSPF and SWAT. This beta version demonstrates a fundamental change in the developmental philosophy of BASINS. BASINS 3.0 will be distributed as a core system and several extensions. This modular and open architecture will allow users to customize their BASINS projects, more easily upgrade systems, and develop extensions for BASINS.

The Mad River Sub Basin

The Mad River sub basin as delineated in the BASINS model occupies 645 mi² of the eastern portion of the Upper Great Miami River Basin and includes the Mad River and eight major tributaries (Figure 2). It ranges in elevation from 457 m (1499 ft) above MSL in the northeastern corner of the sub basin to 235 m (784 ft) MSL in the vicinity of Dayton, Ohio (Figure 3). Land use in the study area is greater than 75% agricultural and approximately 15% urban or built up (Figure 4). The remaining 10% is comprised of forest land and water cover.

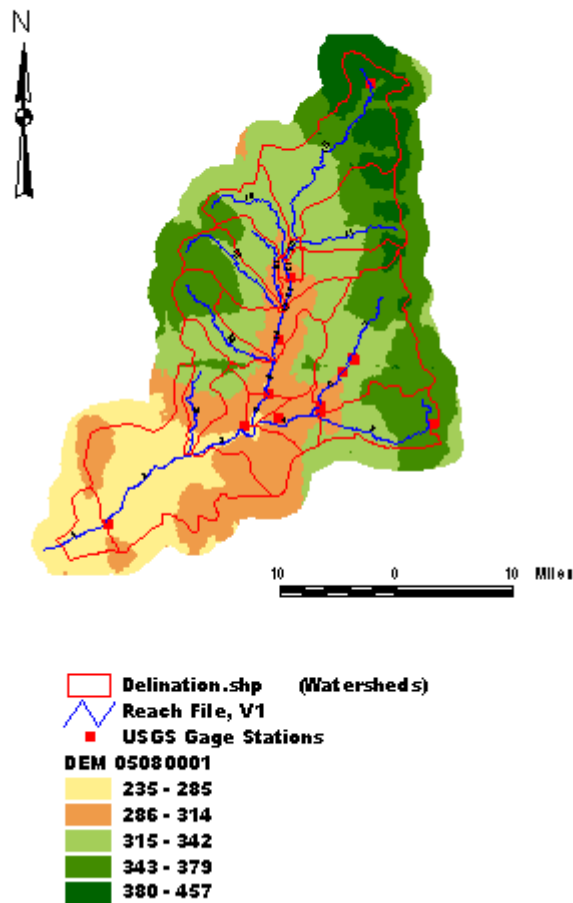


Figure 3. DEM Elevations Within the Mad River Sub Basin

A total of 20 individual watersheds ranging in size from approximately 0.01 to 106 mi² were delineated within the Mad River sub basin based on topographical information and/or the location of USGS stream gaging stations (Table 1; Figure 5). Each watershed contains a segment of or tributary to the Mad River ranging in length from 0.4 to 21 miles (Table 1; Figure 5). Watershed 6, which was delineated before data were available listing the inactive status of the gaging station, contains two segments of Buck Creek (segments 6 and 7). The active USGS gaging stations in the Mad River sub basin are located at Dayton (03270000), Springfield (03269500), St. Paris (03267900), and Urbana (03267000).

Preliminary NPSM Model Results

Preliminary NPSM and postprocessor results have been completed for the Mad River sub basin. Initial efforts have focused on calibrating and validating stream flow data for the Mad River sub basin. However, two factors have become apparent that presently limit the usefulness of the 2.0 BASINS/NPSM model:

- While there is no limit to the number of watersheds that the BASINS/NPSM model will run, there is a limit of 200 total operations. The number of operations depends on the number of land use types, number of watersheds, number of reaches, etc. (Choudhury, 2000). Consequently, it has not been possible to run the NPSM model for the entire 20 watersheds within the Mad River sub basin. Only 10 combinations of watersheds can be successfully run at one time.
- In launching the NPSM, there are only 6 individual discharge years (1991 to 1996) that can be selected for Permit Compliance System (PCS) data to be incorporated into the model. Combined with limitations on the number and years of record of the USGS gaging stations in the Mad River sub basin, restrictions are placed on the time span for which water quality analyses within the study area can be performed, and available years of record for calibration and validation.

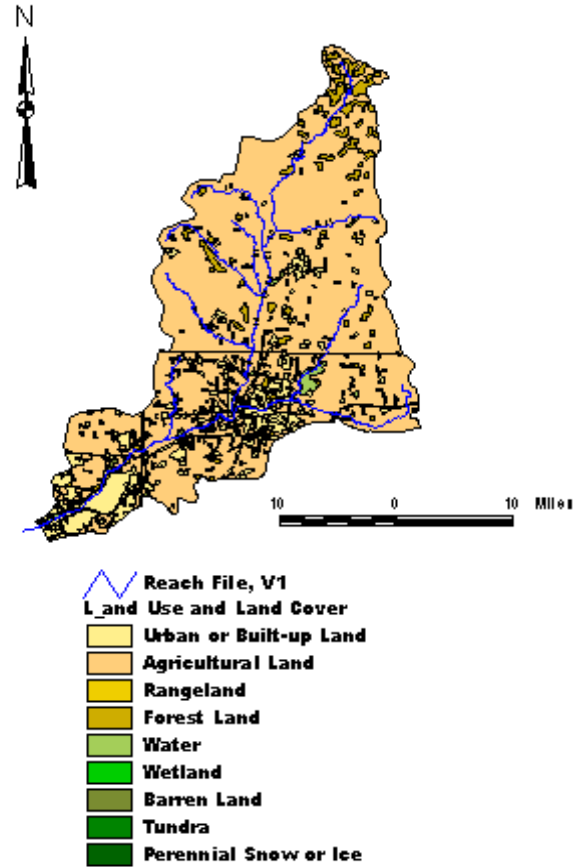


Figure 4. Land Use and Cover Within the Mad River Sub Basin

Table 1. Delineated Mad River Watersheds and Associated Stream Segments

Watershed Designation	Area (mi²)	Stream Segment	Length (mi)	Mean Flow (cfs)
5080001001	16.7	Mad River	6.2	633.9
5080001002	105.9	Mad River	10.6	633.9
5080001003	38.4	Mad River	7.8	522.6
5080001004	16.3	Buck Creek	5.9	139.4
5080001005	40.8	Beaver Creek	15.7	42.3
5080001006	80.5	Buck Creek	14.4*	75.8
5080001008	6.1	Mad River	3.8	340
5080001009	29.8	Mad River	3.3	340
5080001010	32.7	Mad River	4.8	256.7
5080001011	21.9	Mad River	3.2	156.1
5080001012	4.6	Mad River	2.1	156.1
5080001013	1.5	Mad River	2.3	101
5080001014	47.4	Kings Creek	9.8	29.7
5080001015	83.2	Mad River	21	64.4
5080001016	23.7	Muddy Creek	12.1	36.6
5080001017	0.1	Nettle Creek	0.4	82.3
5080001018	16.5	Anderson Creek	8.6	32.8
5080001019	28.1	Nettle Creek	12.6	47.9
5080001020	25.5	Chapman Creek	12.3	46.8
5080001021	<u>25.4</u>	Donnels Creek	9.4	51.2
	645.1			
*Watershed contains stream segments 6 and 7				

An example of preliminary, uncalibrated 1992 NPSM model results for discharge on the Mad River at Dayton, Ohio, are presented on Figure 6. This can be compared to the 1992 Mad River discharge as recorded at the USGS gaging station 03270000 at Dayton, Ohio (Figure 7), and precipitation at the Dayton WSO Airport (Figure 8). (The outflow

point for the NPSM model is located at the USGS gaging station.) If the above limitations can be resolved, the NPSM model results will be calibrated with the USGS stream gage result by adjusting individual model parameters, especially percent land use category perviousness and stream cross section characteristics. In addition, all pertinent watershed information will be updated to confirm model accuracy.

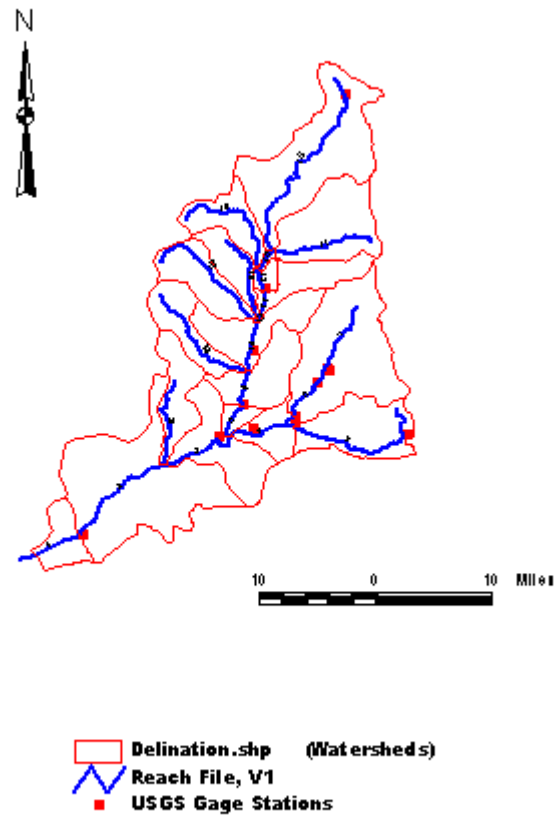


Figure 5. Mad River Sub Basin Watersheds and USGS Stream Gaging Stations

Prospective Project Approach

The limitations of the BASINS/NPSM model discussed above may be insuperable. Consequently, an attempt was made to directly apply the HSPF program to the Mad River sub basin for estimating instream concentrations resulting from loadings from point and non-point sources. However, a major disadvantage of HSPF is that it has no graphical user interface (GUI) and the user must manually create a user control input (UCI) files, which inform HSPF of modules (e.g., watershed and land use delineation, meteorological inputs, etc.) to be used in the model run, watershed and stream network connectivity, and model parameters. Given the complexities of HSPF and the number of

Figure 6. Preliminary 1992 NPSM Model Discharge for Mad River at Dayton, Ohio

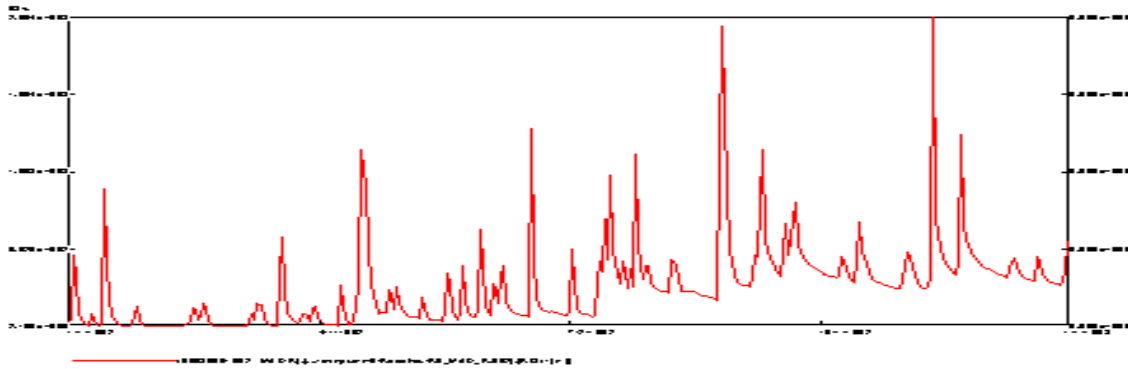


Figure 7. 1992 Discharge for Mad River at Dayton, Ohio, USGS Gaging Station 03270000

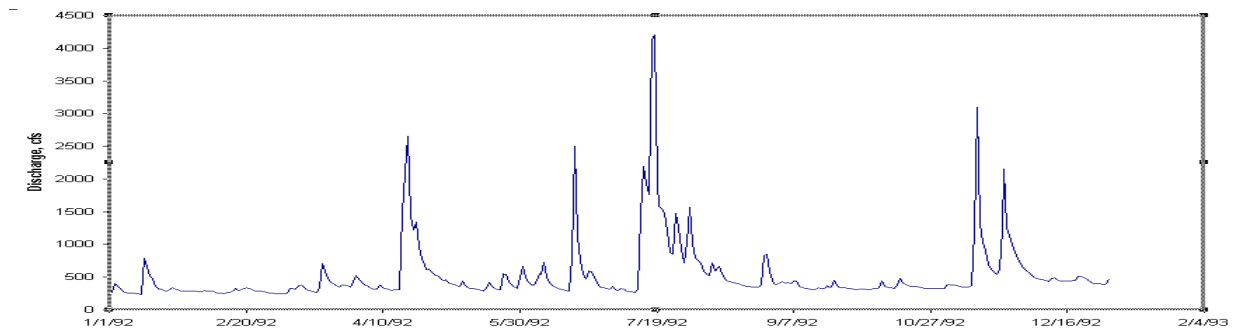
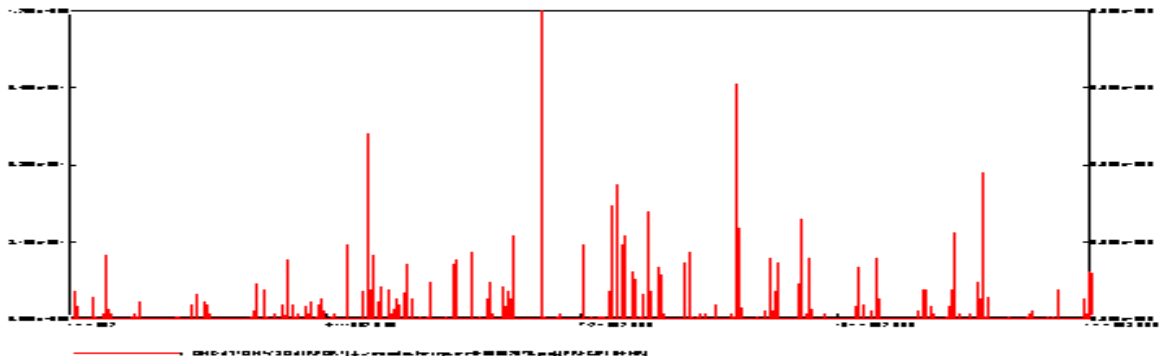


Figure 8. 1992 Dayton WSO Airport Precipitation (in/hr)



tasks it can perform, the manual nature of HSPF can present serious obstacles that require an extremely high level of user knowledge and effort.

An alternative to the multipurpose BASINS system, which integrates the HSPF program with a GIS environment, is the Watershed Management System (WMS). This system has been now been interfaced with HSPF to provide graphical representation of HSPF data as well as automate the definition of many of the required parameters. The strength of WMS as a modeling environment lies in the digital terrain modeling functions that can be used for automated watershed delineation, geometric parameter computation, hydrological parameter computation, and result visualization using GIS data, Digital Elevation Models (DEMS), or Triangulated Irregular Networks (TINs). Efforts are now underway to apply WMS to the Mad River sub basin study area. Many of the data files generated with the BASINS modeling effort can be used directly in WMS. This compatibility should streamline efforts in developing the watershed model.

The successful modeling of the Mad River sub basin using WMS and verification of the fate and transport components of the developmental SWAT module will mark an integral step in the completion of the multiple project tasks and study objectives for estimating the TMDL in the Great Miami River Basin.

References

Choudhury, S. H., 2000, Personal Communication: Schoudhu@CH2M.com.

Dumouchelle, D. H., 1998, Simulation of Ground-Water Flow Dayton Area, Southwestern Ohio: U.S. Geological Survey Water-Resources Investigations Report 98-4048, 57p.

Gardener, K. M., 1999, The Importance of Surface Water/Ground Water Interaction, Issue Paper: Office of Water/Water Quality Unit, Environmental Protection Agency, Seattle, Washington.

HydroGeoLogic, 1998, Development and Verification of VAM3DF: A Numerical Code for Modeling Flow and Transport in Ground Water, Final Report, July 1998: Prepared for Fluor Daniel Fernald.

IT Corporation, 1993, Ground Water Modeling Report Summary of Model Development: Prepared for U.S. Department of Energy, Fernald Field Office, Fernald, Ohio.

Koltun, G. F. 1995, Determination of Base-Flow Characteristics at Selected Streamflow-Gaging Stations on the Mad River, Ohio: U.S. Geological Survey Water-Resources Investigations Report 95-4037, 12p.

Lahlou, M., Shoemaker, L., Choudhury, S., Elmer, R., Hu, A., Manguerra, H., and Parker, A., 1998, Better Assessment Science Integrating Point and Non-Point Sources, Version 2.0, User's Manual: Tetra Tech, Inc., 348p.

Ritzi, R. W., Jr., Jayne, D. F., Zahradnik, A. J., Jr., 1994, Geostatistical Modeling of Heterogeneity in Glaciofluvial, Buried-Valley Aquifers: Ground Water, v. 32 (July/August), p. 666-674.

U.S. Environmental Protection Agency, 1999a, Report of the Federal Advisory Committee on the Total Maximum Daily Load (TMDL) Program: The National Advisory Council for Environmental Policy and Technology (NACEPT), Washington, D.C.

U.S. Environmental Protection Agency, 1999b, WDMUtil: A Tool for Managing Watershed Modeling Time-Series Data, User's Manual (DRAFT), Version 1.0 (BETA): Office of Water, Washington, D.C., 91p.

Basic Information

Title:	Degradation of Groundwater Quality from Pumping-Induced Surface-Water Infiltration: Bacterial Contamination
Project Number:	G-03
Start Date:	9/1/1997
End Date:	9/1/1999
Research Category:	Ground-water Flow and Transport
Focus Category:	Ecology, Groundwater, Hydrology
Descriptors:	Autochthonous-allochthonous microbial interactions, Bacterial transport, Groundwater quality modeling, Surface-groundwater relationships
Lead Institute:	Water Resources Center
Principal Investigators:	Jonathan Levy, Robert H. Findlay

Publication

1. Kreeger, A.L. (2000) Comparison of hydraulic conductivity estimates using a variety of techniques at a field site in southwestern Ohio. Master of Science thesis. Department of Geology, Miami University, Oxford, Ohio, 83 pp.
2. Rossman, A.J. (2001) Determining the significance of the autochthonous (indigenous) microbial community on the fate and transport of allochthonous (invasive) bacteria. Master of Science thesis. Department of Geology, Miami University, Oxford, Ohio, 85 pp.
3. Schran, H.L. (2001) Microbial biomass and community structure of shallow, glacial-outwash aquifer sediment. Master of Science thesis. Department of Microbiology, Miami University, Oxford, Ohio, 47 pp.
4. Brannock, J.M., A.P. Tomaras, K. Sun, J. Levy, R.H. Findlay (2000) Comparison of *Escherichia coli* transport through natural sediment and laboratory sand columns. Undergraduate Research 2000, Miami University, Oxford OH.
5. Lustig, A.G. and J. Levy (1999) Comparison of hydraulic conductivity estimates using a variety of techniques at a field site in southwestern Ohio. Abstract 51644. 1999 Fall meeting of the Geological Society of America.
6. Mignery, M.B. and J. Levy (1999) Impact of induced infiltration on water quality at a wellfield in southwest Ohio. Abstract 51512. 1999 Fall meeting of the Geological Society of America, Denver, CO.
7. Schran, H.L., A. Lustig, J. Levy and R.H. Findlay (1999) Microbial biomass and community structure of a shallow glacial-outwash aquifer sediment. Abstract for 1999 meeting of the American Society for Microbiology.
8. Sun, K., A.J. Rossman, J. Levy, R.H. Findlay and H.L. Schran (1998) Bacterial transport through intact sediment cores: variability of transport parameters and controlling aquifer characteristics. Abstract 51051, 1998 Fall meeting of the Geological Society of America, Toronto, Ontario.
9. Schran, H.L., A.J. Rossman, J. Levy, R.H. Findlay (1998) Microbial community structure of a shallow groundwater sediment and coliform bacterial transport. 1998 Ohio, Allegheny, Kentucky

- & Tennessee ASM Branch Meeting, p. 40.
10. Schran, H.L., AJ Rossman, J. Levy, R.H. Findlay (1998) Microbial community structure of a shallow groundwater sediment. 8th International Symposium on Microbial Ecology, Halifax Canada, p. 296.
 11. Findlay, R.H., H.L. Schran, A.J. Rossman, J. Levy (1998) Microbial community structure of a shallow groundwater sediment and coliform bacterial transport. Abstract for the Joint Meeting of the Ohio & West Virginia Branches of the American Society for Microbiology, April 24-25, 1998, Ohio State University, Columbus, OH.
 12. Sun, K (2001) Comparative study of bromide and bacterial transport through different porous media: controlling sediment characteristics and mathematical modeling. Ph.D. dissertation. Department of Geology, Miami University, Oxford, Ohio, 350 pp.
 13. Mignery, M.B. (In progress) Assessing water quality impacts from induced infiltration at a well field in southwest Ohio. Master of Science thesis. Department of Geology, Miami University, Oxford, Ohio.
 14. Roa, S.D., J.A. Hardgrove, A.P. Tomaras, J.M. Brannock, K. Sun, F. Farruggia, J. Levy and R.H. Findlay (2001) Comparison of *Escherichia coli* transport through undisturbed and re-packed groundwater sediment columns. 101st General Meeting of the American Society for Microbiology.
 15. Sun, K., J. Levy, R.H. Findlay, J. Brannock, A. Tomaras, K.L. Mumy, J.A. Porter (2000) Effect of sediment characteristics on bacterial transport through intact aquifer sediment cores. Abstract 50436. 2000 Fall meeting of the Geological Society of America, Reno Nevada.
 16. Sun, K., R.H. Findlay, J. Levy, J. Brannock, A. Tomaras, K.L. Mumy (2000) Bacterial transport through relatively undisturbed aquifer sediments. Midwest Ground Water Conference, Oct. 17-19, 2000, Columbus, Ohio.
 17. Mignery, M.B., J. Levy, R.A. Sheets, B. Whitteberry (2000) Extent and impact of induced infiltration at a well field in southwest Ohio. Abstract 51853. 2000 Fall meeting of the Geological Society of America, Reno, Nevada.
 18. Gollnitz, W.D., B. Whitteberry, J. Vogt, R.A. Sheets, G.L. Rowe, J. Levy, R.H. Findlay, M.B. Mignery, (2000) Introduction to the flowpath study at the City of Cincinnati C.M. Bolton well field A case study for monitoring induced infiltration. Midwest Ground Water Conference, Oct. 17-19, 2000, Columbus, Ohio.
 19. Brannock, J.M., AP Tomaras, K Sun, J Levy, RH Findlay (2000) Transport of *E. coli* through Natural Sediments and Laboratory Sand Columns. 100th General Meeting of the American Society for Microbiology, Los Angeles, CA. p. 596.
 20. Brannock, J.M., AP Tomaras, K Sun, J Levy, RH Findlay (2000) Analysis of *Escherichia coli* transport through groundwater sediments. Ohio Branch of the American Society for Microbiology Annual Meeting. Hueston Woods State Park, OH.
 21. Sheets, R.A., J. Levy and M.B. Mignery (In progress) Flow paths and travel times from a river to municipal wells at a site with induced infiltration: modeling and ground truth. For submission to Ground Water.
 22. Gollnitz, W.D., B. Whitteberry, J. Vogt, R.A. Sheets, G.L. Rowe, J. Levy, R.H. Findlay, M.B. Mignery (In progress) The effect of induced infiltration on drinking water quality. For submission to Ground Water Monitoring and Remediation.
 23. Levy, J., K. Sun, R.H. Findlay and F.T. Farruggia (In progress) Factors controlling bacterial transport in glacial outwash aquifer sediment. For submission to Water Resources Research.
 24. Sun, K., J. Levy and R.H. Findlay (In progress) Comparison of bacterial transport through artificial, intact-natural and repacked-natural sediment columns. For submission to Journal of Contaminant Hydrology.
 25. Levy, J. and K. Sun (In progress) Nonideal transport of bromide through heterogeneous sediment: investigating the meanings of the two-region model parameters. For submission to Journal of

Contaminant Hydrology.

26. Porter J., and R. H. Findlay (In progress) Microbial biomass and community structure in groundwater sediments. For submission to *Microbial Ecology*.

Final Report

Project Number: G-03

Start. 09/97

End. 09/99

Title: **Degradation of Groundwater Quality from Pumping-Induced Surface-Water Infiltration: Bacterial Contamination**

Investigators: Jonathan Levy, Miami University, Oxford, OH 45056
Robert H. Findlay, Miami University, Oxford, OH 45056
Kerang Sun, Miami University, Oxford, OH 45056
Heidi L. Schran, Miami University, Oxford, OH 45056
Amy Lustig, Miami University, Oxford, OH 45056
Anthony J. Rossman, Miami University, Oxford, OH 45056

Congressional District: Ohio 8th

Focus Category: ECL, G&G, GW, HYDGEO, HYDROL, MOD, NPP, ST, WQL, WS

Problem and research objectives:

Drinking water pumped from shallow glacial-fluvial aquifers may be contaminated with fecal coliform bacteria derived from nearby polluted surface waters. Municipal wells located adjacent to polluted streams and rivers are especially susceptible to contamination. Due to downward hydraulic gradients induced by pumping, contaminated surface water may be drawn into the underlying aquifer and move towards drinking-water wells. Under US EPA guidelines, wells less than 50 ft from surface water are considered under the direct influence of surface water. From a regulatory standpoint, the Ohio EPA mandates that such groundwater be treated as if it were surface water and therefore requires the water to be treated with techniques for coagulation/flocculation, settling, filtration and disinfection. Upgrading typical groundwater treatment to include these techniques can be quite costly and in many circumstances prohibitive, resulting in well abandonment and the costly search for new water supplies. Studies in bacterial transport through groundwater suggest that the 50-ft criterion will not be cautious enough in some settings and too cautious in others. Adequate guidelines for appropriate separation distances need to be developed and should be based on our best ability to predict bacterial transport in a variety of hydrogeologic settings. Private wells are also susceptible to bacterial contamination. In a recent study of well-water quality in Iowa, 78% of wells in a volunteer sampling program were found to test positive for total coliform bacteria. The majority of these wells were shallow (67%) and were located > 100 ft from the closest active barnyard/feedlot and > 50 ft from a septic system (92%). Clearly, both rural populations obtaining drinking water from private wells and municipal populations obtaining drinking water from aquifers adjacent to polluted surface waters are at risk of waterborne disease. Our objective in this study is to help develop the ability to predict allochthonous

(invasive, nonindigenous) bacterial transport through groundwater aquifers, allowing greater protection of groundwater that is to be used as a drinking-water source.

Our overall research objective is to advance the ability to predict allochthonous bacterial transport and fate through groundwater aquifers. We note two main deficiencies with current models. The first is that the complexity of current models prohibits their use as regulatory tools for determining appropriate separation distances between bacterial sources and drinking-water wells. While the processes have been theoretically described, little work has been done toward their quantification or their relationship to real-world aquifers. Second, previous studies grounded in real complex systems have paid little attention to the impact of the interactions between allochthonous and autochthonous microbial communities of groundwater. Failure to predict retardation and immobilization or decay of allochthonous species accurately may be due to a failure to incorporate microbial interactions into existing models. With this research we directly address these two deficiencies. We approach the problem with a series of testable hypotheses, which we are investigating using a combination of laboratory column experiments under controlled and variable conditions and statistical and computer modeling. We also are initiating field studies to collect real-world data and test new models.

Hypothesis 1: The autochthonous microbial community significantly affects the transport of allochthonous bacteria through groundwater. The effects of autochthonous microbial communities on pathogenic bacterial transport result from predation and other ammensal or commensal interactions. These interactions result in either apparent decay or retardation of the allochthonous species. Autochthonous bacteria are part of a complex biofilm on aquifer sediments that also includes non-living organic matter. We wish to differentiate the effects of the organic matter from the living indigenous microbial community and we hypothesize that the interactions with autochthonous bacteria are significant apart from the effects of the nonliving biofilm component. Our experimental transport columns will therefore be treated to represent aquifer material with and without a viable autochthonous community and with and without any biofilm present. Apparent decay and retardation rates will be compared between treatments. We predict that interactions with the autochthonous community will result in an apparent difference in bacterial transport velocity compared to a conservative tracer and a decrease in the total number of allochthonous bacteria exiting the columns.

Hypothesis 2: A useful predictive model can be developed for allochthonous bacterial transport through aquifer sediments. In Year 2, we will build on the data generated through testing Hypothesis 1. Our goal is to be able to predict allochthonous bacterial transport and fate in groundwater given a set of biotic and abiotic aquifer characteristics. Developing this capability is a two-step process. In the first step, we will conduct dozens of column experiments in addition to those run for testing of Hypothesis 1, and we will measure the biotic and abiotic aquifer characteristics that influence bacterial transport and fate. The columns will comprise sediment taken from a variety of hydrogeological settings and will be run under controlled temperature conditions. For each column we will generate a bacterial breakthrough and dilution curve. In the second step, we will

use a one-dimensional advection-dispersion-reaction model that simulates results comparable to the experimental curves. Each column will have its own associated model parameter values. We will use multiple regression analysis to relate the calibrated transport-model parameter values to the aquifer characteristics that are most likely to control bacterial transport. The end result is a model which uses aquifer characteristics to predict bacterial transport and fate in a wide variety of settings. A strength of such a model is that it can incorporate the spatial variability and uncertainty of the aquifer characteristics to quantify the uncertainty associated with the final transport-model predictions.

Hypothesis 3: The bacterial-transport model developed in the laboratory will accurately predict bacterial transport in the field. We will begin development of a permanent field-test site. We have access to an abandoned City of Oxford, Ohio well that has sporadically tested positive for total coliform bacteria. The well is under the direct influence of Four Mile Creek. We will use the well to induce a vertical hydraulic gradient and use that gradient to perform conservative tracer tests and observe bacterial transport and fate along flow paths from the creek toward the well. A combination of single piezometers, nested piezometers and multilevel sampling devices will be used to determine the horizontal and vertical concentrations of chemical and microbiological components of groundwater. Biotic and abiotic aquifer characteristics will be determined from sediments recovered during piezometer placement. We will predict bacterial fate and transport using our model and the predictions will be compared to the observed bacterial concentrations.

Methodology:

Hypothesis 1: The autochthonous microbial community significantly affects the transport of allochthonous bacteria through groundwater.

Undisturbed groundwater sediments are collected using a drilling rig and a split-spoon sampler. The sediment is collected into a polycarbonate, split-spoon liner from which a 10-cm section is chosen. The ends of the sediment sample are sampled three times for phospholipid fatty acid (PLFA) analysis and the remaining sample is incorporated into a flow-through column apparatus. The sediment core is kept saturated throughout this process. A flow rate of about 12-ml/hr is then established through the column to simulate local natural groundwater flow conditions. Bacterial and bromide breakthrough experiments are run by pulling a pulse of either bacterial suspension in natural groundwater or bromide solution through the column using a peristaltic pump. For the bacterial-breakthrough experiment, the column effluent is sampled at six-minute intervals using an autosampler, and the samples are analyzed with membrane filtration techniques. For the bromide breakthrough experiment, the effluent is analyzed using an ion-specific electrode or samples are collected for analysis by high-performance liquid chromatography (HPLC).

If possible, data from the breakthrough experiments are reproduced with a computer analytical model of contaminant transport. Matching the model predictions to the bromide experiment data, velocity and dispersivity are

determined. Knowing the pumping rate and velocity allows calculation of an effective porosity. Knowing the effective porosity allows determination of groundwater flow velocity in the bacterial breakthrough experiment. Using the computed velocity and the dispersivity calculated from the fitted dispersion coefficient from the bromide experiment, bacterial-reaction coefficients are determined by fitting model results to the bacterial-breakthrough data. To test Hypothesis 1, this process is repeated with replicates on intact sediment (Treatment 1) and on sediment after killing off the autochthonous microbial community (Treatment 2). The reaction coefficients obtained from each treatment are then compared using analysis of variance techniques.

Hypothesis 2: A useful predictive model can be developed for allochthonous bacterial transport through aquifer sediments. We are attempting to investigate the factors that affect the transport of allochthonous bacteria through groundwater sediments. These factors will be quantifiable aquifer system characteristics. The primary factors affecting allochthonous bacterial transport include hydraulic conductivity, effective porosity, mineralogy, organic matter content and grain-size distribution of aquifer material. We will run bacterial and bromide breakthrough experiments on sediment cores collected from a variety of locations. The procedures for running the experiments, quantifying the autochthonous microbial community and fitting the breakthrough curves, will be the same as described for Hypothesis 1. Upon completion of the flow-through experiments, the column sediments and/or sediments from the original cores close to the column sediments will undergo abiotic characterization. We will then perform multiple linear regression analysis to relate calibrated transport model parameter values to aquifer characteristics. Various regression models will be explored for good fits. Forward selection and backward elimination procedures will be employed. Correlation between possible independent variables will be investigated. Only those variables with t-ratios > approximately 2.0 will be included in the final regression models. Equation robustness to changes in variable inclusion will be considered. To improve fits, transformations on the regression variables will be explored including logarithmic, square root and reciprocal transformations. Multiple linear regression models will be selected on the basis of the highest R^2 value with statistically significant variables. Plots of standardized residuals versus the fitted dependent variable value will be examined to judge the model fit.

Hypothesis 3: The bacterial-transport model developed in the laboratory will accurately predict bacterial transport in the field. We have developed a field site in the Four Mile Creek basin near Oxford, Ohio for eventual field-testing of our model. The site will use a drinking-water well formerly operated by the City of Oxford. The well is set in a 12-m layer of heterogeneous, permeable, glacial outwash deposits. A dense, clayey glacial till underlies the outwash, confining groundwater flow. The pumping well is a Ranney® collector with horizontal, screened collector arms, installed at depth and extending radially out from a vertical caisson. Water is drawn from the adjacent Four Mile Creek. Water from this well has sporadically tested positive for fecal coliform bacteria. The field area near the Ranney collector provides an excellent site for investigation of bacterial

transport through groundwater. We will use a single arm of the Ranney collector to induce a hydraulic gradient and use that gradient, to perform conservative tracer tests and observe bacterial transport and fate along flow paths from the creek toward the pumping well. Field data will be used to test the modeling approaches presented.

A combination of single and nested piezometers and multilevel sampling devices have been used to determine hydraulic conductivities and will be used to determine the horizontal and vertical concentrations of chemical and microbiological components of groundwater. Hydraulic conductivities are investigated using an aquifer pumping test, piezometer slug tests and laboratory permeameters.

Forced-gradient tracer tests will be performed using a bromide solution. Approximately 100 liters of groundwater with a bromide concentration of 180 mg/l will be injected into 3 piezometers placed directly below the Four Mile Creek bed. Bromide will be used as a conservative tracer because of its low background concentration in the aquifer. The injection wells will be located so that they are directly upgradient of the multilevel sampling array under pumping-induced gradients. Based on our experience with this aquifer, expected travel time from the creek to the radial arm is one to two days. Samples will be collected and brought to the laboratory for bromide analysis with the HPLC. Moment analysis on bromide concentrations will be used to determine the movement of the center of mass for velocity determination and the change in concentration variance for determination of apparent longitudinal dispersivity. Using these data we will predict allochthonous bacterial distribution within the flow path. Concurrent with the bromide tracer studies the distribution of allochthonous bacteria within the flow field will be determined and compared with model predictions.

Principal findings and significance:

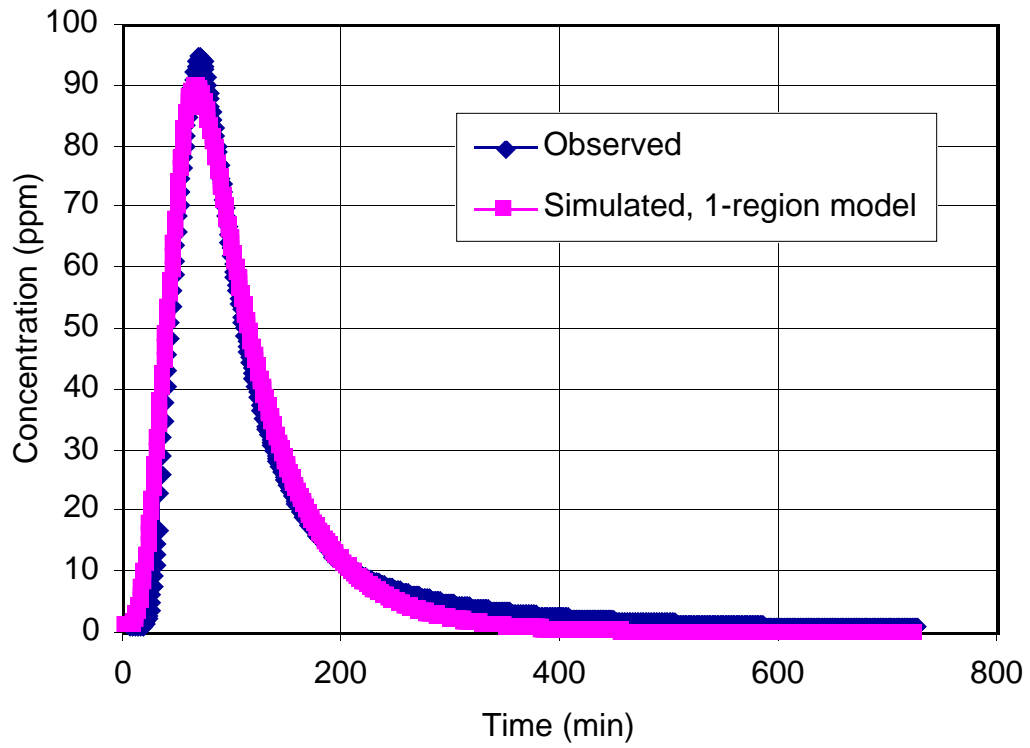
Hypotheses 1 and 2

Our initial column apparatus was designed to incorporate 3.4-cm ID columns. The design allows for natural sediments to be used in a controlled laboratory setting without disturbing the physical structure of the aquifer sediments or the autochthonous microbial community. These features are essential for investigating the role of the indigenous microbial community on the transport of invasive bacteria. Natural sediment cores were taken from the local groundwater aquifer and 10-cm sections of these cores were chosen and incorporated into the column apparatus. Bromide and bacterial flow-through experiments were performed on those columns to test our hypothesis that the indigenous microbial community has interactions that significantly affect the survival and retardation rates of invasive pathogens in groundwater. The column apparatus, along with a technique to kill the indigenous microbial community, allowed us to set up two treatments for our experimental design. Results from the two treatments were compared and the effect of indigenous microbial community on invasive bacterial transport was studied.

A 10-ml, 200 $\mu\text{g/ml}$ bromide slug, prepared from local groundwater, was used in the experiments. A bromide ion-specific electrode (ISE), connected in-line to the effluent tubing, was used to measure the bromide concentrations in the effluent. All the breakthrough curves obtained from bromide experiments were asymmetrical and exhibited long tailing. The cause of the skewness and tailing for non-reactive tracers such as bromide is probably the existence of immobile or stagnant water regions and solute exchange between the mobile and immobile regions. A physical non-equilibrium, two-region model that explicitly accounts for the mass exchange between the mobile and immobile regions was therefore applied to better simulate the experiment data. CXTFIT2.0 software (Toride et al., 1995) was used to simulate the breakthrough experimental data. This program can be used to estimate transport parameters in both the equilibrium mode and the non-equilibrium, two-region mode. Model parameter values are estimated by fitting the observed data with a simulated curve. The simulated and observed curves are matched by minimizing the sum of the squared differences using a nonlinear least-squares inversion method. Figure 1 shows the bromide breakthrough data for the 9-11-98 core modeled with both the equilibrium model and the two-region model. The two-region model better simulates the entire curve, especially the long tail. Since the two-region model better represents the bromide breakthrough data, it was chosen for all bromide modeling. Values of effective porosity and dispersivity were calculated based on the modeling results from two-region model.

It is essential that the column apparatus be able to reproduce experimental data. The reproducibility of the bromide breakthrough experiment was tested with replicate runs on each core. All the replicate bromide runs were performed under similar conditions. However, with the pump we were using, the flow rate varied slightly among the replicate runs. Figure 2 shows the breakthrough curves of the replicate runs for the 9-11-98 core. Run 1 had a slightly higher flow rate, and therefore has a larger peak concentration than Runs 2 and 3. The two-region model was used to reproduce the experiment data; values for transport parameters are presented in Table 1. The values for effective porosity obtained from the replicate runs vary only slightly; however, fitted dispersivity values have a larger variance.

a.



b.

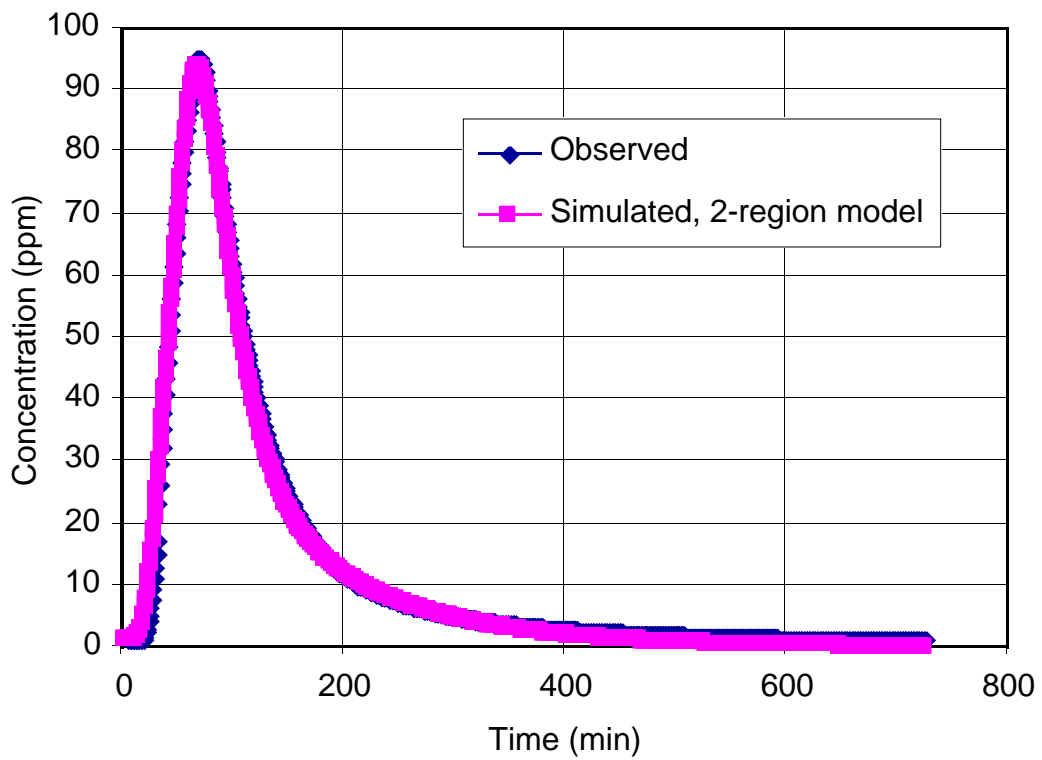


Figure 1. Bromide breakthrough data and model predictions for a) the equilibrium model and b) the physical non-equilibrium, two-region model.

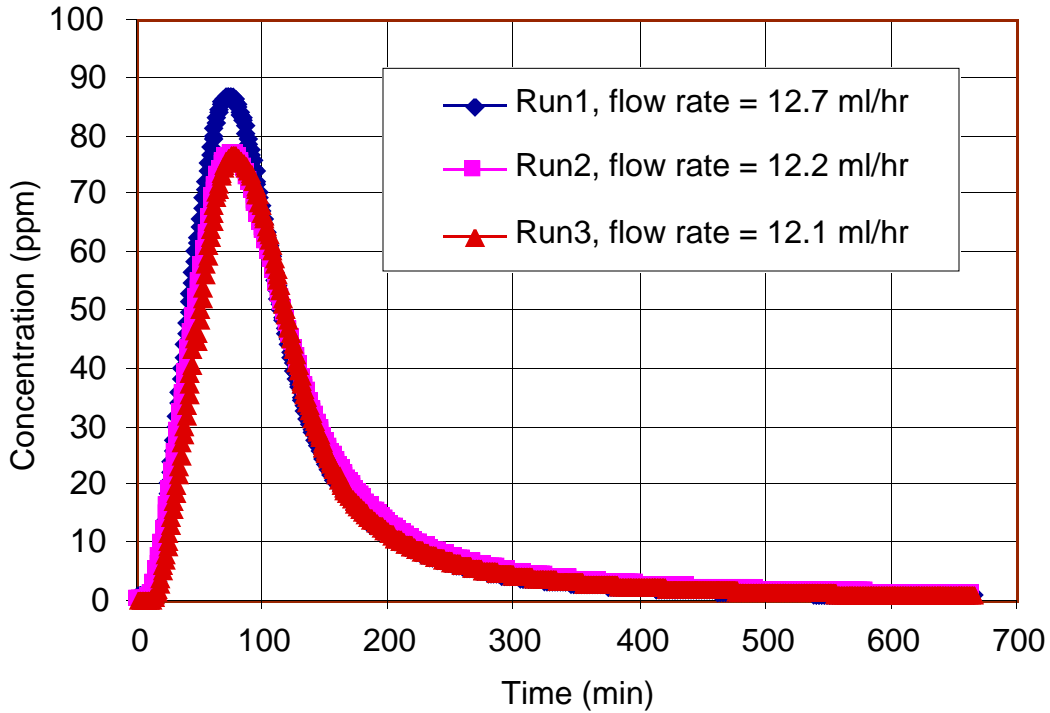


Figure 2. Breakthrough curves obtained from three duplicate runs on the same core

Table 1. Parameters of duplicate bromide runs before and after pasteurization

Pasteurization	Run #	Flow rate (ml/hr)	C_{max}/C_0	C_{max} arrival time (pore volumes)	θ	Dispersivity (cm)
Before	1	12.7	0.436	1.13	0.14	2.98
	2	12.2	0.386	1.09	0.15	3.53
	3	12.1	0.386	1.06	0.15	2.63
After	1	13.5	0.475	1.24	0.13	1.63
	2	6.8	0.466	1.23	0.15	1.56
	3	10.6	0.428	1.14	0.15	1.89

Pasteurization was employed to kill the autochthonous microbial community. It is critical that the physical structure of the aquifer sediments is not altered by pasteurization. Bromide flow-through experiments were also used to check the effect of pasteurization on sediment physical structure. This was tested by comparing bromide breakthrough results obtained from the same core before and after pasteurization. Figure 3 shows the bromide breakthrough curves obtained

from the experiments before and after pasteurization of the 9-11-98 core. Again, the difference in peak concentration is due to a slightly different flow rate. Effective porosity values obtained from the two runs are very similar (Table 1). Dispersivity values are smaller after pasteurization. Based on the effective porosity values and the similarities in the breakthrough curves, we concluded that pasteurization does not substantially affect the sediment's physical properties.

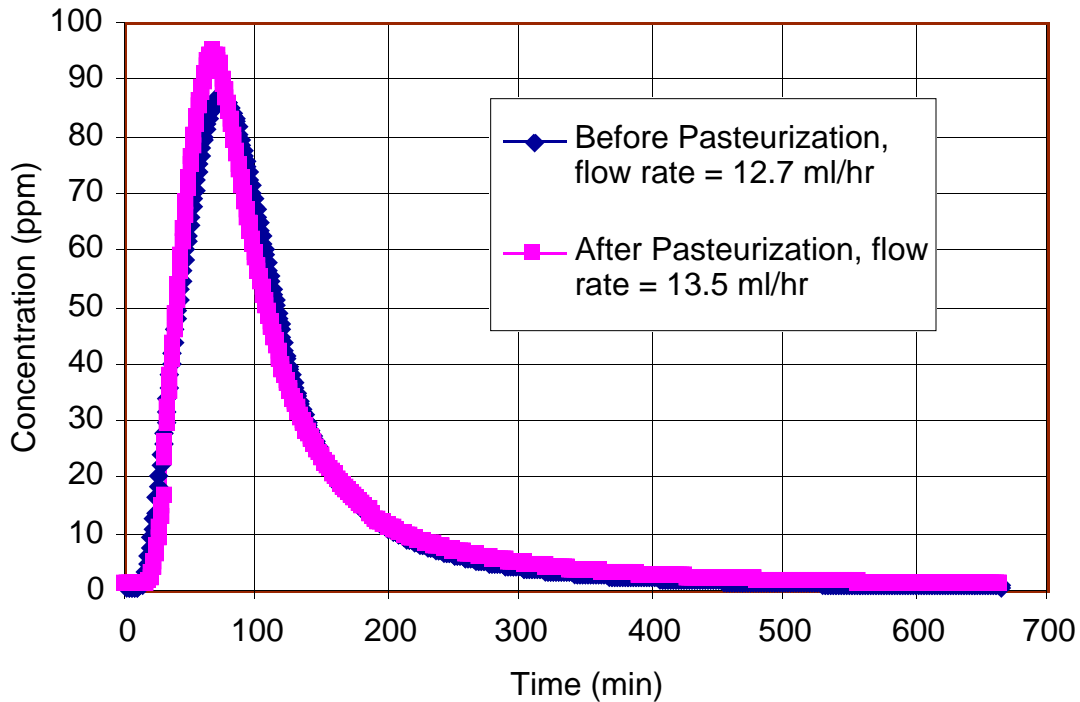


Figure 3. Bromide breakthrough curves before and after pasteurization.

To test our hypothesis that the indigenous microbial community has interactions that significantly affect the survival and retardation rates of invasive pathogens in groundwater, bacterial breakthrough results before and after pasteurization were compared. Figure 4 shows the breakthrough curves obtained from bacterial flow-through experiments before and after pasteurization for the 9-11-98 core. The two experiments were performed under similar conditions. The bacterial slug had a concentration of 10^9 CFU/mL and the slug injection period was 400 minutes for both experiments. Unlike the bromide curves, the bacterial breakthrough curves have non-classical shapes. Both curves drop quickly after reaching the peak concentrations; the decrease occurs within the slug injection period. The arrival of peak concentrations is delayed for both curves compared to a conservative tracer (bromide). The relative peak concentrations are also much lower than those of bromide. In other words, both attenuation and retardation are observed in bacterial breakthrough.

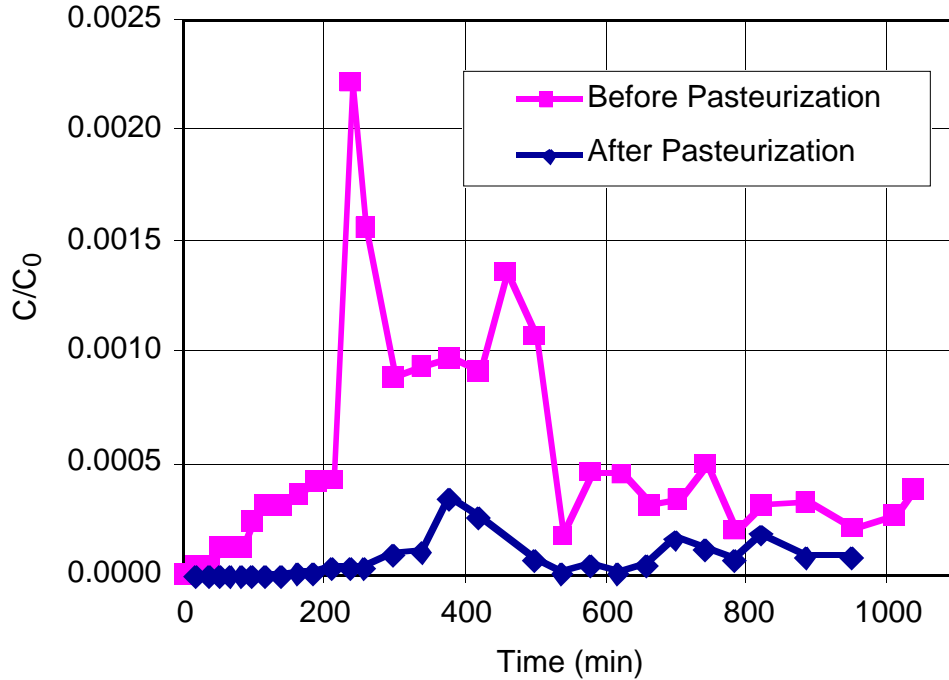


Figure 4. Comparison of bacterial breakthrough before and after pasteurization.

The non-classical shape of the breakthrough curves prohibited modeling the curves and obtaining a retardation or attenuation rate. To compare the two bacterial breakthrough curves, two alternative parameters were chosen: the relative peak concentration (C_{\max}/C_0) and the arrival time (in pore volumes) of C_{\max} . Both parameters changed to a great extent after pasteurization (Table 2). Based on the results of this experiment, pasteurization increases bacterial attenuation and retardation. It is possible that pasteurization may have altered the physical structure of the sediments; however, pasteurization has little effect on the bromide transport. It is, therefore, reasonable to conclude that pasteurization does not significantly affect the physical structure of natural sediments. A second explanation is that the sorption properties of the natural sediments were changed by pasteurization, which, in turn, resulted in the change of bacterial breakthrough. A third explanation is that the autochthonous bacteria may compete for reversible and/or irreversible sorption sites. Killing the autochthonous bacteria frees sorption sites, making the sites available for allochthonous bacterial sorption. This suggests that the presence and nature of the autochthonous microbial communities significantly affects the transport of allochthonous bacteria transport through groundwater. More work needs to be done to confirm the experiment results.

Table 2. Effect of pasteurization on bacterial breakthrough

Pasteurization	C_{\max}/C_0	C_{\max} arrival time (pore volumes)
Before	0.0022	3.8
After	0.00025	6.8

Results from new experimental setup

Towards the end of this project, we began to work with bigger columns. Bigger columns allow collection of more representative samples from the field. With a larger split-spoon sampler and liner we are able to include larger-sized particles and obtain more sample with less chance of sampling refusal. The experiment protocol is basically kept the same as that with the original columns, with a few changes made to improve the experiment setup. A new column apparatus was made to incorporate a 10-cm long by 6-cm diameter column rather than the previous 3.4-cm diameter column. We have also decided to inject fluids into the column bottom and flow upwards. An upward flow helps remove any air bubbles trapped in the column and, in the case of the bacterial experiment, can also minimize the effect of gravity on bacterial transport. A variable-speed, digital Masterflex L/S peristaltic pump was purchased to better maintain a constant flow rate. We also changed the bromide analysis method. The bromide ion-specific electrode (ISE) was originally used to collect bromide data. However, minor drifting of the ISE reading often occurred and we could not obtain the desired accuracy. We are now collecting samples for HPLC analysis with a Dionet DX500 chromatography system and Peaknettm software.

In order to test the new column setup, quartz sand columns were packed and both bromide and bacterial flow-through experiments were performed, collecting column effluent in a fraction collector at an 8-minute interval. Figure 5 shows the breakthrough curves obtained from two bromide flow-through experiments performed on the same sand column. The new digital pump allowed us to establish a constant flow rate of 0.6 mL/min; a slug of 6 mL of 99.68 ppm bromide solution was used. The two curves are almost identical. In addition, total mass recoveries were very close to 100%. Based on these results, the bromide breakthrough data appear highly reproducible and the new column setup works very well. For quartz sand columns, equilibrium transport of bromide can be expected. Therefore, an equilibrium model was used to simulate the experiment data. Table 3 gives the transport parameters obtained from model simulation. Again, the values for the effective porosity and dispersivity obtained from the two replicate runs are almost identical.

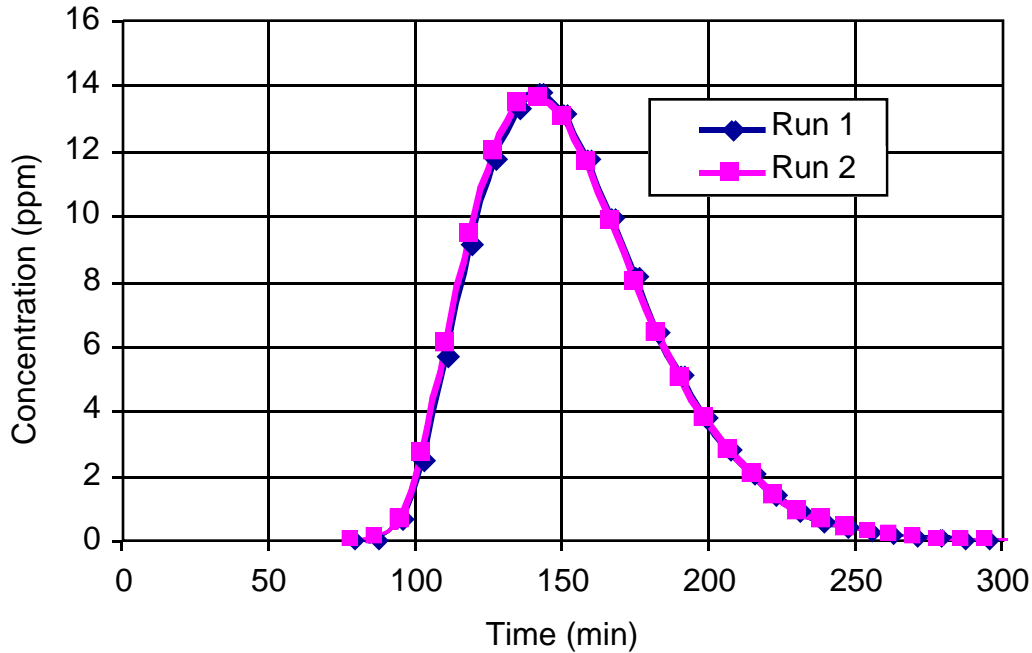


Figure 5. Two replicate bromide runs performed on the same sand column.

Table 3. Transport parameters obtained from the two bromide experiments.

	Effective Porosity	Dispersivity (cm)	Model fit R²	Mass Recovery (%)
Run 1	0.3035	0.2154	0.9956	101.41
Run 2	0.3049	0.2117	0.9960	101.10
Difference (%)	0.46	1.74	NA	NA

A bacterial flow-through experiment was also performed on the same sand column. The slug concentration of the bacterial experiment was 1.9×10^9 CFU/mL, and the flow rate and slug duration time were the same as those of the bromide experiments. Figure 6 shows a comparison between the bacterial and bromide breakthrough curves. Even with the quartz sand column, the bacterial breakthrough curve is non-classical. Table 4 lists the breakthrough curve parameters in comparison to those of bromide experiments. Interestingly, the peak arrival of bacteria was slightly earlier than that of bromide. This can result from the effect of size exclusion. Due to their size, bacteria preferentially follow the flow paths consisting of bigger pores with larger flow velocities, resulting in relatively earlier breakthrough of bacteria. The relative peak concentration of bacteria, however, is much lower than that of bromide and exhibits a much longer tail. Bacterial concentrations level off after about 3 pore volumes (about 400 minutes) but last up to about 38 pore volumes (not shown in the figure). Mass recovery of the first 3 pore volumes was only 48.64%. We sampled for about 90 hours (38 pore volumes) and the last sample taken still had a concentration of about 10^5 . Bacteria were retarded in the sand by sorption or filtration and were flushed out slowly for long periods of time.

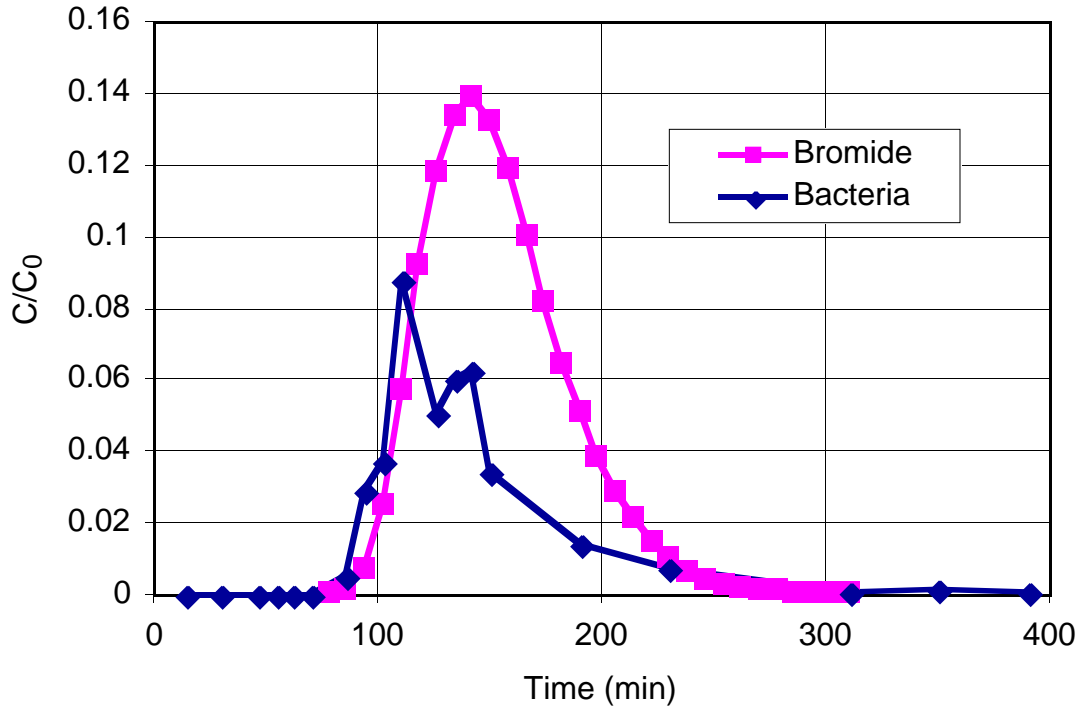


Figure 6. Bacterial breakthrough curve in comparison with bromide breakthrough curve.

Table 4. Comparison of bacterial and bromide breakthrough through quartz sand.

	C_{\max}/C_0	C_{\max} arrival Time (min)	Mass recovery (%)
Bromide	0.1395	142	101.10
Bacteria	0.0372	102	48.64*

*Mass recovery of the first 3 pore volumes.

Based on the results of both bromide and bacterial flow-through experiments, it is clear that the new column setup worked as expected. At the end of this project in September 1999, we began to collect natural sediments and perform flow-through experiments on natural cores using the 6-cm diameter setup.

Investigation of Autochthonous Microbial Community

Groundwater aquifer sediment has been and continues to be analyzed so that the microbial biomass and microbial community structure can be characterized. Sediments are also being analyzed for sediment grain size. We hypothesize that there is variability in microbial biomass and the microbial community structure at differing depths that is related to grain size. In fact, it appears that there is a relationship between biomass and the location of interfaces of two distinct sediment types.

To test these hypotheses, three sediment cores were extracted from a field site near Four Mile Creek and the Water Treatment Facility in Oxford, OH. The 5/13/98 and 8/20/98 bore holes were drilled to the base of the aquifer using hollow-stem augers. The 1/22/99 bore hole was drilled using a hydraulic drill rig supplied and operated by Geoprobe Systems. The 5/13/98 and 8/20/98 cores were retrieved using a sterile split-spoon sampler, and the 1/22/98 core was recovered in a sterile plastic liner. Samples were taken from the sediment cores at 0.6m intervals, and at sediment interfaces. Sediment samples were also taken immediately above and below the biological sampling sites for grain-size analysis. For biological sampling, the outside of the core was removed and samples were taken using a sterile spoon. These were placed in sterile test tubes and kept on ice in the field for no more than 8 hours, then brought to the laboratory for biological analysis. The microbial lipids were then extracted using a modified Bligh-Dyer lipid extraction (3, 10, 26). Once harvested, a portion of the lipid was analyzed in a colorimetric assay for the amount of phospholipid phosphate (PLP) present. This amount was quantified spectrophotometrically, and converted to microbial biomass. The remaining lipid was partitioned on a silicic acid column. The phospholipid fraction was collected, and the glycolipid and neutral lipid fractions were discarded. The purified phospholipids underwent a mild alkaline methanolysis, and the resultant fatty acid methyl esters, (FAMES) were purified using a C18 column. These FAMES were then analyzed with gas chromatography. The presence, absence and abundance of certain fatty acids were analyzed and used to determine the types of microorganisms present in the sample (7, 9, 25).

Two of the three sediment cores have already been processed for PLP. The data obtained from the PLP analysis have been used to determine microbial biomass profiles (Figures 7 and 8). Both sediment cores displayed large variations in microbial biomass with depth. At the different depths sampled, the 5/13/98 core's biomass varied between 0.13 and 0.56 nmol PLP/g DW. The 8/20/98 core's biomass was highest in samples taken above 2.8 m below the surface. Below 2.8 m, there was variation at the different depths sampled similar to the 5/13/98 core.

PLFA data were used to determine microbial community structure. Fatty acids present were predominately 14-19 carbons in length and included saturated, straight-chained fatty acids 14-18 carbons in length, terminally-branched fatty acids, branched, monoenoic fatty acids and straight-chained, w 5,7, and 9 monoenoic fatty acids. Unusually abundant fatty acids were 16:1 ω 5, 10me16:0, cy17:0 and several branched 19:0 fatty acids. PLFAs including 10me16:0 and the branched, odd-chain fatty acids indicated the presence of anaerobic bacteria including sulfate-reducing bacteria. The polyenoic fatty acids 20:4 ω 6 and 20:5 ω 3 occurred at low abundances. This indicated that the microbial community contained heterotrophic microeukaryotes and that these organisms were a minor component of the community.

Microbial biomass and community structure for the third core will be analyzed using PLP and PLFA analysis. Grain size analyses of the second and third cores are being conducted to determine the sediment characteristics at the same depths where the biological samples were taken. By combining these data with the abiotic

conditions of the aquifer, a description and location of the autochthonous microorganisms will be correlated with various groundwater sediment types. This novel data set will provide a basis for future work involving the prevention of groundwater contamination and the remediation of contaminated aquifers.

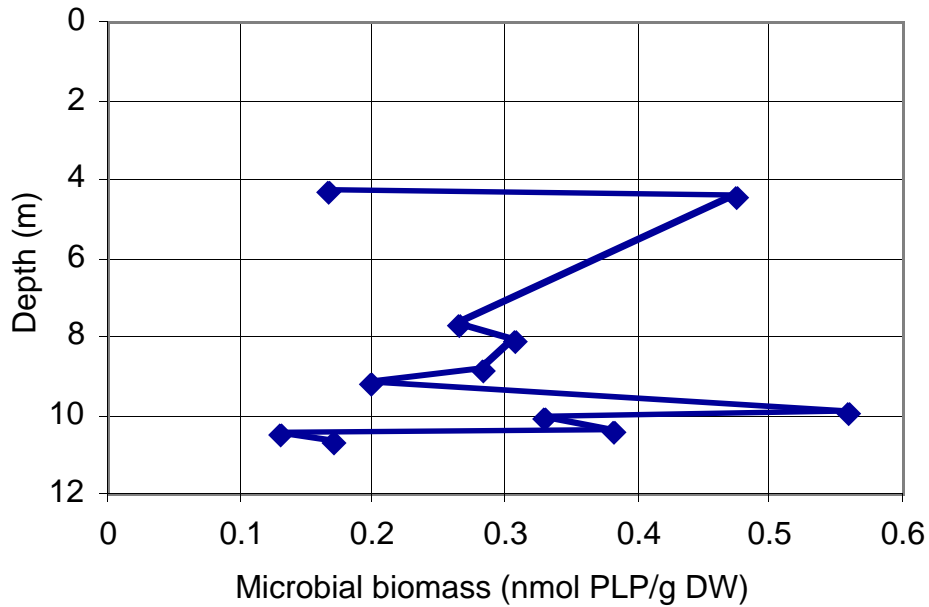


Figure 7. The microbial biomass profile for a groundwater sediment core taken on 5/13/98.

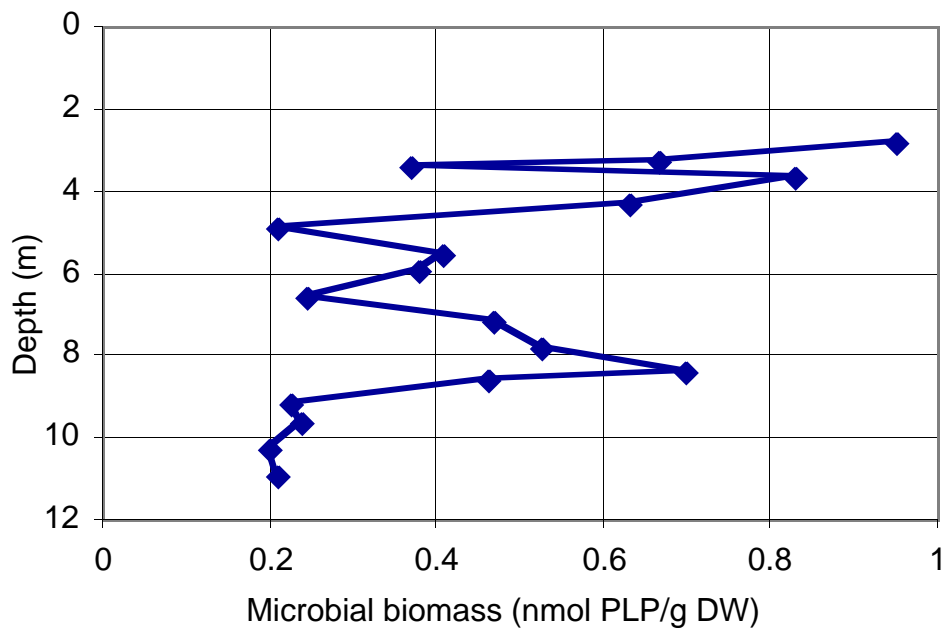


Figure 8. The microbial biomass profile for a groundwater sediment core taken on 8/20/98.

Hypothesis 3: Progress and results associated with establishing the field site

Site Description

Four Mile Creek Valley area bedrock lithology is characterized by interbedded limestone and shale of Ordovician age. During the early Pleistocene, a river carved a valley into the bedrock. The valley was carved to far greater depths than present elevation. During the Pleistocene, glaciers advanced and retreated, filling the valley with alternating layers of sand and gravel glacial outwash and dense glacial till. The result is a heterogeneous sediment sequence of coarse and fine layers. The shallowest layers are highly permeable sands-and-gravels with some silt and cobbles. The aquifer of interest for this study is the shallow, unconfined aquifer lying above a thick, impermeable layer of glacial till.

The specific field site of interest within the Four Mile Creek valley is located adjacent to Four Mile Creek, less than one mile east of Oxford, Ohio, adjacent to State Road 73 (Figure 9). A municipal pumping well was installed at this site in 1961. This municipal well is a Ranney collector (Figures 9 and 10), comprising a central vertical caisson equipped with a pump. From the base of this caisson, radial arms extend horizontally into the aquifer. When pumping, drawdown in the central caisson induces flow of water from the aquifer into the radial arms and into the caisson where it is pumped to the water treatment plant.

The radial arms vary in length and depth (Figure 10). The depth of the upper

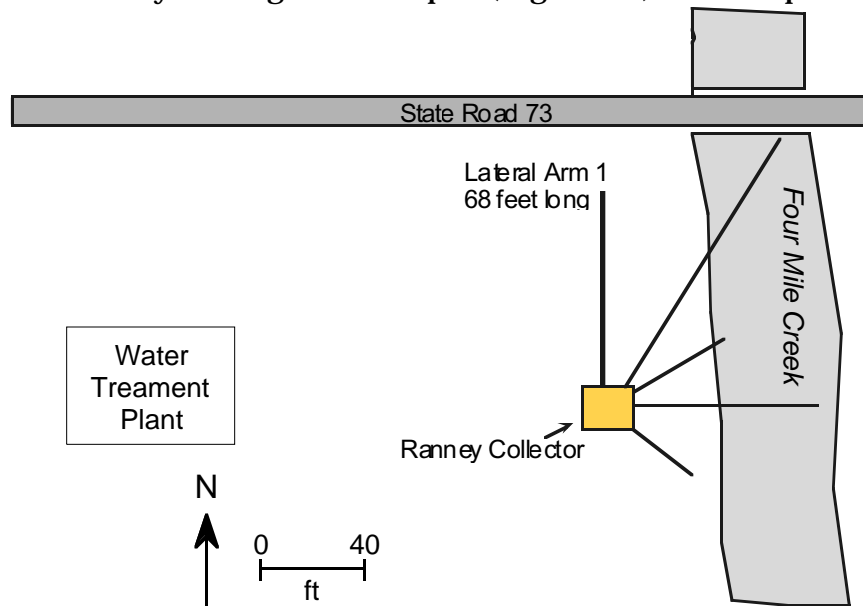


Figure 9. Plan view of Ranney collector and field site.

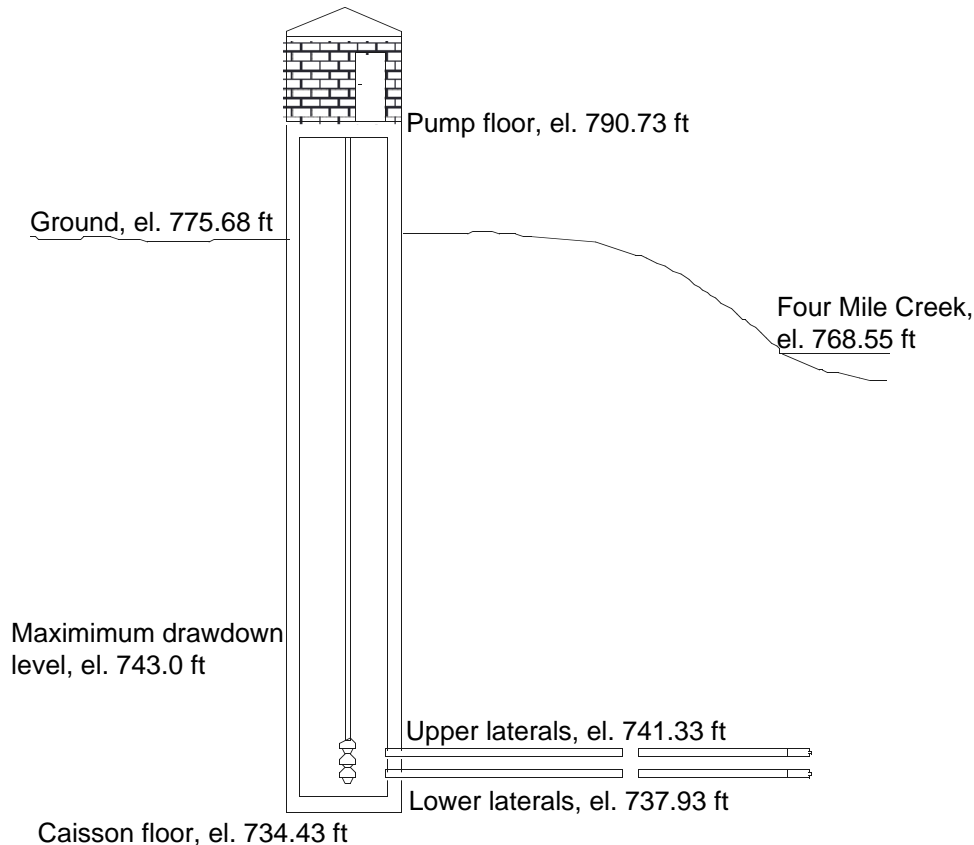


Figure 10. Profile view of Ranney construction.

laterals is less than 50 feet below the bed of Four Mile Creek. According to US EPA standards, this municipal well is considered to be under the direct influence of surface water in Four Mile Creek.

In 1996 the Ranney production well was taken offline due to the presence of coliform bacteria in water samples. The City of Oxford has allowed the use of this well and surrounding area as a research site to examine the fate and transport of bacteria from Four Mile Creek to the municipal well.

Design and Development of Field Site

At the beginning of this project, Laterals 1 and 2 were open; the rest were closed. Because Lateral 1 is parallel to the creek, we wanted only that lateral open to induce flow perpendicularly from the creek to the lateral. Therefore, in December 1998 we contracted Reynolds, Inc. to dive into the caisson and close off Lateral 2.

Placement of monitoring wells was based on the stream-pumping well configuration and expected flow paths. Ten monitoring wells have been installed using a hollow-stem auger drilling rig (Figure 11). The monitoring wells were installed in 5 nested pairs: TS1A&B, TS2A&B, TS3A&B, TS4A&B, and TS5A&B, where the "A" wells are approximately 8-10 feet shallower than the "B" wells.

Multilevel sampling wells – TS6, TS7 and TS8 – were also installed (Figure 11). The monitoring wells consist of 1.25 inch diameter PVC casing with a 1-ft long screened interval of 20 slot screen at the bottom. The multilevel sampling wells are StrataSamplers® manufactured by Timco, Inc. They consist of 2-inch diameter, 1-ft long screened interval stainless steel with a sediment sump. Three-foot long, 2 inch diameter PVC casing separates the sampling ports.

The heterogeneity of the aquifer sediments were characterized by analyzing sample cores. Some samples were acquired by drilling with a hollow-stem auger rig, capable of drilling to a depth of 45 ft below ground surface. The sample cores were taken with a 2-inch diameter steel split-spoon sampler. Other samples were acquired by a direct hydraulic push system designed by Geoprobe Systems and a 1.5 inch diameter split spoon sampler at boreholes GP1 and GP2. Using the Geoprobe system, downhole electrical conductivity data was also collected at boreholes GP1, GP2, GP3, GP4, GP5 (not shown) and GP6 (not shown). The electrical conductivity profile for GP1 was used for calibration against an actual sediment log. Using GP1 as a benchmark, lithology for the other GP boreholes was inferred from the conductivity profiles.

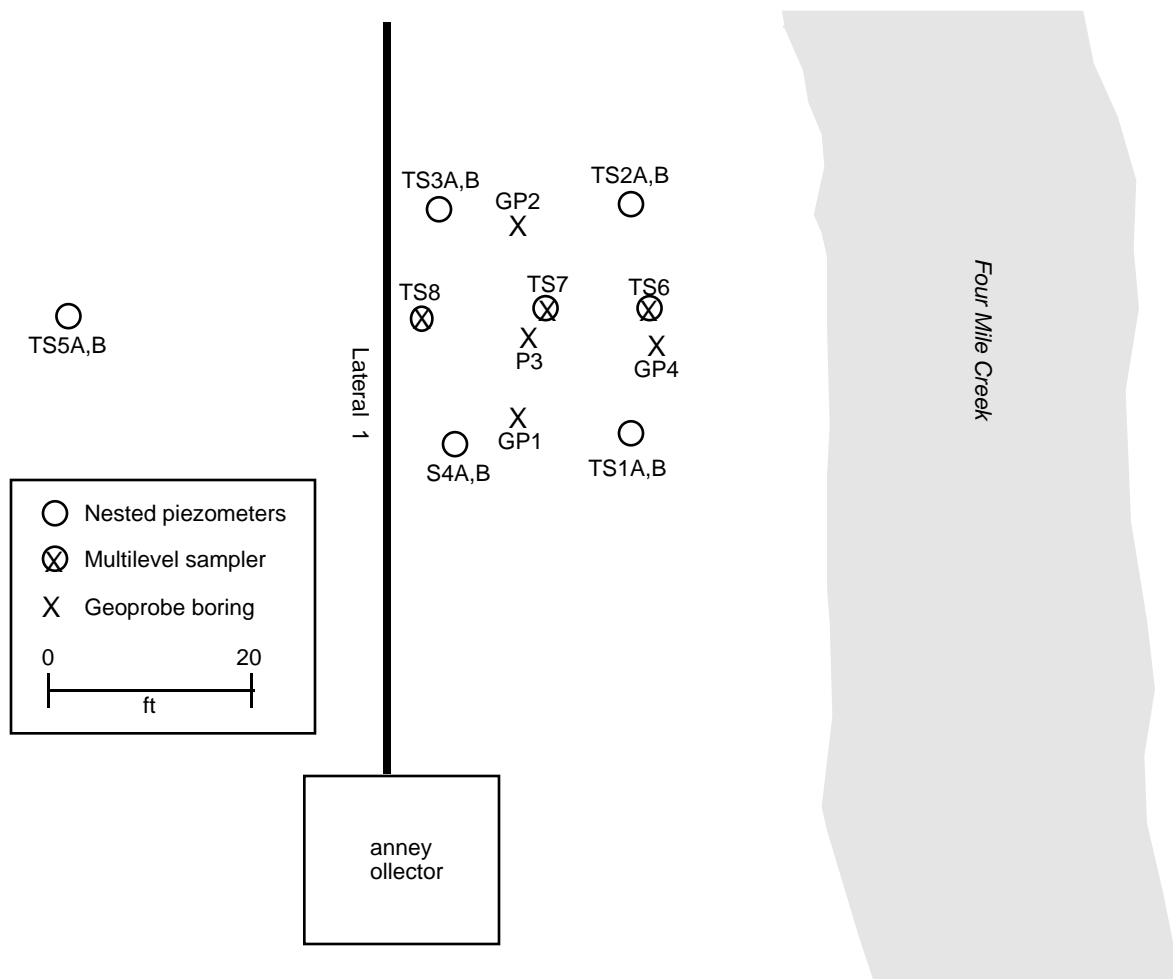


Figure 11. Locations of monitoring wells and Geoprobe borings.

Piezometer Slug Tests

Slug tests provided estimations of hydraulic conductivity on the scale of approximately 3-15 ft – larger than that of the column permeameter experiments, but smaller than most aquifer pumping tests. Multiple slug tests were performed at each piezometer to demonstrate reproducibility of response curves at the same and different displacements (Butler, 1998).

Due to the high hydraulic conductivity of the formation, many of the slug tests exhibited oscillatory behavior caused by the inertial energy and momentum of the water column. (Springer and Gelhar, 1991). These tests were analyzed using a method by Springer and Gelhar (1991). The method uses curve matching to Kipp type curves (Kipp, 1985). Tests not exhibiting the oscillatory behavior were analyzed with the method by Bouwer and Rice (1976).

The delivery of the “slug” or change in water level in a slug test must be done instantaneously. Traditional methods where a volume of water is displaced or removed create complications of splashing and spilling thus resulting in a non-instantaneous slug. We therefore developed a pneumatic apparatus in which air pressure is used to lower the water level. A large diameter, quick release valve allows instantaneous release of the pressure. A pressure transducer located at the screened interval of the well measures the recovery. The design for the slug test can be seen in Figure 12. It consists of an airtight cap that fits over the top of a 1-inch well top, a port for the pressure transducer cord and water level sensor, a port for the air intake regulator, and a port for an air evacuation valve. The intake air valve and regulator are connected to an air compressor. To ensure that the water level is not pushed below the pressure transducer, the water level sensor is lowered to the depth of the maximum induced head change, with the pressure transducer at a greater depth. The water level is lowered slowly until the water sensor beeps. At this point the water level is held constant by the regulator. The data logger is started and the pressure is then instantaneously released.

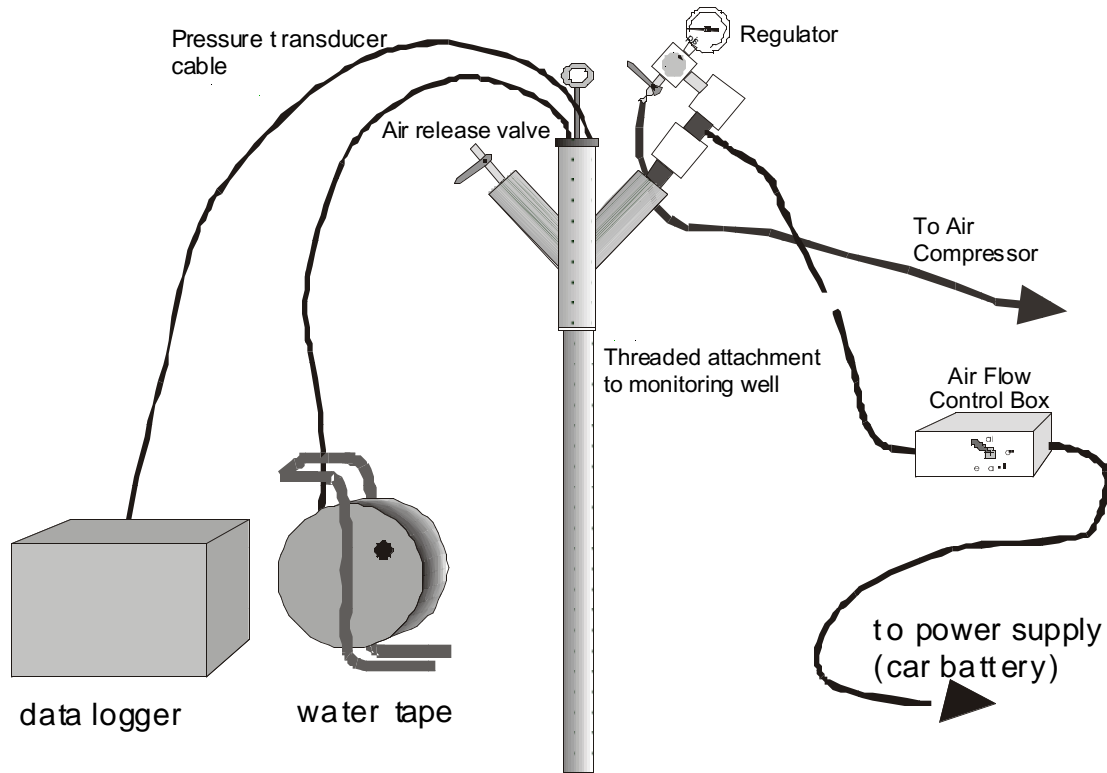


Figure 12. Diagram of air-slug apparatus.

Values of hydraulic conductivity obtained from these analyses ranged from 70 to 607 ft/day (0.050 to 0.214 cm/sec) with an arithmetic mean of 329 ft/day and a geometric mean of 275 ft/day (Table 5). No wells were screened in the shallow fine layer; the range of values reflects only hydraulic conductivity within the outwash deposits.

Oscillatory responses were found in TS4A, TS4B, TS5A, and TS5B. The values of hydraulic conductivity found for these wells were higher than in most of the other wells. Sediment samples taken at the screened intervals of the highest conductivity boreholes (TS4B and TS5B) showing oscillatory responses were characterized in the field as being a fairly well sorted coarse sand and gravel with little to no fine sand or silt. Grain analysis showed that a sample taken at the screened interval of TS5B was 2% gravel, 90% sand, and 8% silt/clay. Field descriptions of sediment samples obtained from the screened intervals of the other boreholes were characterized by more poorly sorted sand and gravel with a larger percentage of fine sand or silt.

Aquifer Pumping Tests

A larger scale measurement was obtained by conducting an aquifer pumping test. Due to the unusual configuration of the lateral pumping arms and the creek, the hydraulic conductivity cannot easily be solved for using classical analytical methods. Instead, we have solved for hydraulic conductivity

numerically by designing and calibrating a flow model to steady-state non-pumping and pumping conditions.

Table 5. Summary of hydraulic conductivity values from slug tests.

Piezometer	K (ft/day)	K (cm/sec)
TS1A	141	0.050
TS1B	394	0.139
TS2A	121	0.043
TS2B	70	0.025
TS3A	359	0.127
TS3B	341	0.120
TS4A	342	0.120
TS4B	398	0.140
TS5A	375	0.132
TS5B	557	0.197

A pumping test was conducted February 4, 1999 with only Lateral 1 open to the aquifer. This test was run for 50 hours at a pumping rate of 40.65 ft³/min. During this time, the groundwater system appears to have reached or nearly reached steady state. Based on calibration of the groundwater-flow model the pumping-test data yield a hydraulic conductivity for the outwash sediments of 440 ft/d. This value is somewhat higher than the slug-test geometric mean of 275 ft/d. The groundwater-flow modeling is described in detail in the following section.

Groundwater Flow Modeling

In this study, a flow model was developed to attain numerical solutions for aquifer pumping tests and predict contaminant flow paths from the creek to the Ranney collector.

1. **Conceptual Model.** The aquifer being modeled was considered an unconfined system. The upper boundary of the aquifer is therefore the water table. The bottom of the aquifer is the impermeable glacial till layer. The western and eastern boundaries of the modeled area are the Four Mile Creek valley walls. The north and south boundaries were set far from the zone of influence of the pumping. The uppermost stratum is composed of brown, organic-rich, soil which grades into brown silt, sand and gravel. This layer is underlain by a gray, fine-grained layer characterized by very high clay and silt content. This layer was assumed to be horizontally continuous, consistent with drilling core logs. Beneath the fine layer is a sand-and-gravel layer. This layer has lenses with higher percentages of cobbles, gravel and sand. Four Mile Creek runs generally north to south across the area. Recharge was assumed to occur at a constant rate over the entire land surface.

2. **Model Code and Grid Discretization.** MODFLOWwin32 was the program used to numerically simulate the groundwater flow. Grid cells are as large as 30 ft by

30 ft but telescope down to as small as 5 ft by 5 ft in the area of the Ranney collector and monitoring wells. Such a fine grid was needed to differentiate between different monitoring wells in the area of interest and to properly simulate pumping in Lateral 1. The model consists of seven layers. Layer thicknesses were determined by examination of drilling core logs. The lower boundary is the impermeable till. Layers 3-7 represent the glacial outwash and are modeled with a homogenous value of hydraulic conductivity. Layers 3-7 are either 4 or 5 feet thick for the purpose of representing varying depths of the monitoring wells' screened intervals and the depth of the pumping well lateral arm. Layer 2 represents the fine grain facies of silt/clay and is continuous and assumed homogeneous across the study area. Layer 2 is modeled as 5-ft thick, which represents an average thickness of this layer. Layer 1 represents the sediments above the silt/clay layer. From core sample data, this layer typically grades from silty top soil to sand and gravel. It is modeled with a homogeneous value of hydraulic conductivity.

3. Stream-Aquifer Interaction. Four Mile Creek was modeled using measured stream width, depth, and streambed and stream stage elevation data. MODFLOW's river package was used to simulate the interactions between Four Mile Creek and the aquifer. The river was modeled with a gradient of 0.002, width of 65 ft, depth of 2 ft, length of 164 ft, stream bed thickness of 1 ft, stream bed conductivity of 2.62 ft/day, and stream conductance of 2.49×10^4 ft²/day.

4. Initial Parameter Values. The value for recharge rate was set to approximately 1/3 the average annual precipitation rate (0.003 ft/day). Initial values for hydraulic conductivity were estimated based on slug test measurements and sediment size and distribution. Vertical hydraulic conductivity values were based on the assumption of the anisotropy (K_v/K_h) ratio of 0.1. Other parameter values were based on the literature. All of the initial values are summarized in Table 6.

5. Calibration. The goal in calibration of the model was to match the field-measured target points in the modeled area. The model was calibrated in two phases. First it was calibrated to a set of targets on January 31, 1999 when there was no pumping. During this calibration, the model was insensitive to changes in parameter values. The model was then calibrated to a set of targets achieved at the end of the February 4, 1999 aquifer pumping test. This model was much more sensitive to changes in values of hydraulic conductivity. Table 6 shows the calibrated model parameter values.

Summary statistics to evaluate the accuracy of the model in predicting the measured head values are shown in Table 7. The residual refers to the difference between measured and simulated heads. Figure 13 shows the model-predicted head values plotted against the observed values for nonpumping and pumping scenarios. The points plot close to the one-to-one trendline. The well with the greatest residual is FC5. The reason for its large residual is unknown, but the well is far outside the area of pumping.

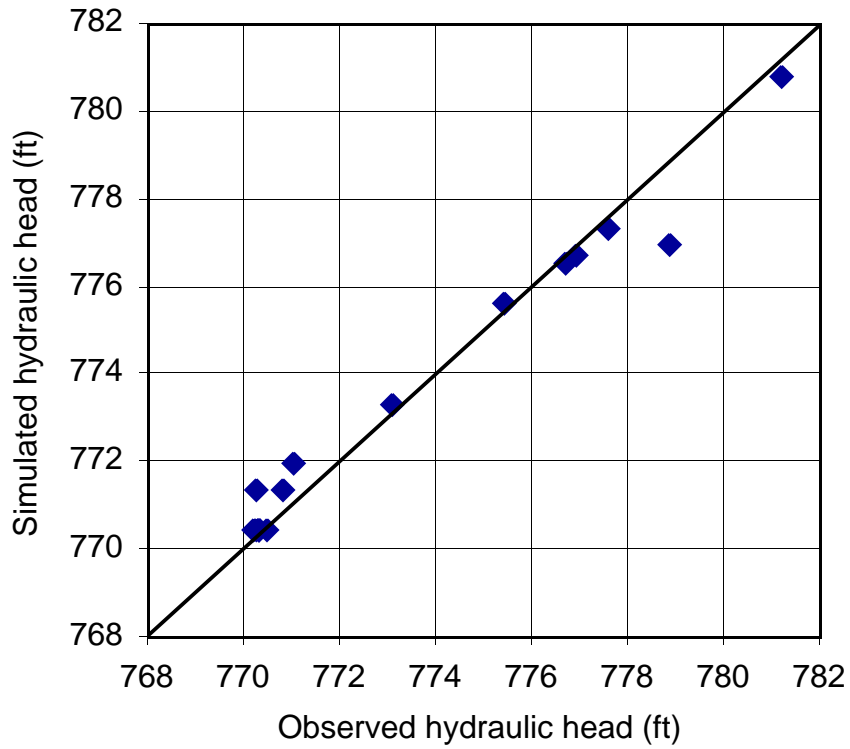
Table 6. Summary of calibrated model parameters.

Parameter	Initial value	Calibrated value
Layer 1 K_h (soil and outwash)	190 ft/day	231 ft/day
Layer 1 K_v (soil and outwash)	19.0 ft/day	21 ft/day
Layer 2 K_h (silt and clay)	1 ft/day	1 ft/day
Layer 2 K_v (silt and clay)	0.1 ft/day	0.225 ft/day
Layer 3-7 K_h (outwash)	279 ft/day	440 ft/day
Layer 3-7 K_v (outwash)	27.9 ft/day	58.08 ft/day
Recharge rate	0.003 ft/day	0.003 ft/day
Well discharge rate	58608 ft ³ /day	58608 ft ³ /day
Stream bed conductance	2.49x10 ⁴ ft ² /day	2.49x10 ⁴ ft ² /day
Effective porosity	0.3	0.3

Table 7. Summary of statistics for pumping and nonpumping scenarios.

Statistic	Nonpumping	Pumping
Residual Mean (ft)	-0.14	0.07
Residual Sum of Squares (ft ²)	7.04	5.10
Absolute Residual Mean (ft)	0.45	0.35
Minimum Residual (ft)	-1.19	-0.83
Maximum Residual (ft)	1.85	1.88
Head Range (ft)	11.01	17.02

a.



b.

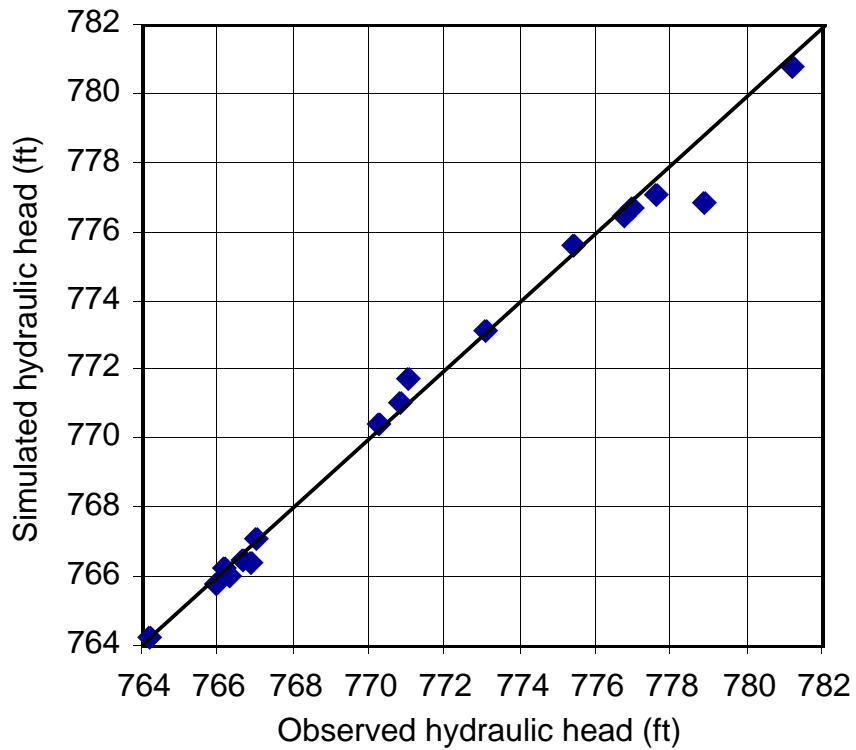


Figure 13. Model-predicted (computed) versus observed heads during a) pumping and b) nonpumping conditions.

6. Sensitivity Analysis. A sensitivity analysis was performed to assess which parameters are most influential in model calibration. Both the pumping and nonpumping scenarios are sensitive to changes in K_h of the silt/clay layer and the outwash layer. The model with pumping is far more sensitive than the non-pumping model since the drawdown created by the pumping is dependent on hydraulic conductivity. The calibrated values of K_h are optimal (in terms of minimizing the residual sum of squares) for all three facies in the pumping model. With the non-pumping model, the calibrated values are optimal for the uppermost top soil layer and the silt/clay layer. For the sand-and-gravel layer under nonpumping conditions, a lower value of K_h would be optimal, but only slightly improves the calibration. The high degree of sensitivity allows a high degree of confidence in the calibrated K_h values of those two facies.

The model was insensitive to increases in K_v in both scenarios. The non-pumping scenario is highly sensitive to a decrease in K_v of the silt/clay layer. The model with pumping is sensitive to decreases in K_v of the sand-and-gravel outwash layer as well. The calibrated value is nearly optimal in both scenarios.

The model with no pumping is sensitive only to an increase in recharge rate. The pumping model is only sensitive to the pumping discharge rate. The calibrated recharge and pumping rate values are also optimal.

Tracer Tests

On approximately the same scale as the pumping test, conservative tracer tests were performed to attain additional values of hydraulic conductivity, likely to be most representative of actual groundwater movement between Four Mile Creek and the Ranney collector. During the pumping test, hydraulic heads were measured to determine the groundwater flow directions within the monitoring-well network. Because the well network was placed toward the northern end of the Ranney pumping arm, the groundwater flow past the wells was northeast to southwest rather than directly from the east. An additional monitoring well, TS9, was therefore installed between TS2 and TS3 (Figure 11) so that it could be used as an injection well for the tracer tests. TS9 is a 2-in diameter well with a 5-ft long screen set about 8 to 13 ft below the water table. The multilevel sampling well TS8, 15-ft downgradient of TS9, was used as the detection well. TS8 has sampling ports installed at evenly spaced depths and only one port was monitored per tracer test starting with the deepest and working towards the shallowest. Tracer tests were run after the official completion of this project in October 1999, November 1999, March 2000 and July 2000. For each of the tracer tests, 48 L of 5000-ppm bromide solution were injected into TS9 followed by injection of 25 L of untreated, unbrominated groundwater to flush the well of any residual injectate. At TS8, water was sampled continuously at very slow flow rates with a peristaltic pump and monitored with a bromide-specific electrode connected to a laptop computer using an Orion Sensorlink[®] PC card and software. During the tests, the hydraulic heads in both wells were monitored to calculate the hydraulic gradient and allow estimation of an effective or apparent hydraulic conductivity. Results from the four tests are summarized in Table 8.

The first three tests indicate that the travel velocity and apparent conductivity are highly dependent on the amount of vertical distance traveled by the tracer. This result confirms the high vertical to horizontal anisotropy predicted by the flow-model calibration. The apparent K value for the near-horizontal test of March 2000 is close to the calibrated model value of 440 ft/d. The July 2000 test, however, complicates the picture. In this test, there was an arrival of bromide up to 270 ppm at about 2.8 hours into the test after which time the concentration fell to zero. At about 8 hours, the concentration began to rise again peaking at just over 2000 ppm at about 14.5 hours. The July 2000 test brings into question which peak is appropriate to use and whether there might have been later, higher-concentration peaks associated with the other tests that were not observed simply because the tests were not run long enough. We recommend that the tracer tests be repeated in the future with a longer duration.

Table 8. Results of bromide tracer tests.

Date	Depth of monitoring port below injection (ft)	Approximate breakthrough time (hours)	Peak concentration (ppm)	Apparent K (ft/d)
Oct 1999	11 to 16	23	52	26
Nov 1999	6 to 11	13	24	41
Mar 2000	1 to 6	4	88	570
Jul 2000	0	2.8 and 13*	270 and 2040	Unclear

*There were two breakthroughs observed during the July 2000 test

Time of Travel from the Creek to the Municipal Well: Model Predictions and a Natural-Tracer Test

The program MODPATH was used in conjunction with the calibrated MODFLOW simulation to investigate travel paths and travel times from Four Mile Creek to the municipal well under pumping conditions. Prediction of the transport of particles placed below the streambed along the western edge of Four Mile Creek shows flowpaths from the stream to Lateral 1 that intersect the monitoring wells. Predicted travel times were highly dependent on the existence of a silt/clay lens a few feet below the water table. In 1999, it was unclear whether this lens extended underneath the creek bed. If it did not extend that far, then predicted travel times were expected to be about 2.3 days. Such short travel times would allow a field test to be conducted in which the effects of induced infiltration could be observed. On the other hand, if the lens did extend beneath the creek, estimated travel times would be more on the order of 24 days, making a field test difficult within the scope of this project.

In Summer 2000, following the completion of this project, additional drilling and sampling with Geoprobe® equipment indicated that it was likely that the silt/clay lens was continuous underneath the creek. A pumping test was then performed for 4.5 days to establish steady-state conditions and look for the movement of creek water towards the pumping arm. A new monitoring well, TS10, was installed between TS8 and TS4 (Figure 11). This well has a 2-in diameter, large enough to house a YSI® datasonde that allows continuous

monitoring of pH, temperature, specific conductance and dissolved oxygen. Before beginning the test, creek water and well water were sampled; creek water had a substantially higher temperature, dissolved oxygen content and lower specific conductance than the aquifer water. Shortly after the pump was turned on, creek piezometers indicated that the creek near the Ranney well went from being a gaining creek to a losing creek indicating that pumping does draw water directly out of the creek. Over the 4.5-day pumping period, however, no substantial differences in water chemistry were detected in the monitoring wells indicating that over this period there was no arrival of creek water to the monitoring wells. It is hoped that future work will allow a longer pumping test to be performed to measure travel times between the creek and the pumping arm. Given the probable existence of the silt/clay lens, however, it is unlikely that bacterial arrival at any of the monitoring wells will be observed.

Related Research as an Outgrowth of this Project:

The work on this project led to our inclusion in another project entitled “Fate and transport of pathogens in areas of induced surface-water infiltration,” a joint effort by ourselves, the US Geological Survey and the Cincinnati Water Works. The project was funded by the Ohio Water Development Authority and we were subcontracted by the City of Cincinnati for \$46,900. Work on the new project began in 1999 and will continue through September 2001. As with the original project, this new research involved both field and laboratory investigations of water and pathogen transport under induced infiltration. Specifically, the new field site was the Bolton wellfield in Fairfield, Ohio which consists of 10 municipal wells set in the Great Miami River buried-valley aquifer and placed very close to the Great Miami River to benefit from induced infiltration. A monitoring well network was established between the river and two of the municipal wells. The monitoring wells were extensively sampled to observe the movement of chemicals and pathogens along flowpaths from the river to the municipal wells. During the drilling of the boreholes for these wells, 3-m long, 10-cm diameter intact cores were collected using Rotasonic® drilling. Towards the end of 1999, we began using these larger cores in our column experiments. To date we have run bromide- and bacterial-breakthrough experiments on 22 10-cm long sections of these cores.

The experiments performed on the 10-cm diameter core sections have been highly successful. On average, bacteria move through this material faster than does bromide resulting in a faster peak arrival. However, the bacteria continue to exit the column at a fairly constant concentration for as long as we run the experiment (up to 50 pore volumes in some cases). We have been able to simulate the observed bacterial breakthrough using a model incorporating kinetic sorption. We have developed regression models that indicate that much of the variability of bacterial transport observed from one core to the next can be explained by the variability associated with the median grain size of the core section. The hydraulic conductivity and sorting coefficient are also important factors controlling the time of peak arrival and rate of bacterial desorption. In contrast to the results of the original project, there was no significant effect from the variability associated with the indigenous biomass of the columns. There was

also no discernable effect from the organic-matter content.

Many field data have been collected showing the reduction in bacterial concentrations at various points along flow paths towards the municipal wells. In future work, the transport-model parameters estimated from the laboratory experiments will be used in a field-scale transport model to see how well actual concentrations can be predicted based on the laboratory results.

References:

- Bouwer, H (1989) The Bouwer and Rice slug test; an update. *Ground Water*, 27:304-309.
- Bouwer, H and R.C. Rice (1976) A slug test for determining hydraulic conductivity of unconfined aquifers with completely or partially penetrating wells. *Water Resources Research*, 12:423-428.
- Butler, J. J., Jr. (1998) *The design, performance, and analysis of slug tests*. Lewis Publishers, Boca Raton, US.
- Hvorslev, M.J. (1951) Time lag and soil permeability in ground Water observations. U.S. Army Corps of Engineers Waterway Experimentation Station, Bulletin 36.
- Kipp, K.L., Jr. (1985) Type curve analysis of inertial effects in the response of a well to a slug test. *Water Resources Research*, 21:1397-1408.
- Springer, R.K. and L.W. Gelhar (1991) Characterization of large-scale aquifer heterogeneity in glacial outwash by analysis of slug tests with oscillatory responses, Cape Cod, Massachusetts, *U.S. Geological Survey Water Resources Investigations Report*. 91-4034, 36.
- Toride, N., F.J. Leij and M.Th. van Genuchten (1995) The CXTFIT code for estimating transport parameters from laboratory or field tracer experiments, Version 2.0. Research Report No. 137, US Salinity Laboratory, Agricultural Research Service, US Department of Agriculture, Riverside, CA, 121 pp.

Descriptors:

Autochthonous-allochthonous microbial interactions, Bacterial transport, Groundwater quality modeling, Surface-groundwater relationships.

Theses and Dissertations:

- Kreeger, A.L. (2000) Comparison of hydraulic conductivity estimates using a variety of techniques at a field site in southwestern Ohio. Master of Science thesis. Department of Geology, Miami University, Oxford, Ohio, 83 pp.
- Rossmann, A.J. (2001) Determining the significance of the autochthonous (indigenous) microbial community on the fate and transport of allochthonous (invasive) bacteria. Master of Science thesis. Department of Geology, Miami University, Oxford, Ohio, 85 pp.

Schran, H.L. (2001) Microbial biomass and community structure of shallow, glacial-outwash aquifer sediment. Master of Science thesis. Department of Microbiology, Miami University, Oxford, Ohio, 47 pp.

The following thesis and dissertation are products of our latest funding and indirectly stem from this project:

Sun, K (2001) Comparative study of bromide and bacterial transport through different porous media: controlling sediment characteristics and mathematical modeling. Ph.D. dissertation. Department of Geology, Miami University, Oxford, Ohio, 350 pp.

Mignery, M.B. (In progress) Assessing water quality impacts from induced infiltration at a well field in southwest Ohio. Master of Science thesis. Department of Geology, Miami University, Oxford, Ohio.

Conference Abstracts:

Brannock, J.M., A.P. Tomaras, K. Sun, J. Levy, R.H. Findlay (2000) Comparison of *Escherichia coli* transport through natural sediment and laboratory sand columns. Undergraduate Research 2000, Miami University, Oxford OH.

Lustig, A.G. and J. Levy (1999) Comparison of hydraulic conductivity estimates using a variety of techniques at a field site in southwestern Ohio. Abstract 51644. 1999 Fall meeting of the Geological Society of America.

Mignery, M.B. and J. Levy (1999) Impact of induced infiltration on water quality at a wellfield in southwest Ohio. Abstract 51512. 1999 Fall meeting of the Geological Society of America.

Schran, H.L., A. Lustig, J. Levy and R.H. Findlay (1999) Microbial biomass and community structure of a shallow glacial-outwash aquifer sediment. Abstract for 1999 meeting of the American Society for Microbiology.

Sun, K., A.J. Rossman, J. Levy, R.H. Findlay and H.L. Schran (1998) Bacterial transport through intact sediment cores: variability of transport parameters and controlling aquifer characteristics. Abstract 51051, 1998 Fall meeting of the Geological Society of America.

Schran, H.L., A.J. Rossman, J. Levy, R.H. Findlay (1998) Microbial community structure of a shallow groundwater sediment and coliform bacterial transport. 1998 Ohio, Allegheny, Kentucky & Tennessee ASM Branch Meeting, p. 40.

Schran, H.L., AJ Rossman, J. Levy, R.H. Findlay (1998) Microbial community structure of a shallow groundwater sediment. 8th International Symposium on Microbial Ecology, Halifax Canada, p. 296.

Findlay, R.H., H.L. Schran, A.J. Rossman, J. Levy (1998) Microbial community structure of a shallow groundwater sediment and coliform bacterial transport. Abstract for the Joint Meeting of the Ohio & West Virginia Branches of the American Society for Microbiology, April 24-25, 1998, Ohio State University, Columbus, OH.

The following abstracts are products of our latest funding and indirectly stem from this project:

Roa, S.D., J.A. Hardgrove, A.P. Tomaras, J.M. Brannock, K. Sun, F. Farruggia, J. Levy and R.H. Findlay (2001) Comparison of *Escherichia coli* transport through undisturbed and re-packed groundwater sediment columns. 101st General Meeting of the American Society for Microbiology.

Sun, K., J. Levy, R.H. Findlay, J. Brannock, A. Tomaras, K.L. Mumy, J.A. Porter (2000) Effect of sediment characteristics on bacterial transport through intact aquifer sediment cores. Abstract 50436. 2000 Fall meeting of the Geological Society of America

Sun, K., R.H. Findlay, J. Levy, J. Brannock, A. Tomaras, K.L. Mumy (2000) Bacterial transport through relatively undisturbed aquifer sediments. Midwest Ground Water Conference, Oct. 17-19, 2000.

Mignery, M.B., J. Levy, R.A. Sheets, B. Whitteberry (2000) Extent and impact of induced infiltration at a well field in southwest Ohio. Abstract 51853. 2000 Fall meeting of the Geological Society of America

Gollnitz, W.D., B. Whitteberry, J. Vogt, R.A. Sheets, G.L. Rowe, J. Levy, R.H. Findlay, M.B. Mignery, (2000) Introduction to the flowpath study at the City of Cincinnati's C.M. Bolton well field—A case study for monitoring induced infiltration. Midwest Ground Water Conference, Oct. 17-19, 2000.

Brannock, J.M., AP Tomaras, K Sun, J Levy, RH Findlay (2000) Transport of *E. coli* through Natural Sediments and Laboratory Sand Columns. 100th General Meeting of the American Society for Microbiology, Los Angeles, CA. p. 596.

Brannock, J.M., AP Tomaras, K Sun, J Levy, RH Findlay (2000) Analysis of *Escherichia coli* transport through groundwater sediments. Ohio Branch of the American Society for Microbiology Annual Meeting. Hueston Woods State Park, OH.

Articles:

The following articles are all in progress. They are products of our latest funding and indirectly stem from this project:

Sheets, R.A., J. Levy and M.B. Mignery (In progress) Flow paths and travel times from a river to municipal wells at a site with induced infiltration: modeling and ground truth. For submission to *Ground Water*.

Gollnitz, W.D., B. Whitteberry, J. Vogt, R.A. Sheets, G.L. Rowe, J. Levy, R.H. Findlay, M.B. Mignery (In progress) The effect of induced infiltration on drinking water quality. For submission to *Ground Water Monitoring and Remediation*.

Levy, J., K. Sun, R.H. Findlay and F.T. Farruggia (In progress) Factors controlling bacterial transport in glacial outwash aquifer sediment. For submission to *Water Resources Research*.

- Sun, K., J. Levy and R.H. Findlay (In progress) Comparison of bacterial transport through artificial, intact-natural and repacked-natural sediment columns. For submission to *Journal of Contaminant Hydrology*.
- Levy, J. and K. Sun (In progress) Nonideal transport of bromide through heterogeneous sediment: investigating the meanings of the two-region model parameters. For submission to *Journal of Contaminant Hydrology*.
- Porter J., and R. H. Findlay (In progress) Microbial biomass and community structure in groundwater sediments. For submission to *Microbial Ecology*.

Information Transfer Program

Basic Information

Title:	Ohio Water Resources Center Information Transfer Activities
Start Date:	3/1/2000
End Date:	2/28/2001
Descriptors:	
Lead Institute:	Water Resources Center
Principal Investigators:	Earl Whitlatch

Publication

A series of tasks were continued, including; the administration of the Water Resources Center at The Ohio State University and activities to transfer and disseminate information and technology developed by researchers affiliated with the WRC to a wide range of state, federal, county, and municipal agencies; to the private sector, academic community, and to private citizens throughout Ohio. Specific tasks were: the initiation and administration of a Special Water and Wastewater Treatment Grants Competition; administration of the 104(B) In-State Competition and the National Competitive Grants Program; continuation of the Water Luncheon Seminar; assemblage of a directory of college and university water resources research publications and capabilities in Ohio; and continued administrative support for the Water Management Association of Ohio and the Ohio Water Education Program.

USGS Summer Intern Program

Student Support

Student Support					
Category	Section 104 Base Grant	Section 104 RCGP Award	NIWR-USGS Internship	Supplemental Awards	Total
Undergraduate	0	3	0	0	3
Masters	2	5	1	0	8
Ph.D.	2	4	1	0	7
Post-Doc.	0	1	0	0	1
Total	4	13	2	0	19

Notable Awards and Achievements

None

Publications from Prior Projects